

**THEORETICAL STUDIES ON THE REACTION MECHANISMS OF  
CATALYTIC ORGANIC REACTIONS**

**SSS**

**LAU BOON WEI**

**NATIONAL UNIVERSITY OF SINGAPORE**

**2007**

**THEORETICAL STUDIES ON THE REACTION MECHANISMS OF  
CATALYTIC ORGANIC REACTIONS**

**LAU BOON WEI**

**B.Sc. Chemistry (Distinction), University of Minnesota, Twin Cities, USA**

**B.A. Japanese, University of Minnesota, Twin Cities, USA**

**A THESIS SUBMITTED**

**FOR THE DEGREE OF MASTER OF SCIENCE**

**DEPARTMENT OF CHEMISTRY**

**NATIONAL UNIVERSITY OF SINGAPORE**

**2007**

## Acknowledgements

---

*“Few people have the greatness to change history;  
but each one of us can affect a small portion of events,  
and in the sum of all these activities,  
shall be written the history of our generation.”*

***Robert F. Kennedy***

This academic journey has witnessed several vicissitudes in my life here. I have to go through much pain and effort to complete this research degree and, in the process, I have also learned tremendously. I thank God for giving me the spiritual fortitude to complete whatever I have started out and also for taking care of my mental and physical well-being, hence allowing me to successfully graduate from NUS.

I would like to extend my gratitude to my main supervisor Assoc. Prof. Wong Ming Wah, who has been patient with my progress throughout the course of my study. I am also grateful to my co-supervisor, Assistant Prof. R.P.A Bettens, whose incisive comments every now and then never cease to amuse me.

One can hardly be more thankful to NUS for its financial support in the form of the NUS Research Scholarship, a veritable helping hand especially since I am on a no-pay study leave from the Economic Development Board of Singapore to pursue this Masters degree by Research.

I would like to express my sincere thanks to my lab colleagues, namely Dr.Wang Li, Dr. Ran Jiong, Adrian Mak, Chong Mien Han, and last but not least, Eugene Ng, who has tirelessly provided me with help on the finer details of my projects. To him I owe much.

Indeed, the contributions of my research on the body of knowledge may not be earth-shattering. However, I take comfort in the fact that even smallest contribution matters in the larger scheme of things. For as Robert Kennedy -a true giant amongst us- said, we may be small but in the total all our contributions, shall be written the history of our generation. I invite you, my reader, to partake in this journey with me.

# Table of Contents

---

<i>Acknowledgements</i>	<i>i</i>
<i>Table of Contents</i>	<i>ii</i>
<i>Summary</i>	<i>vii</i>
<b>List of Symbols and Abbreviations</b>	<i>ix</i>
<b>Chapter 1 Introduction</b>	<b>1</b>
1.1 The Concept of Organic Reaction Mechanisms	1
1.2 Elementary and Stepwise Reactions in a Reaction Mechanism	2
1.3 Importance of Studying Reaction Mechanisms	3
1.4 Transition States and Intermediates in Reaction Mechanisms	4
1.4.1 <i>Hammond Postulate/ Early and Late Transition States</i>	5
1.5 Use of Computational Chemistry in Investigating Reaction Mechanisms	6
1.5.1 Theoretical Studies on Alkylation of Benzaldehyde using TiTaddolates	7
1.5.2 Theoretical Studies on Mercaptan-catalyzed Condensation of BPA	9
1.6 References	10
<b>Chapter 2 Theory and Methods</b>	<b>11</b>
2.1 Introduction	11
2.2 Molecular Mechanics	13
2.3 Semi-Empirical Methods	15
2.3.1 <i>Limitations of Semi-Empirical Methods</i>	15
2.4 Ab Initio Methods	16
2.5 The HF Equations	19

2.5.1	Calculating the Atomic or Molecular Energy	21
2.5.2	The Variational Method	21
2.6	Hartree-Fock Method	24
2.7	Basis Sets	26
2.8	Post-HF Calculations: Electron Correlation	30
2.8.1	The Moller-Plesset Approach to Electron Correlation	32
2.9	Density Functional Theory Methods	35
2.9.1	Current DFT Methods: The Kohn-Sham approach	35
2.9.2	The Kohn-Sham Energy and the KS equations	36
2.9.3	The exchange-correlation energy functional: Local Density Approximation	38
2.9.4	The Local Spin DENSITY Approximation (LSDA)	39
2.9.5	Hybrid functionals	39
2.9.6	IMOMM, IMOMO, and ONIOM methods	40
2.10	Solvent Effects	42
2.10.1	The Onsager SCRF Method	44
2.10.2	The Polarizable Continuum Model Method	45
2.11	References	46
<b>Chapter 3 Titanium Taddolate Catalyzed Asymmetric Alkylation Reactions</b>		48
3.1	Development of chiral catalyst (TiTaddolates) for highly enantioselective alkylation reactions of benzaldehydes	48
3.2	Alkylation Nucleophilic Addition of Dialkyl Zinc to Aldehydes catalyzed by TiTaddolates—The R <sub>2</sub> Zn Approach	49
3.3	Alkylation Nucleophilic Addition of R-Ti(OiPr) <sub>3</sub> to Aldehydes catalyzed by TiTaddolates—The Zinc-Free Approach	52
3.3.1	<i>R-Ti(OiPr)<sub>3</sub> as alkylating reagent</i>	53

<b>3.3.2</b> <i>TiTaddolate Catalysts in Alkyl Titanium Derivatives Nucleophilic Addition</i>	54
<b>3.4</b> Experimental Work Done by Various Research Groups	55
<b>3.4.1</b> D. Seebach et al.-Alkyl-Titanium Derivatives as Alkylating Agents	55
<b>3.4.2</b> Y.D. Wu et al. - Experimental Studies on the H-bonded Promoted Enantioselective HDA reaction of Danishefsky's diene with Benzaldehyde	56
<b>3.4.3</b> P.J.Walsh et al.- Titanium Catalyzed Enantioselective Additions of Alkyl group to Aldehydes	57
<b>3.5</b> Methodology and Theoretical Calculations	59
<b>3.5.1</b> 2 types of Uncatalyzed Benchmark Nucleophilic Addition Reactions	59
<b>3.5.2</b> Activation Energy Barrier of Uncatalyzed Reaction	61
<b>3.5.3</b> Monometallic Variant	62
<b>3.5.4</b> Investigation on pre-TS complexes	63
<b>3.5.4.1</b> BE of Benzaldehyde and Alkyl-TiTaddolate pre-TS complexes	63
<b>3.6</b> Bimetallic Variant	70
<b>3.6.1</b> Uncatalyzed benchmark reaction for bimetallic variant	
<b>3.6.2</b> Transition States Complexes in Bimetallic variant	71
<b>3.7</b> Further Developments and Qualitative Predictions	74
<b>3.7.1</b> ONIOM Integrated MO/MM method	74
<b>3.7.2</b> Introduction on ONIOM methods	75
<b>3.7.3</b> Problems with the ONIOM method	76
<b>3.8</b> Methodology in ONIOM calculations	77
<b>3.8.1</b> 2-layer ONIOM calculations	77
<b>3.8.2</b> 3-layer ONIOM calculations	79
<b>3.9</b> Results and Discussion	81

<b>3.10</b>	Conclusion on the Use of ONIOM in structural calculations	82
<b>3.11</b>	Using Reverse Docking	83
<b>3.12</b>	References	85
<b>Chapter 4</b>	<b>Acidic Condensation Reaction of Bisphenol-A using Methyl Mercaptans as Co-catalysts</b>	<b>87</b>
<b>4.1</b>	Introduction	87
<b>4.2</b>	Methyl Mercaptan as Co-catalyst in BPA Condensation Reaction	90
<b>4.3</b>	Improvements on Mercaptan Co-catalysts	91
<b>4.3.1</b>	Dithiolketals as Mercaptan Co-catalysts	92
<b>4.3.2</b>	Experimental and Theoretical calculations on Methyl Mercaptan as Co-catalysts	94
<b>4.4</b>	Calculations: Heats of Formation of BPA Condensation Reaction	95
<b>4.4.1</b>	Discussion and Interpretation on the E values of the Reaction Steps	99
<b>4.4.2</b>	Problems with Protonation-Deprotonation Hypothesis	100
<b>4.4.3</b>	Reaction Mechanism Involving pericyclic rearrangement reaction transition states—[1,3] H-shift	101
<b>4.5</b>	Methodology and Theoretical Calculations	103
<b>4.5.1</b>	Optimal Method of Calculation—DFT B3LYP/6-31G*	103
<b>4.5.2</b>	Energies and Frequency Calculations	104
<b>4.6</b>	PES Energy Profile of Acid and Mercaptan Catalyzed Pathways	104
<b>4.7</b>	Transition States and Conformers of Acid Pathway	107
<b>4.7.1</b>	C—C bond forming transition states in Acid Pathway	107
<b>4.7.2</b>	[1,3] H-shift Transition States	109

<b>4.8</b>	<b>Transition States of Mercaptan Pathway</b>	111
<b>4.8.1</b>	<b>C—C bond forming transition states</b>	111
<b>4.8.2</b>	<b>[1,3] H-shift transition states</b>	113
<b>4.9</b>	<b>Discussion and Interpretation</b>	114
<b>4.9.1</b>	<b>Stability of carbocation intermediates</b>	114
<b>4.9.2</b>	<b>Energy barriers of transition states formed</b>	115
<b>4.9.3</b>	<b>Single point reaction energy barrier heights at B3LYP/6-311+G**</b>	116
<b>4.10</b>	<b>Further Developments through Kinetic Investigation</b>	117
<b>4.11</b>	<b>References</b>	117
	<b>Chapter 5 Conclusion</b>	119
<b>5.1</b>	<b>A common thread between the projects</b>	119
<b>5.2</b>	<b>References</b>	120



## Summary

---

This thesis deals with the computational quantum chemical study of some of the interesting aspects of a few important catalytic organic reactions.

1. Effect of intramolecular formyl C-H hydrogen bonds to the oxygen atom of isopropoxide ligands in complexes of TiTaddolate and benzaldehyde on the stabilization of the pre-TS intermediate
2. Mechanistic basis of enantioselectivity of the alkylation of benzaldehyde by TiTaddolate catalyst in terms of transition-state structures
3. Application of formyl H-bond as an organizing stereochemical element to the understanding of the catalytic reactions involving benzaldehyde and TiTaddolate
4. Effect of methyl mercaptan co-catalyst on the rate of condensation reaction of bisphenol-A
5. Possibility of a pericyclic [1,3] H-shift in the condensation reaction of bisphenol-A

Chapter 1 gives a general introduction to the work done in this thesis.

Chapter 2 then provides the theoretical background of all type of calculations included in this thesis.

Chapter 3 deals with the study of TiTaddolate catalyzed alkylation of benzaldehyde to form secondary alcohol. Specifically, the enantioselective alkylation of benzaldehyde by dimethyl zinc catalysed by TiTaddolates is being examined. It has been found that the  $\alpha$ ,  $\alpha'$ -aryl substituents in the TADDOL molecules are found to exert a significant impact on both the activity and the enantioselectivity of the catalysis. Steric and electronic effects are examined in this chapter, using Density Functional Theory (DFT) methods.

Meanwhile, certain stereochemical elements contributing to the high enantioselectivities

observed in these reactions, namely the weak CH—O H-bonds are also located in the optimized structures of pre-TS intermediates. In combination with the DFT quantum mechanical calculations, the mechanism of the reaction is also studied theoretically using the integrated Molecular Orbital/Molecular Orbital method (ONIOM) in order to ascertain the feasibility of obtaining reliable optimized structures at highly reduced computational costs, so as to facilitate subsequent high-level calculations.

Chapter 4 deals with the study of the reaction mechanism behind the condensation reaction of bisphenol-A (BPA), an important specialty chemical which is used industrially for the manufacture of polycarbonate resins and epoxy resins. In this chapter, the mechanism and geometric aspects of BPA condensation reaction under both conventional acid catalysts and methyl mercaptan (MeSH) co-catalysed conditions are being investigated. We discovered some interesting mechanistic aspects within the acid and methyl mercaptan co-catalysed environments, namely, the possibility of a pericyclic reaction-like [1,3] H-shift mechanism. The entire PES of both acid and methyl mercaptan catalyzed pathways are elucidated as well.

Chapter 5 provides a conclusion to the thesis as well as presents an insight on possible future developments in the projects within this thesis.

## List of Symbols and Abbreviations

---

$\Delta G_{\text{aq}}$  = Gibbs free energy changes in the aqueous phase

$\Delta G_{\text{gas}}$  = Gibbs free energy changes in the gaseous phase

$\Delta E_{\text{aq}}$  = Electronic energy changes in the aqueous phase

$\Delta E_{\text{gas}}$  = Electronic energy changes in the gaseous phase

**TADDOL** =  $\alpha, \alpha', \alpha'', \alpha'''$  - tetraaryl-1,3-dioxalane-4,5-dimethanol

**TiTaddolate** = ( $\alpha, \alpha', \alpha'', \alpha'''$  - tetraaryl-1,3-dioxalane-4,5-dimethanolato)-  
Titanate

**AM1** = Austin Model 1

**BPA** = Bisphenol-A

**B3LYP** = Becke's three parameter hybrid functional with Lee-Yang-Parr  
correlation functional

**DFT** = Density Functional Theory

$E_{\text{calc}}$  = Calculated electronic energy excluding Zero Point Energy

$E_{\text{total}}$  = Calculated electronic energy including Zero Point Energy

$G_{\text{calc}}$  = Calculated Gibb's free energy excluding thermal correction

$G_{\text{total}}$  = Total Gibb's free energy including thermal correction

**HF** = Hartree Fock Theory

**LYP** = Lee, Yang, and Parr's correlation functional including local and non-  
local terms

**OM** = Onsager Model

**ONIOM** = A variant of the Integrated Molecular Orbital Molecular Mechanics  
Method designed by K. Morokuma et al.

**PCM** = Polarized Continuum Model

**PES** = Potential Energy Surface

**ZPE** = Zero Point Energy or Zero Point Vibrational Energy

# Chapter 1

## Introduction

---

---

### 1.1 The Concept of Organic Reaction Mechanisms

The complexity of organic chemistry involves thousands of different reactions which allow chemists to synthesize and interconvert millions of compounds, some of great complexity. The key to understanding this vital branch of chemistry is the concept of reaction mechanism. An increasing knowledge and understanding of organic reaction mechanisms through computational chemistry, harnessing the principles of Quantum Mechanics, has been a major factor in the rapid advancement of organic chemistry, biochemistry and pharmacology in the last few decades.

Organic reactions generally involve covalent bond breaking and forming. How these bond-breaking and bond-forming processes occur along the reaction pathway provides the basis of organic reaction mechanisms. There are 2 main types of reactions, namely, elementary reactions, which involve just one step, and stepwise reactions, which have more than one step and involve the production of reactive intermediates that reacts further down the reaction pathway. We will encounter both kinds of reactions in this thesis, namely the nucleophilic addition of alkyl groups to benzaldehydes by titanium taddolate catalysts and the mercaptan-catalyzed condensation of bisphenol-A (BPA).

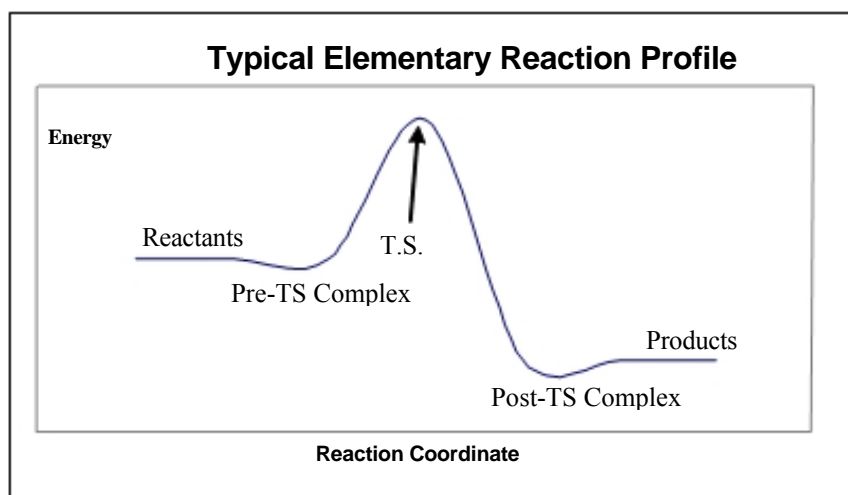
## 1.2 Elementary and Stepwise Reactions in a Reaction Mechanism

In elementary reactions, the reacting molecule or molecules are transformed into products directly, without the formation of reactive intermediates. In a stepwise reaction, one or more intermediate species are formed, which react further down the reaction pathway to give the products. A stepwise reaction can therefore be split up into two or more elementary reactions.

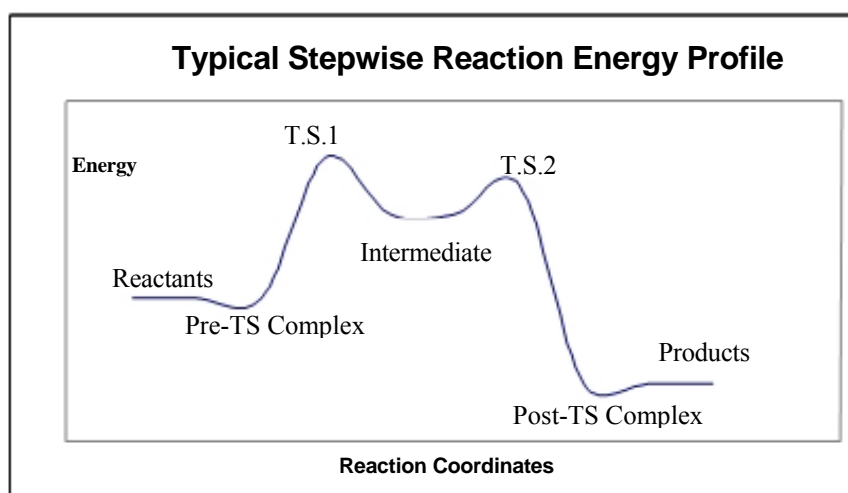
As an elementary reaction proceeds, the Gibbs free potential energy increases up to maximum value and then goes down to a value corresponding to that of the products. The position of the highest potential energy along the PES is called the transition state, and is a key feature of the reaction, which is experimentally almost impossible to observe but can be investigated through the principles of quantum chemistry.

In a stepwise reaction, at least one of the products of the first elementary reaction reacts further in a second elementary reaction. This may be followed by further elementary reactions until the reaction is complete. Any molecules or products in the course of a stepwise reaction which react further and are not present at the end of the reaction are known as intermediates. In Chapter 5, we shall observe the various intermediates involved in the condensation reaction of BPA.

Figure 1.1.a shows a typical free energy diagram for an elementary reaction and Figure 1.1.b for a stepwise reaction with 2 elementary steps.



*Fig. 1.1-a*



*Fig: 1.1-b*

### 1.3 Importance of studying reaction mechanisms

There are many reasons why chemists seek to understand reaction mechanisms. Firstly, reaction mechanisms form a framework on which the factual detail of organic chemistry, necessary for a good understanding of experimental results, can be established. Knowledge about the reaction mechanism of an organic reaction also allows chemists to intelligently vary the reaction conditions such as temperatures, mole equivalence of reactants or any other reaction parameters in order to maximize yields of pure products. In the

biochemical and pharmaceutical industries, the reactions involved in metabolism in living organisms are often organic, and many are understood in only limited details. Therefore, the establishment of the correct reaction mechanism of these vital bio-organic reactions can help biochemists design new drugs which could assist or prevent particular biochemical reactions.

#### **1.4 Transition States and Intermediates in Reaction Mechanisms**

A composite stepwise reaction consists of a number of elementary reactions. Each process along a path is defined by the free energy surface connecting reactants to products. The reaction proceeds along the potential energy surface or PES. The point of maximum free energy is called the transition state of the reaction. A transition state and its associated attributes are traditionally symbolized by the symbol  $\ddagger$ . The difference between the standard free energy of the reactants and of the transition state is termed the standard Gibbs free energy of activation, symbolized as  $\Delta G^\ddagger$ . The transition state refers both to the maximum position on the reaction coordinate diagram as well as to the geometry of the transition state complex formed. Theoretical chemistry seeks to understand the activation process, with the help of experimental kinetics information obtained from practical experiments, in order to understand the change of structures and energetics as reactants proceed towards the transition state. Each step in the reaction has its own transition state. The kinetic scheme will show whether these transition states occur in succession or in parallel and whether kinetically significant reaction intermediates arise at any state.

There is a difference between transition states and intermediates. An intermediate occupies a potential energy minimum along the reaction coordinate. Additional activation, whether by an intramolecular process (distortion, rearrangement, dissociation) or by a

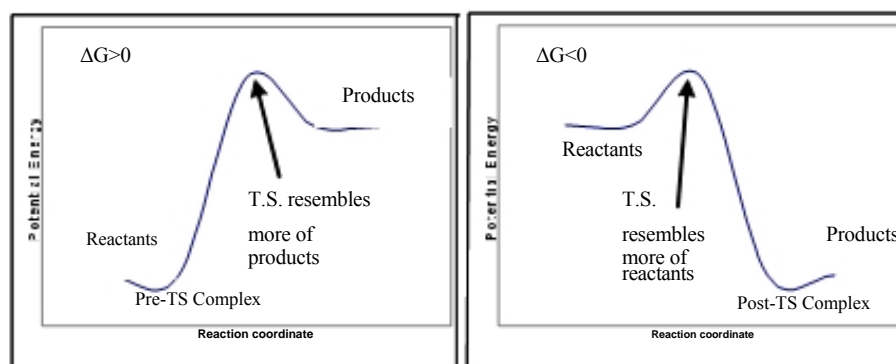
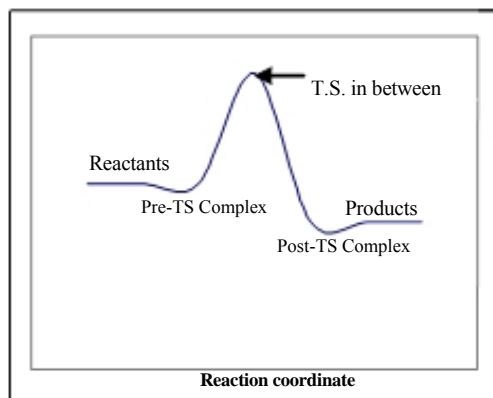


bimolecular reaction with another component, is needed to enable the intermediate to react further; it may then return to the starting materials or advance to the products. The transition state, on the other hand, is a species that reacts without further activation. It is defined as the state corresponding to the energy maximum along the reaction coordinate. At this point, assuming a perfectly irreversible reaction, colliding reactant molecules will go on to form products and will not be diverted to an alternative product; on the other hand, an intermediate, at a free-energy minimum, can still be preceded or followed by a transition state. In addition, an intermediate often has the same “composition” as one of its adjacent transition states and perhaps both.

Unlike the transition states, the intermediate has a choice of reactions. It is not possible to isolate the transition state of a chemical reaction, nor is it feasible to study it by spectroscopic methods (with the exception of perhaps the simplest gas-phase unimolecular reactions observable via femtosecond laser spectroscopy) which rely on the presence of at least appreciable concentrations of species with particular energy and geometry.

#### **1.4.1 Hammond Postulate/ Early and Late Transition States**

The Hammond's Postulate states that if 2 states, for example, a transition state and an unstable intermediate occur consecutively during a reaction process and have nearly the same energies, their interconversion will usually involve only a small reorganization of molecular structures. In other words, for very endothermic reactions, the transition state resembles the products almost completely, with a late transition state (Figure 1.4.1-b) whereas for very exothermic reactions, the transition state is more like the reagents, i.e. an early transition state (Figure 1.4.1-c). For a thermo-neutral reaction, with the products of the reaction identical with the reactants, the transition state would lie in between the reactant and the product (Figure 1.4.1-a).



*Fig. 1.4.1-a (top); Fig. 1.4.1-b (left, bottom); Fig.1.4.1-c (right, bottom)*

Hammond's postulate connects the reaction process with the structural features of those states that form part of it, by saying that the molecular reorganizations have to be small in those steps that involve two states that are very close in energy<sup>1</sup>. This allows for chemists to do structural comparison between the starting materials, products, and the possible "stable intermediates" that lead to the understanding that the most stable product is not always the one that is favored in a reaction process.

## 1.5 Use of Computational Chemistry in Investigating Reaction

### Mechanism

Computation quantum chemistry is one of the most dynamic fields of contemporary chemistry, providing a solid foundation for all chemistry, and serving as

the basis for practical, computational methodologies with applications in virtually all branches of chemistry. Quantum computational chemistry is a field of computational science that attempts to apply the laws of quantum mechanics to chemical systems. In the 1980s supercomputers appeared on the scene, making it possible to carry out highly sophisticated quantum mechanical calculations on the energetics of reactant and product molecules of investigated reactions. The results demonstrated that quantum chemistry is not only capable of providing qualitative answers but can allow the accurate determination of reaction energy profiles and transition states.

The importance of the area is amply demonstrated by the fact that the 1998 Nobel Prize for chemistry was awarded for the development of this field of knowledge. John Pople received the award for showing that computational quantum chemistry is a practical, viable proposition in understanding the reaction mechanisms of complex reactions and Walter Kohn received it for the development of density function theory which is the preferred theory used in this thesis<sup>2</sup>.

Dirac's famous words from 1929 were quoted in the recommendation of the Nobel Committee: "The fundamental laws necessary for the mathematical treatment of large parts of physics and the whole of chemistry are thus fully known, and the difficulty lies only in the fact that the application of these law leads to equations that are too complex to be solved."

### **1.5.1 Theoretical Studies on Alkylation of Benzaldehydes using TiTaddolates**

Taddolates have been introduced as chiral ligands in organotitanium reagents starting from as early as 1982. The TADDOLs (or Taddols hereinafter) can be prepared (in a combinatorial way) from aldehydes, ketones, *L*-tartaric acid, aryl Grignard reagents,

and hetero-atom nucleophiles, as to be fit for multitude of applications ranging from stoichiometric chiral reagents, through chiral ligands on various organometallic centers to polymer-incorporated or silica gel-bound immobilized enantioselective catalysts. For example, Taddol-grafted zeolite medium, which was patented by D. Seebach et al. in 1997 used precisely the abovementioned technique to recycle TiTaddolate catalysts. The strategy of using diaryl-methanol groups as part of chiral reagents has been extremely successful in the hands of researchers around the world. Eminent groups that have focused on Taddolates as catalysts include D. Seebach of ZTH, Zurich; K. Narasaka at the University of Tokyo; as well as P.J. Walsh at the University of Pennsylvania.

The application of modern computational techniques to organometallic chemistry has experienced a renaissance in recent years. Through hard work and perseverance of numerous research groups around the world, many of the challenges involved in modeling heavy metals, particularly those concerning the reliable and efficient modeling of metallic transition elements, have been addressed. Computational chemists now have a wider range of computational techniques to accurately model organometallic compounds. Chapter 3 describes the DFT methods used to model the alkylation of benzaldehydes via titanium taddolate catalysts as well as the theoretical calculations and results found from the DFT studies which allow us to provide possible reaction mechanisms of this important nucleophilic addition reaction.

One important point to note in the description of metallic organic compounds is the property of chemical diversity. Chemical diversity can be defined as the ability of metals to stabilize distinct bonding environments involving different bonds like dative, single, multiple bonds and ligating atoms (hard/soft donors, bond types, spin states and

formal oxidation states, co-ordination numbers and geometries) The myriad of catalytic transformations involving organometallic species which includes processes like changes in oxidation states, coordination numbers, and ligand types adds to the complexity of these calculations. It is this property of chemical diversity which makes the elucidation of catalytic organometallic reaction mechanism such a challenging yet rewarding task.

### **1.5.2 Theoretical Studies on Mercaptan-catalyzed Condensation of BPA**

Bisphenol A (4, 4'-isopropylidene diphenol), or more commonly known in the petrochemical industry as BPA, is composed of 2 phenyl rings attached to a central carbon of propane moiety. In conventional industrial production methods, an inorganic acid such as HCl or H<sub>2</sub>SO<sub>4</sub> is used to catalyze the production of BPA from acetone and phenol feedstock. The inorganic acid acts as the catalyst for the condensation addition reactions to produce BPA from acetone and phenol. The aim of Chapter 4 is to elucidate the reaction mechanism of acid-catalyzed production of BPA as well as to shed light on the reasons behind engaging mercaptan or thiol promoters to enhance the product yield of high-purity BPA along ion-exchange resins column. We shall look at the reaction mechanism between the traditional acid catalysed condensation reaction of BPA versus a co-catalyzed (with methyl mercaptan) reaction which has been observed experimentally to have a higher reaction rate as well as a higher chemical yield of BPA. In addition, we shall seek to shed light on the reaction mechanisms behind these 2 pathways and explain how methyl mercaptan, as a co-catalyst, could possibly reduce the energy barrier of some elementary reactions within the reaction profile. DFT calculations were used to study the reaction profiles of the 2 reactions.

The last chapter wraps up the thesis and shows the reader the common thread behind the 2 projects incorporated within this thesis. It appears that, with the increasing complexity of reactions carried out nowadays, it is no longer as simple as increasing the rate of reaction of a reaction process using only one catalyst. More often than not, a co-catalyst (or more) is required to further accelerate the reaction rate and chemoselectivity of a reaction. In the TiTaddolate case, the co-catalyst is  $\text{Ti}(\text{OiPr})_4$  while in the BPA case, the co-catalyst is MeSH.

#### **References:**

---

<sup>1</sup> Hammond, G. S., *A Correlation of Reaction Rates*, J. Am. Chem. Soc. **1955**, 77, 3

<sup>2</sup> [http://nobelprize.org/nobel\\_prizes/chemistry/laureates/1998/](http://nobelprize.org/nobel_prizes/chemistry/laureates/1998/)

# Chapter 2

## Theory and Methods

---

---

### **2 Introduction**

Computational chemistry is used increasingly by researchers to test out the suitability of model systems which are deployed to simulate real-life conditions. It is extremely adaptable for different types of theoretical studies, especially in situations where experimental studies are physically impossible to be carried out- for example, in the elucidation of extremely short-lived intermediates or transition states. Short of using ultra-short laser pulse spectroscopy (for example, Ahmed Zewail's femtosecond spectroscopic studies on transition states reaction mechanisms), such reaction mechanisms are hard to observe experimentally.

In addition, computational chemistry methods can be used to compute molecular energies and structures, energies and structures of transition states, bond and reaction energies and intrinsic reaction pathways. Computations can either be carried out in the gas phase or the solvated phase (Onsager, 1936; Wong et al., 1991) as well as in the ground states or excited states. It serves as a powerful auxiliary tool for exploring areas of chemical interest like substituent effects, reaction mechanisms, potential energy surfaces and excitation energies, at merely a fraction of the time and effort which would be needed during real-life experiments.

Theoretical chemistry is basically defined as the mathematical description of chemical systems investigated. The term computational chemistry is usually used in replacement of theoretical chemistry when a mathematical method is sufficiently well developed that it could be automated for implementation on a supercomputer.

Every quantum chemical calculation seeks to obtain an exact solution to the famous Schrodinger equation:

$$H|\Psi\rangle = E|\Psi\rangle$$

Although it is practically impossible to obtain an exact solution to the Schrodinger equation for any system except for the hydrogen atom (or perhaps, in a loose definition of the word “solving”, perhaps a helium cation as well), it is possible to obtain a fairly good approximation for a variety of molecular systems. Solving a mathematical equation as complex as a Schrodinger would be impossible without the help of supercomputers we fortunately possess today. With the advent of dual-core –and quad-core processors, astronomical amounts of cheap memory, the prospect of theoretical calculations seems increasingly appealing to chemists and biochemists alike.

Theoretical calculations are broadly classified into 3 categories

1. Molecular Mechanics Calculations
2. Quantum Mechanics Calculations
3. Density Functional Theory Calculations

A common thread runs through these 3 types of calculations: they all perform energy calculations, geometry optimizations and vibrational frequency calculations. However, the principles in which the calculations are done are vastly different in the three categories.



The level of theory plays a key role in the prediction of the molecular geometry of molecular complex. Each level of theory has its own advantages and disadvantages. Short of solving the complete Schrödinger equation from first principles, the only way one can determine the chemical and, to some extent, the physical properties, of the chemical system in question, would be to introduce approximations and other parameters which would simplify the otherwise onerous task of solving the Schrödinger equation. In order to obtain the quickest results, the first geometry optimization is usually done with a fast but lower quality level of theory such as semi-empirical method or HF method. Once the geometry of a molecule is optimized with this lower level of theory, it can then be utilized as a starting point for a further geometry optimization leading to a more accurate result. In a nutshell, the level of theory is the extent to which the various methods emulate the solving of the real Schrödinger's equation.

## **2.1 Molecular Mechanics**

Molecular mechanics is, by far, the most accessible of all computational methods, concepts of which are most accessible to the vast majority of scientists and students alike. It's based on the laws of classical physics. It takes no more than freshman college physics to understand the foundation of molecular mechanics, where a molecule is considered as a group of hard spheres (atoms) attached by springs (bonds). Electrons are not considered explicitly in these calculations and the energy of a molecule is represented as the sum of contributions due to

- a) bond stretching
- b) bond bending
- c) van der Waals attractions and repulsions between non-bonded atoms

- d) electrostatic interactions due to polar bond and
- e) energy changes accompanying internal rotation about single bonds

A variety of computer programs like Sybyl, Amber, MM3 are available to perform MM calculations. Each molecular mechanics method has its own unique force field, parameters of which are determined by the computational chemists through benchmark experiments which might differ from one program to another. A force field consists of

1) A set of equations which define how the potential energy of a molecule changes with the position of its component atoms

2) A series of atom types which define the characteristics of an element with specific chemical context (for example a carbon atom in a carbonyl is treated differently from a carbon atom bonded to three hydrogen atoms ( $sp^2$  versus  $sp^3$ ))

3) One or more parameter sets that fit the equations and atom types to the experimental data

As stated earlier, the MM calculations do not explicitly include electrons for any molecular system and they perform calculations based on the interaction among the nuclei. MM calculations have been used by scientists, especially bio-molecular chemists, to perform calculations on very large bio-molecules (hundreds of kDa) containing many thousands of atoms. However, with the oversimplifications inherent within MM comes the various drawbacks which are:

1. Using MM method, one can obtain good results only for the exact molecules, or functional groups for which parameters are available experimentally and which have been thereafter incorporated into the program

2. Since MM method does not treat electrons explicitly, molecular systems where electronic effects predominate (hydrogen bonding, weak CH- $\pi$  interaction etc) are not suitable systems to calculate.
3. Making and breaking of bond cannot be achieved in MM methods, i.e. simulation of reaction dynamics is impossible using MM methods alone.

## 2.2 Semi-Empirical Methods

Semi empirical methods, in general, are very computationally efficient but lose accuracy when the parameters introduced cannot fully describe the chemical system at hand. These methods limit the choice of molecular orbital and it considers only valence electrons. Several semi-empirical methods are available, namely AM1, PM3, PM3(tm), MNDO and it is easily found in commercially available software packages like Trident, Spartan, and HyperChem. These semi-empirical methods are, in a nutshell, parameterized from experimental data or *ab initio* data on a sample collection of common organic molecules, comparatively much more computationally efficient than quantum mechanics, generally in the order of magnitude of  $10^3$  to  $10^4$  applicable to large number of molecules, and hence commonly used in drug-like molecules and medium-sized proteins.

### 2.2.1 Limitations of semi-empirical method

Having stated the advantages of semi-empirical method, one has to note that semi-empirical methods are generally applicable only for systems where parameters have been developed for the component functional groups. Outside the description of the parameters, semi-empirical methods basically lose their computational luster, for lack of

a more poetic description, and fails miserably in describing electronic properties of the chemical system.

### 2.3 Ab Initio Methods

Theoretical methods that do not include empirical or semi-empirical parameters in their equations and that are derived directly from theoretical principles, with no inclusion of experimental data are generally called *ab initio* methods- the term *ab initio* being the Latin phrase “from the beginning”. Most of the time, this specifically refers to the approximate quantum mechanical calculations. The approximations made in these cases, however, are usually mathematical in nature, such as using a simpler functional form (i.e. using Gaussian Type Orbitals (GTO) to model Slater Type Orbitals (STO) in MO calculations) or getting an approximate solution for a complicated differential equation. The simplest kind of *ab initio* calculation is the Hartree-Fock (HF) calculation. Modern molecular HF calculations grew out of calculations first performed on atoms by D.R.Hartree in 1928.<sup>1</sup> The problem that Hartree addressed arises from the fact that for any atom (or molecule) with more than one electron, an exact analytical solution of the Schrödinger equation is not possible, because of the electron-electron repulsion terms. For a two electron system e.g. He, the Schrödinger equation in SI units is:

$$\left[ -\frac{\hbar^2}{8\pi^2m}(\nabla_1^2 + \nabla_2^2) - \frac{Ze^2}{4\pi\epsilon_0r_1} - \frac{Ze^2}{4\pi\epsilon_0r_2} + \frac{e^2}{4\pi\epsilon_0r_{12}} \right] \psi = E\psi \quad (2.1)$$

where  $m$  is the mass (kg) of the electron,  $e$  is the charge (coulombs, positive) of the proton, the variables,  $r_1$ ,  $r_2$  and  $r_{12}$  are the distances (meters) of electrons 1 and 2 from the nucleus and from each other,  $Z=2$  is the number of protons in the nucleus, and  $\epsilon_0$

refers to the permittivity of vacuum. In atomic units (a.u.), the Schrödinger equation can be simplified into:

$$\left[ -\frac{1}{2}\nabla_1^2 - \frac{1}{2}\nabla_2^2 - \frac{Z}{r_1} - \frac{Z}{r_2} + \frac{1}{r_{12}} \right] \psi = E\psi \quad (2.2)$$

It consists of five terms, representing, from left to right, the kinetic energy of electron 1

( $-\frac{1}{2}\nabla_1^2$ ), the kinetic energy of electron 2 ( $-\frac{1}{2}\nabla_2^2$ ), the potential energy of the attraction

of the nucleus for electron 1 ( $-\frac{Z}{r_1}$ ), the potential energy of the attraction of the nucleus

for electron 2 ( $-\frac{Z}{r_2}$ ) and the potential energy of the repulsion between electron 1 and 2

( $+\frac{1}{r_{12}}$ ). This is however not the exact Hamiltonian as it neglects effects due to relativity

and to magnetic interactions such as spin-orbit coupling.<sup>2</sup> Fortunately, for most chemical systems investigated, these effects are rarely important in calculations involving lighter

atoms. The problem of solving the Schrödinger equation lies with the  $+\frac{1}{r_{12}}$  term which

makes it impossible to separate the Schrödinger equation for helium into two one-

electron equations which, like the hydrogen atom equation, can be solved exactly. The

impossibility of an analytic solution to the many electron systems prompted

D.R.Hartree's approach to calculating wavefunctions and energy levels for atoms.

Hartree's methods were to write a plausible approximate wavefunction for an atom as the product of one-electron wavefunctions:

$$\Psi_0 = \psi_0(1)\psi_0(2)\psi_0(3)\dots\psi_0(n) \quad (2.3)$$

This function is called a Hartree product. Here  $\Psi_0$  is a function of the coordinates of all the electrons in the atom,  $\psi_0(1)$  is a function of the coordinates of electron 1,  $\psi_0(2)$  is a function of the coordinates of electron 2, etc; these one electron functions are called atomic orbitals (or molecular orbitals, if the system under discussion is a molecule).

In the first instance, we first solve for electron 1, a one-electron Schrödinger equation in which the electron-electron repulsion comes from one and an average, smeared out electrostatic field calculated from  $\psi_0(2)\psi_0(3)\dots\psi_0(n)$ , due to all the other electrons. The only moving particle in this equation is electron 1. Solving this equation gives  $\psi_1(1)$ , an improved version of  $\psi_0(1)$ . We then move on to solve for electron 2, a one-electron Schrödinger equation with electron 2 moving in an average field due to the electrons of  $\psi_1(1), \psi_0(3), \dots, \psi_0(n)$ , continuing to electron  $n$  moving in a field due to  $\psi_1(1), \psi_1(2), \psi_1(3), \dots, \psi_1(n-1)$ . This completes the first cycle of calculations and gives us:

$$\Psi_1 = \psi_1(1)\psi_1(2)\psi_1(3)\dots\psi_1(n) \quad (2.4)$$

The process is continued for  $k$  cycles till a wavefunction  $\psi_k$  and/or an energy calculated from  $\psi_k$  that are essentially the same (within a certain tolerance threshold) as the wavefunction and/or energy from the previous cycle. This happens when the functions  $\psi(1), \psi(2), \psi(3)\dots\psi(n)$  are varying so little from one cycle to the next that the smeared-out electrostatic field used for the electron-electron potential has ceased to change. At this stage, the field of cycle  $k$  is essentially the same as that of cycle  $k-1$  i.e. it is consistent with this previous field and so that's why the Hartree procedure is called the self consistent field procedure which is usually abbreviated as the SCF procedure.<sup>3</sup>

The immediate problem with the Hartree product is apparent: electrons are indistinguishable from one another and the overall wavefunction should be symmetric to

exchange but this is clearly not the case in the Hartree product. This major defect was corrected by Slater and Fock in 1930. Slater devised a way to construct a total wavefunction  $\psi$  from one electron functions (i.e. orbitals) such that  $\psi$  will be anti-symmetric to electron switching. Hartree's iterative, average-field approach supplemented with electron spin and anti-symmetry leads to the HF theory and the HF equations.

## 2.4 The HF Equations

The Hartree wavefunction is a product of one-electron functions called orbitals or more precisely, spatial orbitals: these are functions of the usual space coordinates,  $x, y, z$ . The Slater wavefunction however, is composed not just of spatial orbitals but of spin orbitals. A spin orbital  $\psi$  ( $\alpha$  or  $\beta$ ) is the product of a spatial orbital and a spin function  $\alpha$  or  $\beta$ . The spin orbitals corresponding to a given spatial orbital are

$$\Psi(\text{spin } \alpha) = \psi(\text{spatial}) \alpha = \psi(x,y,z)\alpha \quad (2.6)$$

$$\Psi(\text{spin } \beta) = \psi(\text{spatial})\beta = \psi(x,y,z)\beta \quad (2.7)$$

The Slater wavefunction differs from the Hartree function not only in being composed of spin orbitals rather than just spatial orbitals. In addition, the Slater wavefunction is not a simple product of one electron functions, but rather a determinant whose elements are these functions.

Slater determinants enforce the Pauli Exclusion Principle, which forbids any two electrons in a system to have all quantum numbers being the same. This is readily seen for an atom: if the three quantum numbers,  $n, l, m_m$  of  $\psi(x,y,z)$  and the spin quantum number  $m_s$  of  $\alpha$  or  $\beta$  were all the same for any electron, two rows (or columns, in the

alternative formulation) would be identical and the determinant, and hence, the wavefunction, would vanish.

For systems with  $2n$  electrons, the general form of a Slater determinant is the  $2n \times 2n$  determinant:

$$\Psi_{2n} = \frac{1}{\sqrt{(2n)!}} \begin{vmatrix} \Psi_1(1)\alpha(1) & \Psi_1(1)\beta(1) & \Psi_2(1)\alpha(1) & \Psi_2(1)\beta(1)\dots\dots & \Psi_n(1)\beta(1) \\ \Psi_1(2)\alpha(2) & \Psi_1(2)\beta(2) & \Psi_2(2)\alpha(2) & \Psi_2(2)\beta(2)\dots\dots\dots & \Psi_n(2)\beta(2) \\ M & M & M & M & M \\ M & M & M & M & M \\ \Psi_1(2n)\alpha(2n) & \Psi_1(2n)\beta(2n) & \Psi_2(2n)\alpha(2n) & \Psi_2(2n)\beta(2n)\dots\dots\dots & \Psi_n(2n)\beta(2n) \end{vmatrix} \quad (2.8)$$

The determinant (total molecular wavefunction) described aforementioned will lead to  $n$  occupied and a number of unoccupied, component spatial molecular orbitals  $\psi$ . These orbitals from the straightforward Slater determinant are called canonical molecular orbitals. Since each occupied spatial  $\psi$  can be thought of as a region of space which accommodates a pair of electrons, it might be expected that when the shape of these orbitals are displayed, each one would look like a bond or lone pair. However, this is often not the case but it is possible to combine the canonical MOs to get localized MOs which look like the conventional bonds and lone pairs. This is achieved by using the columns (or rows) of the Slater determinant  $\psi$  to create a  $\psi$  with modified columns (or rows). If a column or row of a determinant is multiplied by a constant  $k$  and added to another column/row, the determinant is unchanged. Essentially, a new determinant is formed which also corresponds to the same total wavefunction. The appropriate manipulation of the columns/row of the columns/rows  $\psi$ s can be made to correspond to our ideas of bonds and lone pairs since such localized MOs are often useful.



### 2.4.1 Calculating the Atomic or Molecular Energy

The next step in deriving the HF equations is to express the energy of the molecule or atom in terms of the total wavefunction  $\psi$ ; the energy will then be minimized with respect to each of the component molecular (or atomic) spin orbitals  $\psi_\alpha$  and  $\psi_\beta$ .

From the Schrödinger equation,  $\hat{H}\psi = E\psi$ , we have  $\psi^*\hat{H}\psi = \psi^*E\psi$ . Integrating and rearranging the equation leads to

$$E = \frac{\int \psi^* \hat{H} \psi dv}{\int \psi \psi^* dv} \quad (2.9)$$

The integration variable  $dv$  indicates integration with respect to spatial coordinates ( $x, y, z$  in a Cartesian coordinate system). When orthogonally normal functions are used, the denominator equals unity and  $E = \int \psi^* \hat{H} \psi dv$ . Applying the Dirac notation for integrals gives:

$$E = \langle \psi | \hat{H} | \psi \rangle \quad (2.10)$$

### 2.4.2 The Variational Method

The variational theorem<sup>4</sup> states that if  $\phi$  is any well-behaved function that satisfies the boundary conditions associated with the problem of interest, then the expectation value of  $H$ , calculated using  $\phi$ , will obey the inequality

$$E_{trial} = \frac{\langle \phi | H | \phi \rangle}{\langle \phi | \phi \rangle} \geq E_0 \quad (2.11)$$

where  $E_0$  is the exact ground-state energy. The  $\phi$ 's are termed trial wavefunctions and the expectation value is  $E_{trial}$ . To prove this theorem, one rearranges the inequality to

yield  $I = \langle \phi | H - E_0 | \phi \rangle \geq 0$  (a). Expanding  $\phi$  in terms of exact eigenfunctions of  $H$  i.e. these eigenfunctions satisfy  $H\psi_k = E_k\psi_k$ , one obtains  $\phi = \sum_k c_k \psi_k$ . Substituting this into

(a),

$$I = \sum_{k,l} c_k^* c_l \langle \psi_k | H - E_0 | \psi_l \rangle = \sum_{k,l} c_k^* c_l (E_k - E_0) \delta_{kl} = \sum_k |c_k|^2 (E_k - E_0) \quad (2.12)$$

Each term in the last sum is inherently positive or zero, because the absolute square therein cannot be negative and the energy difference  $(E_k - E_0)$  is also positive or zero, given that  $E_0$  is the ground state energy. The variational theorem is very powerful in that it enables the determination of the trial wavefunction which gives the most accurate energy. The variational theorem, therefore, provides a criterion that needs to be satisfied to achieve optimization and the way it can be implemented can be shown through the simpler albeit limited Hartree theory. Ignoring the Pauli principle, the wavefunction can be written as a product of spherical orbitals, as in

$$\psi = u_1(1)u_2(2)\dots \quad \text{where } u_l = Y_{lm}(\theta_l, \phi_l)g(r_l) \quad (2.13)$$

Considering the effective Hamiltonian associated with each electron, which is the total Hamiltonian averaged over the other electrons, electron  $l$ , for example, will have a kinetic energy and a coulomb attraction to the nucleus and will be expelled by the other electrons. The average repulsion experienced by electron  $l$  due to the charge distribution associated with electron  $j$  is given by the integral of the product of  $1/r_{lj}$  and the charge density of  $j$ . This charge density is simply the electron's charge  $e$ , multiplied by the square of the spatial wavefunction  $u_j$ . In atomic units, this becomes  $\rho(j) = |u_j(j)|^2$  and so the average repulsion induced in electron  $l$  by electron  $j$  is

$v_{1j} = \int |u_j(j)|^2 \frac{1}{r_{1j}} d\tau_j$ . This repulsion is generally written as  $v_{1j} = J_j(1)$  where  $J_j$  is called the coulomb operator. The overall effective one-electron Hamiltonian for the first electron is then

$$\hat{\eta}_1^{eff} = -\frac{\nabla_1^2}{2} - \frac{Z}{r_1} + \sum_{j \neq 1} \int \frac{|u_j(r_j)|^2}{r_{j1}} d\tau_j = -\frac{\nabla_1^2}{2} - \frac{Z}{r_1} + \sum_{j \neq 1} J_j(1) \quad (2.14)$$

Once this Hamiltonian is obtained, the variationally best wavefunction for electron  $1$  can be obtained by solving the one electron Schrödinger equation

$$\hat{\eta}_1^{eff}(r_1)u_1(r_1) = \epsilon_1 u_1(r_1) \quad (2.15)$$

In order to solve this equation, one needs to have the wavefunctions  $u_j$  of all the electrons except electron  $1$ . However, to obtain those functions, equations equivalent to (2.15) have to be solved for the other orbitals  $u_j$ . The widely accepted approach towards solving this problem is by an iterative process i.e. making a guess for all the  $u_j$  and substituting them back into the one-electron Hamiltonians to define Schrödinger equations like (2.15) for each orbital. These equations are then solved and the results are cycled back to redefine the one-electron Hamiltonians. The iteration is continued until it becomes self consistent, which means that the orbitals and energies that are obtained from one step of the iteration to the next are the same to within some tolerance. This procedure is called the self-consistent field (SCF) approximation and its implementation using a wavefunction written as a product of spatial orbitals is called the Hartree theory. Once self-consistency is achieved, the total electronic energy is obtained by calculating the expectation value of the many-electron Hamiltonian as follows:

$$\begin{aligned}
E_{total} &= \langle \psi | \hat{H} | \psi \rangle = \left\langle \psi \left| -\sum_i \frac{\nabla_i^2}{2} - \sum_i \frac{Z}{r_i} + \sum_i \sum_{j<i} \frac{1}{r_{ij}} \right| \psi \right\rangle \\
&= \left\langle \psi \left| \sum_j \left( \frac{\nabla_j^2}{2} - \frac{Z}{r_j} + \sum_{j \neq i} J_j(r_i) \right) + \left[ \sum_i \left[ \sum_{j<i} \frac{1}{r_{ij}} - \sum_{j \neq i} J_j(r_i) \right] \right] \right| \psi \right\rangle \\
&= \sum_i \varepsilon_i + \sum_i \left\{ \sum_{j<i} \left\langle u_i u_j \left| \frac{1}{r_{ij}} \right| u_i u_j \right\rangle - \sum_{j \neq i} \left\langle u_i u_j \left| \frac{1}{r_{ij}} \right| u_i u_j \right\rangle \right\} \tag{2.16}
\end{aligned}$$

When the two sums in (2.16) are combined,

$$E = \sum_i \varepsilon_i - \sum_i \sum_{j>i} J_{ij} \text{ where } J_{ij} \text{ is the same coulomb integral as defined earlier i.e.}$$

$$J_{ij} = \left\langle u_i(1)u_j(2) \left| \frac{1}{r_{12}} \right| u_i(1)u_j(2) \right\rangle \tag{2.17}$$

The total energy is not just the sum of orbital energies; it is necessary to subtract off the sum of coulomb integrals because sum of orbital energies double counts the coulomb interactions.

## 2.5 Hartree-Fock Method

The SCF or Hartree theory is actually an old theory often used to describe the problems in classical mechanics, such as the motions of planets in which the Pauli principle is not relevant. The theory that obeys the Pauli principle while still letting each electron have its own orbital is known as Hartree-Fock theory<sup>5,6</sup>. The assumed form of the wavefunction is a Slater determinant. For a closed shell singlet molecule, in which there are  $\alpha$  and  $\beta$  spins for each spatial orbital, then the Slater determinant can be written as

$$\psi = |u_1(1)\bar{u}_1(1)u_2(1)\bar{u}_2(1)u_3(1)\dots| \tag{2.18}$$

where the  $u_i$ 's are the spatial orbitals analogous to what was used in the Hartree theory

At this point, the Hartree-Fock theory uses the variational theorem described above to optimize the spatial orbitals  $u_i$ 's, with the trial energy evaluated by means of the determinant and the full electronic Hamiltonian. In the Hartree-Fock theory, the equation for a closed shell singlet is

$$\varepsilon_i u_i = \left[ \frac{-\nabla_i^2}{2} - \frac{Z}{r_i} + \sum_{j=1}^N [2J_j(i) - K_j(i)] \right] u_i \quad (2.19)$$

The operator in brackets on the right-hand side of this equation is called the Fock operator. It consists of a kinetic energy operator ( $\frac{-\nabla_i^2}{2}$ ), a nuclear coulomb potential ( $-\frac{Z}{r_i}$ ) and a coulomb operator  $J_j(i)$  similar to that in Hartree theory.  $K_j(i)$  is a new term called the exchange operator. The set of equations, one for each distinct spatial orbital are called the Hartree-Fock equation.

As with the Hartree Fock theory, these equations must be solved by iteration until self-consistency is achieved. Once the self-consistency is obtained, the total electronic energy may be evaluated (closed shell system) using the formula

$$E_{tot} = 2 \sum_{i=1}^N \varepsilon_i - \sum_{i,j=1}^N (2J_{ij} - K_{ij}) \quad (2.20)$$

where  $J$  and  $K$  are the same types of coulomb and exchange integrals as mentioned previously,

$$J_{ij} = \langle u_i | J_j(i) | u_i \rangle = \iint d\tau_1 d\tau_2 \frac{|u_i|^2(1) |u_j|^2(2)}{r_{12}} \quad (2.21)$$

$$K_{ij} = \langle u_i | K_j(i) | u_i \rangle = \iint d\tau_1 d\tau_2 \frac{u_i^*(1) u_j(1) u_j^*(2) u_i(2)}{r_{12}} \quad (2.22)$$

As with the Hartree theory, the  $(2J_{ij} - K_{ij})$  correction term arises because of double counting.

## 2.6 Basis Sets

In quantum chemistry, a basis set is used to create the an atomic or molecular orbital. In fact, a basis set would include a set of mathematical functions which recreates or, –for lack of a more accurate term-, models the spatial configuration of the atomic orbitals and the linear addition of the individual atomic orbitals, with its weighted coefficients, models the molecular orbitals. Usually these functions are atomic orbitals, the traditional form where the functions are centered on the atoms, but there are also functions used which are centered in bonds or lone pairs of atoms.

Given the computational constraint which imposes itself on even the most powerful of supercomputers, quantum chemistry ab initio calculations are typically performed within a finite set of basis functions. In a quantum calculation, the term basis set is applied to a collection of contracted Gaussians representing atomic orbitals, which is optimized to reproduce the desired chemical properties of a system. Larger basis sets can accurately approximate the orbitals by imposing fewer restrictions on the location of electron in space.

In such cases, the wave functions under consideration are all represented as vectors, the components of which correspond to the coefficients in a linear combination of functions used inside the basis set. When one is doing MO calculations, one would commonly used a basis set composed of a finite number of atomic orbitals, which are, in turn, typically centered at the atomic nucleus within the molecule, and then using linear combination of atomic orbitals to model the MO. Ideally, these atomic orbitals should have a “cusp” at

the atomic nucleus of each atom within the molecule, since from a classical physics point of view, the potential energy of the electron when brought infinitesimally close to the nucleus (protons and neutrons), would invariably experience a spike in potential energy. Mathematically, atomic orbitals would be best represented by Slater functions, where a set of functions would decay exponentially with distance from the nuclei, effectively mimicking the cusp at the center of the nucleus. However, anyone who has taken multivariable integral calculus in college would know that the integration of a discontinuous function (of which Slater functions are one of them) is very difficult. A computationally more feasible method would be to further “approximate” the Slater functions by treating them as linear combinations of Gaussian type orbitals (GTO). Because it is easier to calculate overlap and other integrals with Gaussian basis functions, this led to significant computational savings.

In the family of basis sets in use today, a few stand out among the rest.

- 1) Minimal basis sets
- 2) Split valence basis sets
- 3) Polarized basis sets
- 4) Diffuse basis sets

These basis functions themselves are composed of a linear combination of Gaussian functions such basis functions are referred to as contracted Gaussian functions. The component Gaussian functions are primitives. A basis function consisting of just a single Gaussian function would be uncontracted.

In LCAO calculations, it is necessary to choose a set of functions  $b_{\mu}$  to represent the atomic orbitals. In principle, the atomic orbitals can be chosen to be hydrogen-like

wavefunctions, or even Hartree-Fock orbitals, for the atoms. However, neither of these is often used, as their complicated functional form (with lots of nodes near the nucleus for high  $n$  and small  $l$  functions) makes them cumbersome for evaluating integrals.<sup>7,8,9</sup> A more commonly used set of functions is the set of Slater orbitals which have the form

$$b = Ae^{-\xi r} r^n Y_{lm}(\theta, \phi) \quad (2.22)$$

and thus resemble hydrogen orbitals, but without the complicated nodal structure. The parameters  $\xi$  and  $n$  are chosen to make the large  $r$  (valence) part of the orbitals look like atomic Hartree-Fock orbitals.

Slater orbitals have often been used for the Hartree-Fock calculations on linear molecules and they are commonly used in semi-empirical MO calculations, but the complexity of doing multi-center electron repulsion integrals makes their more general use for HF calculations difficult.<sup>5,6</sup>

The most commonly used atomic orbitals are Gaussian orbital, which have the form

$$g = x^a y^b z^c e^{-\alpha r} Y_{lm}(\theta, \phi) \quad (2.23)$$

where  $a$ ,  $b$  and  $c$  are integers and  $\alpha$  is a parameter that is usually fixed. The above equation defines a primitive Gaussian function. Normally, several of these Gaussians are summed to define a more realistic AO basis functions, as in the formula,

$$b_{\mu} = \sum_p k_{\mu p} g_p \quad (2.24)$$

The coefficients  $k_{\mu p}$  in this expansion are chosen to make the basis functions look as much like Slater orbitals as possible. In the simplest version of this basis,  $n$  Gaussians are superimposed with fixed coefficients to form one Slater-type orbital(STO). Such a



basis is denoted STO- $n$ G, and  $n = 3,4,5,\dots$  have been used. The exponent parameters in STO- $n$ G basis sets are chosen so that one Gaussian is sharply peaked near the nucleus, thereby approximating the cusp in the STO. Other exponents are smaller, so as to describe the large  $r$  parts of the wavefunctions.

Split valence basis sets<sup>10,11</sup> use sums of Gaussians such that there is more than one set of basis functions for each subshell. Thus a 3-21G basis set uses three Gaussians, grouped into two Gaussians that are summed with fixed relative coefficients and one that is used directly. These are commonly known as double-zeta-quality basis functions, as they are summed using two Slater functions with different  $\xi$ s. However, the split valence character of basis functions is applied only to the valence subshell and in the 3-21G basis set, the inner shell orbitals are represented using three Gaussians with fixed coefficients. Similarly, a 6-31G basis uses six Gaussians to represent the inner-shell orbitals and a split-valence set of four Gaussians (grouped into subsets of three and one) for the valence orbitals.

Another improvement to STO- $n$ G basis sets involves using polarization functions. These are Gaussians similar to  $g = x^a y^b z^c e^{-ar^2} Y_{lm}(\theta, \phi)$  except that the orbital angular momentum  $l$  is one (or more) larger than is appropriate for the orbital being described. Thus in describing a  $2p$  orbital on an atom, a polarization function would have  $3d$  character. The purpose of a polarization function is to describe distortion of the orbital by the other atomic centers away from what would be expected for a spherically symmetric atomic environment. In Gaussian orbitals, it is typical to denote basis sets that allow for polarization functions using an asterisk (\*) e.g. a split-valence-plus polarization basis might be 6-31G\* (if polarization functions are to be added to atoms other than hydrogen)

or 6-31g\*\*<sup>12,13</sup> (if polarization are to be added to hydrogen as well). A more explicit notation that differentiates between the orbital angular momentum used for H atoms with that for heavier atoms is 6-31G(*kp*, *ld*), where *k* and *l* are integers that indicate the number of *p* (for H) and *d* (for other atoms) polarization functions included in the basis. One other set of orbital basis functions that is commonly used is the set of diffuse functions- Gaussian orbitals that have very small exponent parameters  $\alpha$ , so that they allow the wavefunction to extend far from the nucleus. Diffuse functions are important in describing weakly bound electronic states, such as for anions. A more commonly used notation for diffuse functions is 6-31+G, where the “+” indicates that one diffuse function is included for each valence orbital.

## 2.7 Post-HF calculations: Electron Correlation

Electron correlation<sup>5-8,13</sup> is the phenomenon of the motion of pairs of electrons in atoms and molecules being correlated. The purpose of post-HF calculations is to treat such correlated motion better than the HF method. In the HF method, electron-electron repulsion is handled by having each electron move in a smeared-out average electrostatic field due to all the other electrons and the probability that an electron will have a particular set of spatial coordinates at some moment is independent of the coordinates of the other electrons at that moment. However, this neglects the situation whereby each electron at any moment moves under the influence of the repulsion, not of an average charged cloud, but rather of individual electrons. Because of this enhanced effect whereby each electron has a tendency to stay away from the path of the neighboring electron. The electron-electron repulsion energy is thus consistently over-estimated by a HF calculation and so produces higher electronic energies than the correct ones. Despite

the common notion that HF ignores electron correlation, this method does provide for spin correlation<sup>6,7</sup>, where two electrons of the same spin cannot be in the same place at the same time because their spatial and spin coordinates would then be the same and the Slater determinant representing the total molecular wavefunction would vanish since a determinant is zero if two rows or columns are the same.

Hartree-Fock calculations give an energy that is too high. This is partly because of the over-estimation of the electronic repulsion and partly because of the fact that in any real calculation, the basis set is not perfect. For sensibly developed basis sets, as the basis set size increases, the HF energy gets smaller i.e more negative. The limiting energy that would be given by an infinitely large basis set is called the HF limit.

A distinction is sometimes made between dynamic and non-dynamic (static) correlation energy.<sup>13,14</sup> Dynamic correlation energy is the energy a HF calculation does not account for because it fails to keep the electrons sufficiently far apart; this is the usual correlation energy. Non-dynamic correlation is the energy not accounted for because a calculation uses a single determinant; this problem arises with singlet diradicals e.g. where a closed-shell description of the electronic structure is qualitatively wrong. Dynamic correlation energy can be recovered from post-HF calculations while static correlation energy can be recovered by basing the wavefunction on more than one determinant as in the multi-reference configuration interaction method.

Although HF calculations are satisfactory for many purposes, there are cases where a better treatment of electron correlation is needed. This is particularly true for the calculation of relative energies. The inability of HF calculations to model correctly, hemolytic bond dissociation is commonly illustrated as a case in point.

The fundamental issue here is that the wavefunction is represented as a single determinant and does not permit correct hemolytic dissociation to two radicals because while the H<sub>2</sub> radical is a closed shell species, the products are two radicals, each with an unpaired electron.

### 2.7.1 The Moller-Plesset Approach to Electron Correlation

The Moller-Plesset (MP) treatment of electron correlation is based on perturbation theory, a very general method used in physics to treat complex systems; this particular approach was described by Moller and Plesset in 1934<sup>15</sup> and developed into a practical molecular computational method by Binkley and Pople et al in 1975. The basic idea behind perturbation theory is that if a simple, often idealized system can be suitably tackled then a altered version (perturbed) can be mathematically treated in a none too different manner.

In particular, consider  $H = H_0 + \lambda V$  where  $H_0$  is a zeroth-order Hamiltonian for which solutions to the Schrödinger equation may be obtained easily and  $V$  is a time dependent perturbation that is small compared to  $H_0$ . The eigenfunctions of  $H_0$  are then denoted by  $H_0\phi_n^0 = E_n^0\phi_n^0$

In the perturbation theory approximation, the exact wavefunction  $\psi_n$  may be expanded in powers of  $\lambda$  as

$$\psi_n = \phi_n^0 + \lambda\phi_n^1 + \lambda^2\phi_n^2 + K \tag{2.25}$$

The corresponding energy expansion is

$$E_n = E_n^0 + \lambda E_n^1 + \lambda^2 E_n^2 + K \tag{2.26}$$

Substituting these expressions into the full Schrödinger equation ( $H\psi_n = E_n\psi_n$ ) and equating like powers of  $\lambda$  gives

$$H_0\phi_n^0 = E_n^0\phi_n^0 \quad (\text{zeroth order}) \quad (2.27)$$

$$V\phi_n^0 + H_0\phi_n^1 = E_n^1\phi_n^0 + E_n^0\phi_n^1 \quad (\text{first order}) \quad (2.28)$$

$$V\phi_n^{j-1} + H_0\phi_n^j = \sum_{k=0}^j E_n^k\phi_n^{j-k} \quad (\text{jth order, } j \geq 1) \quad (2.29)$$

The zeroth-order equation is satisfied by assumption which is simply the original 'zero-order' approximation. The other equations permit us to obtain the corrections to this approximation. To solve the first order equation,  $\phi_n^1$  is expanded in terms of the complete set of zeroth-order states,  $\phi_n^1 = \sum_{k \neq n} C_{nk}^1 \phi_k^0$  where  $C_{nk}$  is a coefficient.

$$\text{Subsequently, } E_n^1 = \langle \phi_n^0 | V | \phi_n^0 \rangle \text{ and } C_{nk}^1 = \frac{\langle \phi_k^0 | V | \phi_n^0 \rangle}{E_n^0 - E_k^0} (k \neq n) \quad (2.30)$$

It has been shown that expressions for higher orders can be developed in a similar manner. For example,

$$E_n^2 = \sum_{k \neq n} \frac{\langle \phi_n^0 | V | \phi_k^0 \rangle \langle \phi_k^0 | V | \phi_n^0 \rangle}{E_n^0 - E_k^0} \quad (2.31)$$

“MP0” would use the electronic energy obtained by simply summing the HF one-electron energies. This ignores inter-electronic repulsion except for refusing to allow for more than two electrons in the same spatial MO. “MP1” corresponds to MP0 corrected with the Coulomb and exchange integrals  $J$  and  $K$  i.e. MP1 is plainly the HF energy. MP2 is the first MP level to go beyond the HF treatment and it is the HF energy plus a correction term (a perturbation adjustment) that represents a lowering of the energy brought by allowing the electrons to avoid one another better than in the HF treatment.

$$E_{MP2} = E_{HF}^{total} + E^{(2)} \quad (2.32)$$

The HF term includes inter-nuclear repulsions and the perturbation correction  $E^{(2)}$  is a purely electronic term which is a sum of terms which models the promotion of pairs of electrons (double excitations) from occupied to unoccupied MOs. Formulas for the MP energy corrections  $E^{(3)}$ ,  $E^{(4)}$ , and so on have been derived.<sup>16</sup> The MP  $E^{(4)}$  (ie. MP4) in particular, involves summation over single, double, triple and quadruple substitutions.

In addition to their computational efficiency compared to other methods like CI, MP calculations truncated at any order have been shown to be size consistent. However, MP calculations are not variational and can produce energy below the true energy. Another limitation of MP calculations is that although they work well near the equilibrium geometry, they do not work well at geometries far from equilibrium. For example, calculations using double zeta basis sets on H<sub>2</sub>O showed that at the equilibrium geometry, an MP2 calculation yields 94% of the basis set correlation energy but at a geometry with the O-H bonds at twice their equilibrium lengths, an MP2 calculation yields only 83% of the basis set correlation energy.<sup>17,18</sup> A third limitation is that MP calculations are not generally applicable to excited electronic states<sup>19</sup>. Because of its computational efficiency and good results for molecular properties, the MP2 method is one of the two most commonly used methods for including correlation effects on molecular ground state equilibrium properties, the other being the widely available density functional method.

## 2.8 Density Functional Theory Methods

Density functional theory (DFT)<sup>5,6,8</sup> is not based on the wavefunction but rather on the electron probability density function or electron density function which is

commonly called simply the charge density or electron density, designated by  $\rho(x, y, z)$ . The electron density function is the basis of not only the DFT but also of a whole suite of methods of regarding and studying atoms and molecules<sup>1</sup> and unlike the wavefunction, is measurable e.g. by X-ray diffraction. Apart from being experimentally observable and being readily grasped intuitively, the electron density has another property particularly suitable for any method with claims to being an improvement on, or at least a valuable alternative to wavefunction methods; it is a function of position only, that is of just three variables ( $x, y, z$ ). On the other hand, the wavefunction of an  $n$ -electron molecule is a function of  $4n$  variables, three spatial coordinates and one spin coordinate, for each electron. In contrast, no matter how large the molecule may be, the electron density remains a function of only three variables and density functional theory seeks to calculate all the properties of atoms and molecules from the electron density.

### 2.8.1 Current DFT methods: The Kohn-Sham approach

Nowadays, DFT calculations on molecules are based on the Kohn-Sham approach, the stage for which was set by two theorems published by Hohenberg and Kohn in 1964. The first Hohenberg-Kohn theorem says that all the properties of a molecule in a ground electronic state are determined by the ground state electron density function  $\rho_0(x, y, z)$ . In other words, given  $\rho_0(x, y, z)$ , we can in principle calculate any ground state property, e.g. the energy,  $E_0$ ; we could represent this as

$$\rho_0(x, y, z) \rightarrow E_0 \quad (2.32)$$

where it is understood from the above that  $E_0$  is a functional of  $\rho_0(x, y, z)$ .

The theorem is an existence theorem because the existence of the functional offers little clue on how to locate it and the omission is the main problem with DFT. The significance

of this theorem is that it assures us that there is a way to calculate molecular properties from the electron density and any approximate functionals will give at least approximate answers.

The second Hohenberg-Kohn theorem is the DFT analogue of the wavefunction variation theorem where it says that any trial electron density function will give an energy higher than (or equal to, if it were exactly the true electron density function) the true ground state energy. The exact functional is unknown, so actual DFT calculations use approximate functionals and are thus not variational.

### **2.8.2 The Kohn-Sham Energy and the KS equations**

The two basic ideas behind the KS approach to DFT are:

- (i) To express the molecular energy as a sum of terms, only one of which, a relatively small term, involves the unknown functional.
- (ii) To use an initial guess of electron density  $\rho$  in the KS equations (analogous equations) to calculate an initial guess of the KS orbitals; this initial guess is then used to refine these orbitals, in a manner similar to that used in the HF-SCF method. The final KS orbitals are used to calculate an electron density which in turn is used to calculate the energy.

In 1965, Kohn and Sham devised a practical method for finding  $\rho_0$  and finding  $E_0$  from  $\rho_0$ . Their method is capable, in principle, of yielding exact results, but because the equations of the KS method contain an unknown functional that must be approximated, the KS formulation of DFT yields approximate results. They considered a fictitious non-interacting reference system, defined as one in which the ground state electron density  $\rho_0$  is exactly the same as that in the real ground state system i.e.  $\rho_r = \rho_0$ .



The ground state electronic energy of a real molecule is the sum of the electron kinetic energies, the nucleus-electron attraction potential energies and the electron-electron repulsion potential energies and each is a functional of the ground state electron density:

$$E_0 = \langle T[\rho_0] \rangle + \langle V_{Ne}[\rho_0] \rangle + \langle V_{ee}[\rho_0] \rangle \quad (2.33)$$

$$\text{But } \overline{V_{Ne}} = \left\langle \langle \psi_0 \left| \sum_{i=1}^n v(r_i) \right| \psi_0 \rangle \right\rangle = \int \rho_0(r) v(r) dr \quad (2.34)$$

where  $v(r_i) = -\sum_{\alpha} Z_{\alpha} / r_{i\alpha}$  (in atomic units) and it defines the nuclear attraction potential energy for an electron located at point  $r$ . Thus  $V_{Ne}[\rho_0]$  is known but the functionals  $T[\rho_0]$  and  $V_{ee}[\rho_0]$  are unknown and

$$E_0 = E_v[\rho_0] = \int \rho_0(r) v(r) dr + T[\rho_0] + V_{ee}[\rho_0] = \int \rho_0(r) v(r) dr + F[\rho_0] \quad (2.35)$$

where the functional  $F[\rho_0]$  is independent of the external potential. This, however, does not provide a practical way to calculate  $E_0$  from  $\rho_0$  because the functional  $F[\rho_0]$  is unknown.

However, Kohn and Sham defined the quantity

$$\Delta \langle T[\rho_0] \rangle \equiv \langle T[\rho_0] \rangle - \langle T_r[\rho_0] \rangle \quad (2.36)$$

Where  $\Delta \langle T[\rho_0] \rangle$  is the deviation of the real kinetic energy from that of the reference system,  $\Delta \langle V_{ee}[\rho_0] \rangle$  is the deviation the real electron-electron repulsion energy from a classical charge cloud coulomb repulsion energy. The classical electrostatic repulsion energy is the summation of the repulsion energies for pairs of infinitesimal volume elements  $\rho(r_1)dr_1$  and  $\rho(r_2)dr_2$  separated by a distance  $r_{12}$ , multiplied by half to avoid

double counting the repulsion between similar entities. The sum of infinitesimals is an integral and so

$$\Delta \langle V_{ee} [\rho_0] \rangle = \langle V_{ee} [\rho_0] \rangle - \frac{1}{2} \iint \frac{\rho_0(r_1)\rho_0(r_2)}{r_{12}} dr_1 dr_2 \quad (2.37)$$

Thus we can write

$$E_0 = \int \rho_0(r)v(r)dr + \langle T_r [\rho_0] \rangle + \frac{1}{2} \iint \frac{\rho_0(r_1)\rho_0(r_2)}{r_{12}} dr_1 dr_2 + \Delta \langle T [\rho_0] \rangle + \Delta \langle V_{ee} [\rho_0] \rangle \quad (2.38)$$

The sum of the kinetic energy deviation from the reference system and the electron-electron repulsion deviation from the classical system is called the exchange-correlation energy functional or the exchange-correlation energy,  $E_{XC}$ :

$$E_{XC} [\rho_0] \equiv \Delta \langle T [\rho_0] \rangle + \Delta \langle V_{ee} [\rho_0] \rangle \quad (2.39)$$

The  $\Delta \langle T \rangle$  term represents the kinetic correlation energy of the electrons and the  $\Delta \langle V_{ee} \rangle$  term the potential correlation energy and the exchange energy. Further simplifying, we have :

$$E_0 = \int \rho_0(r)v(r)dr + \langle T_r [\rho_0] \rangle + \frac{1}{2} \iint \frac{\rho_0(r_1)\rho_0(r_2)}{r_{12}} dr_1 dr_2 + E_{XC} [\rho_0] \quad (2.40)$$

### 2.8.3 The exchange-correlation energy functional: Local Density Approximation

The simplest approximation to  $E_{XC} [\rho(r)]$  is within the framework of the local density approximation (LDA); this applies to a uniform (homogenous) electron gas. The term local was probably used because for any point, only the electron density at that point are considered, in contrast to so-called non-local methods in which for each point a gradient, which samples the region a bit beyond that point is taken into account. For the LDA, the exchange-correlation energy functional  $E_{XC}^{LDA}$  and its derivative  $v_{XC}^{LDA}$  can be

accurately calculated. The  $X\alpha$  method of Slater is a special case of the LDA, developed before the KS approach in which the correlation part of the exchange-correlation functional is neglected and the exchange functional used is

$$E_{XC}^{LDA} = E_X^{X\alpha} = -\frac{9}{8} \left(\frac{3}{\pi}\right) \alpha \int [\rho(r)]^{4/3} dr$$

The parameter  $\alpha$  is empirical; values of 1 to 2/3 give reasonable results for atoms.

#### 2.8.4 The Local Spin Density Approximation (LSDA)

Better results than LDA can be obtained by an elaboration of the LDA in which electrons of  $\alpha$  and  $\beta$  spin in the uniform electron gas are assigned different spatial KS orbitals  $\psi_\alpha^{KS}$  and  $\psi_\beta^{KS}$ , from which different electron density functions  $\rho^\alpha$  and  $\rho^\beta$  follow. This unrestricted LDA method is called the local spin density approximation, LSDA and has the advantages that it can handle systems with one or more unpaired electrons, like radicals and systems in which electrons are becoming unpaired, such as molecules far from their equilibrium geometries. For species in which all the electrons are securely paired, the LSDA is equivalent to the LDA.

#### 2.8.5 Hybrid functionals

In actual practice, self-consistent Kohn-Sham DFT calculations are performed in an iterative manner that is analogous to an SCF computation. This similarity to Hartree-Fock theory was also pointed out by Kohn and Sham. Hartree-Fock theory also includes an exchange term as part of its formulation and Becke has formulated

functionals which include a mixing of mixture of Hartree-Fock and DFT exchange along with DFT correlation, conceptually defining  $E^{XC}$  as:

$$E_{hybrid}^{XC} = c_{HF} E_{HF}^X + c_{DFT} E_{DFT}^{XC} \quad (2.41)$$

where the  $c$ 's are constant. For example, a Becke-style three parameter functional may be defined via the following expression:

$$E_{B3LYP}^{XC} = E_{LDA}^X + c_0 (E_{HF}^X - E_{LDA}^X + c_X \Delta E_{B88}^X + E_{VWN3}^C + c_c (E_{LYP}^C - E_{VWN3}^C)) \quad (3.42)$$

Here the parameter  $c_0$  allows any admixture of HF and LDA local exchange to be used.

In addition, Becke's gradient correction to LDA exchange is also included via a scaling parameter  $c_X$ . Similarly, the VWN2 local functional is used and it may be optionally corrected by the LYP correction via the parameter  $c_c$ . In the B3LYP functional, the parameter values are those specified by Becke, which he determined by fitting to the atomization energies and first row atomic energies in the G1 molecule set:  $c_0 = 0.20$ ,  $c_X = 0.72$  and  $c_c = 0.81$

## 2.8.6 IMOMM, IMOMO, and ONIOM Methods

To study macromolecular processes such as large organo-metallic reactions in the Titaddolate catalysed reactions. It is necessary to use a chemical model that is capable of describing the forming and breaking of chemical bonds and is also suitable for capturing the complexity of the system. A fully quantum mechanical treatment of the entire macromolecular system, in principle, satisfies these criteria and quantum mechanical algorithm designed to scale linearly with system size have been developed and applied to protein system sin energy calculations. Though this approach has many attractive features, it is however, very expensive and has only been limited to application

to biological problems. Luckily in most enzymatic reactions, it not necessary to treat the electronic structure of the entire system quantum mechanically. ONIOM or IMOMM comprise of 2 methods, QM is used to solve the most essential parts of the system, or the reaction core of the system, and MM is used for the non-essential part. This method yields a good choice for investigating huge system. Nowadays, this methodology is the most commonly used method to handle over 1000-atom systems. The main advantage of the QM/MM method is its easy implementation in the computational codes while giving good chemical qualitative results. Its main disadvantage especially in enzymatic systems is its inability to go beyond qualitative results and thus to obtain reliable quantitative numbers.

Using quantum mechanics on larger systems or systems with transition metal atoms with many shells and valence electrons using high level methods is very demanding in terms of computer time and is therefore normally out of the question. What seems to be the best alternative at the time being, is to combine high level approximations on the interesting part of our system (the active part) with some appropriate low level approximation on the rest of the system (the non-active part). Methods trying to combine MO (molecular orbital) approximations describing the active part of the system (ab initio, density functional to semi-empirical) with either some lower level MO methods or MM (molecular mechanics) describing the non-active parts, are discussed. These are:

1. **IMOMM:** Integrated MO + MM (molecular mechanics). With this method one treats the active part of one's system with MO methods and the non-active part with MM.

2. **IMOMO:** Integrated MO + MO. With this method one treats the active part of one's system with sophisticated MO method, whereas the non-active part is treated with some lower level MO method.

3. **ONIOM:** N-layered Integrated MO and MM. The ONIOM method divides the system into n-layers like an onion. What is used in this thesis is the ONIOM3 method that divides the chemical system in question into 3 parts. With ONIOM3 we can use high level MO methods to describe the active part, some lower level MO method to the semi-active part and MM to the non-active part of the system. An example could be B3LYP/LANL2DZ on the active part, B3LYP/6-31G\* on the semi-active part and MM on the non-active part of the system.

## 2.9 Solvent Effects

The molecular properties of most calculations are appropriate only for gas-phase molecules at low pressure. However, most of chemistry and biochemistry occurs in solution, and the solvent can have a major effect on the position of chemical equilibrium and on reaction rates.<sup>21</sup> While gas-phase predictions are appropriate for many purposes, they are inadequate for describing the characteristics of many molecules in solution. Indeed the properties of molecules and transition states can differ considerably between the gas phase and solution. For example, electrostatic effects are often much less important for species placed in a solvent with high dielectric constant than they are in the gas phase. The rigorous way to deal with solvent effects on molecular properties is to carry out quantum-mechanical calculations on a system consisting of a solute molecule surrounded by many solvent molecules; one repeats the calculations for various orientations of the solvent molecules and takes a suitable average over orientations to

find average properties at a particular temperature and pressure. Such a calculation is however usually impractical because the primary problem with explicit solvent calculations is the significant amount of computer resources required. The most common way to calculate solvent effects is to use a continuum solvent model. In this model, the molecular structure of the solvent is ignored and the solvent is modeled as a continuous dielectric of infinite extent that surrounds a cavity containing the solute molecule. The continuous dielectric is characterized by its dielectric constant  $\epsilon_r$ , whose value is the experimental dielectric constant of the solvent at a particular temperature and pressure of the solution. The solute molecule can be treated classically as a collection of charges that interacts with the dielectric or it can be treated quantum mechanically. In a quantum-mechanical treatment, the interaction between a solute molecule M and the surrounding dielectric continuum is modeled by a term  $\hat{V}_{\text{int}}$  that is added to the molecular electronic (fixed-nuclei) Hamiltonian  $\hat{H}_M^{(0)}$  where  $\hat{H}_M^{(0)}$  is for M in the vacuum.

In the usual quantum-mechanical implementation of the continuum solvation model, the electronic wave function and electronic probability density of the solute molecule M are allowed to change on going from the gas phase to the solution phase, so as to achieve self-consistency between the M charge distribution and the solvent's reaction field. Any treatment in which such self-consistency is achieved is called a self-consistent reaction field (SCRF) model.<sup>22-25</sup> Many versions of SCRF model exist. These differ in how they choose the size and shape of the cavity that contains the solute molecule M and in how they calculate  $\hat{V}_{\text{int}}$ .

## 2.9.1 The Onsager SCRF Method

In Onsager reaction field theory, the molecular cavity is a sphere of radius  $a$  and the interaction between the molecular charge distribution and the reaction field is calculated by approximating the molecular charge distribution as an electric dipole located at the cavity center with electric dipole moment,  $\mu$ . In 1936, Onsager<sup>29</sup> showed that the electric field in the cavity (the reaction field) produced by the polarization of the solvent by  $\mu$  is (in atomic units)

$$E_R = \frac{2(\epsilon_r - 1)}{(2\epsilon_r + 1)a^3} \mu. \quad (2.43)$$

The potential energy of electrostatic interaction between  $\mu$  and the reaction field  $E_R$  is

$$\hat{V}_{\text{int}} = -\hat{\mu} \cdot E_R \quad (2.44)$$

$$\text{where } \hat{\mu} = -\sum_i r_i + \sum_a Z_a R_a$$

In an SCRF implementation of Onsager's theory, one starts by using a method such as HF, DFT, MP2 or whatever, to calculate an electron probability density,  $\rho^{(0)}(r)$  for the isolated molecule. The electric dipole moment is then evaluated from

$$\mu^{(0)} = -\int \rho^{(0)}(r) dr + \sum Z_\alpha R_\alpha \quad (2.45)$$

Then  $\mu^{(0)}$  is used in (2.43) to give an initial estimate  $E_R^{(0)}$  of the reaction field. From  $E_R^{(0)}$ , one calculates an initial estimate of the operator  $\hat{V}_{\text{int}}$  as  $\hat{V}_{\text{int}}^{(0)} = -\hat{\mu} \cdot E_R^{(0)}$ . Using  $\hat{V}_{\text{int}}^{(0)}$ , one solves the equations of the quantum method being used and obtains an improved electron probability density  $\rho^{(1)}$ . Subsequently, one new value of  $\mu^{(1)}$  is calculated and an improved estimate  $E_R^{(1)}$  for the reaction field is obtained. Iterations are continued until



there is no further change in  $\rho, \mu$  and  $E_R$ . An inherent limitation of the Onsager approach however arises for systems having a zero dipole moment where calculations performed on such models will not exhibit solvent effects and will instead give results similar to the gas phase.

## 2.9.2 The Polarizable Continuum Model method

Accurate ab-initio calculations of solvent effects require the molecular shape to be more realistic than spherical or ellipsoidal shapes. In the polarizable-continuum model (PCM)<sup>30</sup> of Miertus, Scrocco and Tomasi, each atomic nucleus in the solute molecule M is surrounded by a sphere of radius 1.2 times the van der Waals radius of that atom. The cavity region is taken as the volume occupied by these overlapping atomic spheres. The isodensity polarizable continuum model (IPCM)<sup>31</sup> is a modification of the PCM that defines the surface of the molecular cavity as a contour surface of constant electron probability density of the solute molecule M. An isodensity surface is a very natural, intuitive shape for the cavity since it corresponds to the reactive shape of the molecule to as great a degree as is possible (rather than being a simpler, pre-defined shape such as a sphere or a set of overlapping spheres). However, a cavity defined as an isosurface and the electron density are necessarily coupled. The Self-consistent Isodensity Polarized Continuum Model (SCI-PCM) was designed to take this effect fully into account. It includes the effect of solvation in the solution of the SCF problem. This procedure solves for the electron density which minimizes the energy, including the solvation energy-which itself depends on the cavity which depends on the electron density. In other words, the effects of solvation are folded into the iterative SCF computation rather than

comprising an extra step afterwards. SCI-PCM thus accounts for full coupling between the cavity and the electron density and includes coupling terms that IPCM neglects.

## References

---

1. J. C. Slater, *Phys. Rev.*, **1930**, *35*, 210.
2. P. A. M. Dirac, *Proc. Roy. Soc.* **1928**, *A117*, 610; *A118*, 351.
3. D. R. Hartree, *Proc. Cambridge Phil. Soc.* **1928**, *24*, 111.
4. C. Eckhart, *Phys. Rev.* **1930**, *36*, 878.
5. I. N. Levine, **2000**, *Quantum Chemistry*, Prentice Hall
6. M. A. Ratner , G. C. Schatz , **2001**, *Quantum Mechanics in Chemistry*, Prentice Hall
7. L. Pauling, E. B. Wilson, **1963**, *Introduction to Quantum Mechanics (With applications to Chemistry)*, Dover Books
8. J. P. Lowe., *Quantum Chemistry*, **1993**, Academic Press
9. F. L. Pilar, *Elementary Quantum Chemistry*, **2001**, Dover Publications
10. S. Wilson, *Adv. Chem. Phys.* , **1987**, *67*, 439.
11. E. R. Davidson, Feller. D, *Chem. Rev.*, **1986**, *86*, 681.
12. G. A. Petersson, A. Bennett, T. G. Tensfeldt, M. A. Al-Laham, W. A. Shirley and J. Mantzaris, *J. Chem. Phys.*, **1988**, *89*, 2193.
13. G. A. Petersson and M. A. Al-Laham, *J. Chem. Phys.*, **1991**, *94*, 6081.
14. D. Feller, E. R. Davidson, *Reviews in Computational Chemistry*, Vol. 1, 1956, 846-848
15. R. J. Bartlett, *Ann. Rev. Phys. Chem.*, **1981**, *32*, 359.
16. J. A. Pople, *Int. J. Quantum Chem.*, **1978**, *14*, 91.

17. W. D. Laidig et al., *Chem. Phys. Lett.*, **1985**, *113*, 151.
18. N. C. Handy et al., *Theo. Chim. Acta*, **1985**, *68*, 87.
19. V. N. Glushkov, A. Ya. Tsaune, *Chem. Phys. Lett.*, **1996**, *262*, 59.
20. S. J. A. van Gisbergen et al., *Phys. Rev. Lett.*, **1999**, *83*, 694.
21. F. Maseras, K. Morokuma, *J. Comp. Chem.*, **1995**, *16*, 1170
22. Humbel, S., Sieber, S., and Morokuma, K., *J. Chem. Phys.*, **1996**, *105*, 1959-1967
23. Svensson, M., Humbel, S., Froese, R., Matsubara, T., Sieber, S., and Morokuma, K., *J. Phys. Chem.*, **1996**, *100*
24. C. Reichardt, *Solvents and Solvent Effects in Organic Chemistry*, **1998**, VCH
25. K. B. Wiberg, T. A. Keith, M. J. Frisch, M. Murcko, *J. Phys. Chem.*, **1995**, *99*, 9072.
26. M. W. Wong, M. J. Frisch, K. B. Wiberg, *J. Am. Chem. Soc.*, **1991**, *113*, 4776.
27. M. W. Wong, M. J. Frisch, K. B. Wiberg, *J. Chem. Phys.*, **1991**, *95*, 8991.
28. M. W. Wong, M. J. Frisch, K. B. Wiberg, *J. Am. Chem. Soc.*, **1992**, *114*, 1645.
29. L. Onsager, *J. Am. Chem. Soc.*, **1938**, *58*, 1486.
30. S. Miertus, J. Tomasi, *Chem. Phys.*, **1982**, *65*, 239.
31. Foresman, J. B.; Keith, T. A.; Wiberg, K. B.; Snoonian, J.; Frisch, M. J. *J. Phys. Chem.* **1996**, *100*, 16098.
32. Metropolis, N., Rosenbluth, A.W., Rosenbluth, M. N., Teller, A.H. and Teller, E., *J. Chem. Phys.* , **1958**, *21*, 1087.
33. Kirkpatrick, S., Gerlatt, C. D. Jr., and Vecchi, M.P., *Science*, **1983**, *220*, 671.
34. Pincus, M., *Oper. Res.* , **1970**, *18*, 1225.

# Chapter 3

## Titanium Taddolate Catalyzed Asymmetric Alkylation Reactions

---

This chapter describes the deployment of titanium taddolates as a unique class of catalysts driving the highly enantioselective nucleophilic addition of alkyl titanium derivatives to benzaldehydes. It presents the methodology employed and the theoretical calculations done to calculate the Gibbs free activation energy for the alkylation reaction of benzaldehydes to secondary alcohols. We seek to derive the reaction mechanism behind this highly enantioselective nucleophilic alkylation reaction using TADDOL-derived titanates via DFT methods.

### **3.1 Introduction: Development of chiral catalyst (TiTaddolates) for highly enantioselective alkylation reactions of benzaldehydes**

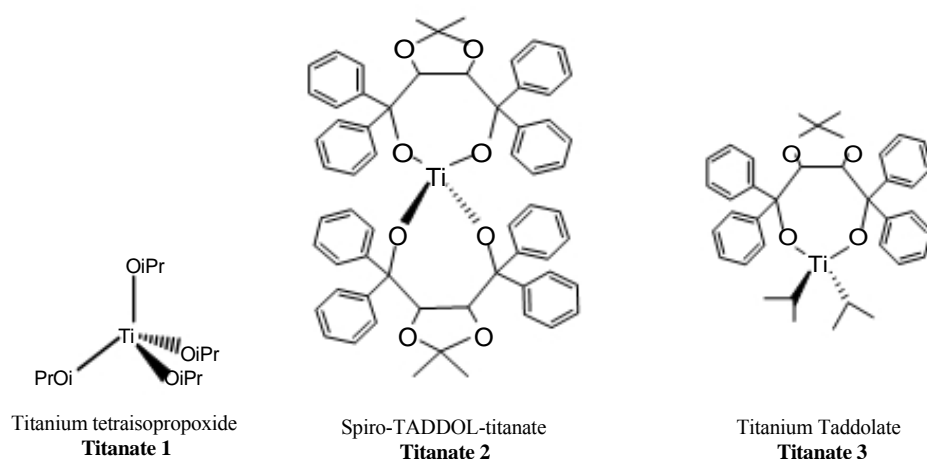
The titanates derived from  $\alpha, \alpha, \alpha', \alpha'$ -tetraaryl-1,3-dioxolane-4,5-dimethanols (commonly known as TADDOLs) act as catalysts for the enantioselective additions of dialkylzinc compounds to aldehydes. There has been much effort to achieve enantioselective C—C bond formation between a carbonyl compound—usually an aromatic aldehyde like benzaldehyde—and an organometallic alkyl or aryl species. Alkylation of benzaldehydes via TiTaddolates has been studied extensively by D. Seebach and A.K. Beck et al.<sup>1</sup> whereas arylation of benzaldehydes has also been similarly

investigated by K. Narasaka et al.<sup>2</sup> Similar reactions involving aldehydes with Ti-based Lewis acid catalysts have also been investigated by K. Maruoka et al.<sup>3</sup> The most successful examples using catalytic amounts of a chiral catalyst were performed with either dialkyl zinc reagents or alkylated Ti derivatives in combination with chiral amino-alcohols<sup>4</sup> or Lewis acid systems<sup>5</sup>, and enantioselectivities better than 99:1 were quite often found.

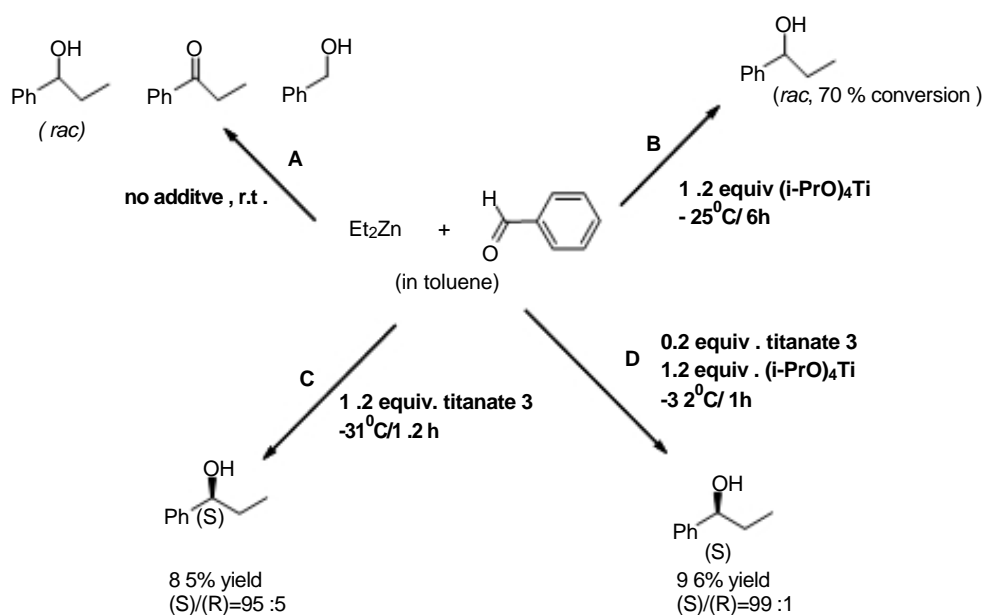
### 3.2 Alkylation Nucleophilic Addition of Dialkyl Zinc to Aldehydes catalyzed by TiTaddolates—the R<sub>2</sub>Zn Approach

Among these reactions, organometallic chemists found that Ti-catalyzed ones, of which TiTaddolates are prime candidates, play a prominent role and they have observed high enantioselectivities for both aromatic and aliphatic aldehydes. This thesis focuses on the industrially important reactions of the alkylation of benzaldehyde to yield aromatic secondary alcohols which are important industrial chemicals. Using chiral TiTaddolate which contains diol ligands and which can be prepared from tartrate acetals and aryl *Gignard* reagents, favorable enantioselectivities of up to 99% e.e. (e.r. =99.5:0.5) were achieved.<sup>6</sup>

Experimental results from previous studies on the TADDOL-titanate catalyzed nucleophilic addition of Et<sub>2</sub>Zn to benzaldehydes are summarized in Scheme 3.2-1 on the following page; various types of TiTaddolates catalysts used are also summarized in Fig. 3.2-1. Specifically, **titanate 1** refers to titanium tetra-isopropoxide, which is added in excess in all alkylation reactions as a co-catalyst; **titanate 2** refers to the dimer complex of titanium taddolate, with 2 taddolate bidentate ligands co-ordinated to a central titanium atom (spiro-TADDOL-titanate) and **titanate 3** refers to the main catalyst used in this project, namely, titanium taddolate.



**Fig. 3.2-1: Various titanates derivatives produced in Seebach's research group**



**Scheme 3.2-1: Reactions of Et<sub>2</sub>Zn with PhCHO under various conditions**

As shown in Path A in Scheme 3.2-1, Et<sub>2</sub>Zn does not react with benzaldehydes to any appreciable extent in toluene at a temperature of around -30°C, whereas at room temperature, an effluent mixture of benzyl alcohol, 1-phenylpropan-1-ol and propiophenone are produced.<sup>7</sup> This strongly indicates that the reaction of Et<sub>2</sub>Zn without the aid of a chiral catalyst like TiTaddolate is unlikely to yield either the desirable product or the favorable enantioselectivity expected of the highly enantioselective alkylation reaction

of benzaldehyde to a secondary alcohol. Path B, in contrast, shows the nucleophilic transfer of an alkyl group to benzaldehyde from  $\text{Et}_2\text{Zn}$  occurring at around  $-25^\circ\text{C}$  in the presence of 1.2 equiv. of  $\text{Ti}(\text{OiPr})_4$ . There is a distinct difference between Path A and Path B in the fact that  $\text{Ti}(\text{OiPr})_4$  catalyses the reaction between  $\text{ZnEt}_2$  and  $\text{PhCHO}$  even at a low temperature of  $-30^\circ\text{C}$  and produces a reasonable chemical conversion rate of a racemic phenyl-alcohol product. Indeed, one can easily deduce that  $\text{Ti}(\text{OiPr})_4$  is a non-enantioselective catalyst for the alkylation of benzaldehydes from diethyl zinc. However, we think that  $\text{Ti}(\text{OiPr})_4$  is not so much an enantioselective catalyst as a co-catalyst which enhances the catalytic activity of the main catalyst, namely the TiTaddolate molecule. This hypothesis will be further investigated in the latter part of this chapter under the bimetallic titanium Taddolate- $\text{Ti}(\text{OiPr})_4$  complex hypothesis. There are several other salient features noted in above schematic path, namely:

- i. There is a significant conversion (70% conversion rate) of benzaldehydes into the desired product (secondary alcohol) albeit being a racemic mixture.  $\text{Ti}(\text{OiPr})_4$  seems to catalyze an otherwise non-reactive, non-chemoselective nucleophilic addition of  $\text{Et}_2\text{Zn}$  to benzaldehydes.
- ii.  $\text{Ti}(\text{OiPr})_4$  is not an enantioselective catalyst since there is no distinct e.e. observed, i.e. the alcohol product is a racemic mixture. In other words, the  $\text{Ti}(\text{OiPr})_4$  catalyzes the nucleophilic addition reaction but does not act as an enantioselective asymmetric catalyst.
- iii. Path C shows a reaction which produces a 95:5 mixture, with the (*S*)-enantiomers predominant under  $-30^\circ\text{C}$ , and Path D is a significantly improved pathway to the increased enantioselectivity, from 90% e.e., 85% product yield, to 99% e.e., 96%

yield, an improvement which is attained by applying 0.2 equiv. of **titanate 3** and 1.2 equiv. of  $\text{Ti}(\text{OiPr})_4$ . Surprisingly, by reducing the amount of the chiral titanate by a factor of six and adding a six fold excess of the achiral  $\text{Ti}(\text{OiPr})_4$ , the chemical system presents the best chemoselective and enantioselective yield.

Seebach proposed that the  $\text{Ti}(\text{OiPr})_4$  in Path B and TiTaddolate in Path C acts as:

(a) an acceptor of alkyl radical group from the  $\text{Zn}(\text{Et})_2$  molecule and then acts as the source of alkyl groups for the alkylation of benzaldehydes; (b) a removing agent for the removal of the product of the alkylation (alkoxide product) away from the TiTaddolate. We shall investigate these proposals systematically in the following sections.

### **3.3 Alkylation Nucleophilic Addition of Me-Ti(OiPr)<sub>3</sub> to Aldehydes catalyzed by TiTaddolates—The Zinc-Free Approach**

Although the alkylation reactions of benzaldehydes by dialkyl zinc catalyzed by TiTaddolates possess impressive chemical yields and enantio-selectivities, there remains an inherent disadvantage in all these dialkyl zinc additions: only one of the two alkyl groups from the dialkyl zinc is transferred to the aldehyde. It is not chemically the most cost-effective way to carry out this reaction because for every dialkyl zinc molecule used; one of the 2 alkyl ligands is inadvertently “wasted”. More importantly, diethyl zinc is a highly toxic substance; it is, in fact, more toxic and harder to remove than TiTaddolate or  $\text{Ti}(\text{OiPr})_4$  from the reaction mixture and it would invariably be a step towards greener chemistry if one could remove zinc-containing compounds from the reaction mixture as early as possible. Several mechanistic investigations have been carried out previously and mechanisms have been postulated. In this thesis, we attempt to provide quantitative explanation on 2 salient features observed, namely, 1) the reason why  $\text{Ti}(\text{OiPr})_4$  is a



supplemental but highly essential co-catalyst which acts as a removing agent to facilitate the production of the desired *S*-enantiomer as well as 2) the reason why Et<sub>2</sub>Zn may not be as important an alkylating agent as once thought (and which has been indicated by P.J. Walsh<sup>8</sup> and D. Seebach) but rather serves as a “middleman” entity which transfers the alkyl group -to be added to benzaldehyde- to the achiral catalyst Titaddolate or Ti(OiPr)<sub>4</sub> to form alkylated Titaddolate or R-Ti(OiPr)<sub>3</sub>. This hypothesis has been supported experimentally by Walsh et al. to be the rate determining factor in the nucleophilic addition reactions<sup>7</sup>. In some examples where dialkyl zinc additions give only moderate selectivities, higher enantiomeric ratios (e.r.) values can be achieved using the “zinc-free” method. For example products *S* and *R* are formed with a 98.5:1.5 selectivity using the reaction sequence which does not involve diethyl zinc, but an e.r. of only 92:8 is found in the corresponding dialkyl zinc reaction. Evidently, the alkyl, or by extrapolation, even the aryl transfer and for aliphatic aldehydes, this “zinc-free” reaction could well be the superior reaction pathway. Last but not least, -without sounding over repetitive-, we wish to emphasize the fact that here the alkyl transfer is also twice as efficient as in any dialkyl zinc addition since only one equiv. of RM (R= alkyl radical attached to M) is needed, i.e. RM vs. RMR. Not only is it more environmentally friendlier to use “zinc-free” nucleophilic addition reactions but also chemically more efficient. Most importantly, it allows both organo-metallic and computational chemists to reduce the ambiguity of the mechanistic interpretation behind this alkylation process.

### 3.3.1 R-Ti(OiPr)<sub>3</sub> as alkylating reagent

Consequently, Seebach et al. improvised and patented a method using R-Ti(OiPr)<sub>3</sub> as the organometallic reagent for the addition to benzaldehydes, and the **titanate 3**

(bidentate bicyclic taddolate) as the main catalyst, immobilized and attached to zeolite nanotubes<sup>9</sup>. This zinc-free monometallic system is also more promising for large scale applications and there is less ambiguity in its mechanistic interpretations. Within the time limit of my M.Sc.candidature, quantum mechanical calculations were carried out to provide mechanistic understanding of the aforementioned reactions which uses R-Ti(OiPr)<sub>3</sub> as the alkylating agent.

### 3.3.2 TiTaddolate Catalysts in Alkyl Titanium Derivatives Nucleophilic Addition to Benzaldehydes—Preparation of the Catalysts

TiTaddolate is normally generated in situ either by ligand exchange from the TADDOL and Ti(OiPr)<sub>4</sub> or by metathesis from **spiro-titanate 2** and Ti(OiPr)<sub>4</sub>. According to D. Seebach<sup>1</sup>, the later route is favored by his research group since **titanate 3** would be generated with the least number of chemical steps, just by mixing the air stable and commercially available spiro-titanate with an equimolar amount of the commercially available Ti(OiPr)<sub>4</sub> in toluene as mixture. The enantioselective addition of alkyl groups to aldehydes is performed with 1.2 equiv. of freshly prepared R-Ti(OiPr)<sub>3</sub>, 0.2 equiv. of TiTaddolate and 1.0 equiv. of benzaldehyde. This combination of molar equivalence has been discovered to produce the highest combination of product conversion rate and enantioselectivity. The reactants are mixed at -78 °C and slowly allowed to warm to room temperature overnight.

Generally, the characteristic features of this reaction are very similar to those of the TiTaddolate catalyzed dialkyl zinc addition to aldehydes.<sup>10</sup> It is therefore entirely possible that no zinc center is involved in the rate determining C—C bond formation step of the previous reported reaction. The results from our quantum mechanical DFT calculations has

also proven that it is possible that no zinc atom is needed to find the transition state complex and that it is not the quintessential component involved in the rate determining step of C—C bond formation, since with R-Ti(Tadolate)(OiPr)<sub>2</sub>, it is still possible to find the 2 transition states represent the *S*- and *R*-enantiomers and the transition state reaction coordinate, as elucidated by subsequent IRC calculations, reveal a clear C—C bond formation between the alkyl group and the formyl carbon.

### 3.4 Experimental Work Done by Various Research Groups

#### 3.4.1 D. Seebach et al.—Alkyl Titanium Derivatives as Alkylating Agents

In experiments carried out by B. Weber and D. Seebach, toluene-ether or toluene-hexane solutions of aryl and alkyl triisopropoxy titanium reagents were prepared from the corresponding Li or Grignard reagents and Cl-Ti(OiPr)<sub>3</sub> with careful removal of the unwanted Mg, or Li salts. The solution of the organotitanium compounds were then combined with one equiv. of aldehydes and 0.2 equiv. of (*R, R*)-diisopropoxy-( $\alpha, \alpha, \alpha', \alpha'$ -tetraphenyl-2,2-dimethyl-1,3-dioxolane-4,5-dimethanolato) titanium, in short Ti-Taddolate at dry-ice temperature. Warming up to room temperature leads to the nucleophilic addition to the *Si*-face of the aldehydes with e.r. as high as 99.5:0.5. The enantioselective addition to aldehydes is performed with 1.2 equiv. of freshly prepared R-Ti(OiPr)<sub>3</sub>, 0.2 equiv. of **titanate 3**, and 1.0 equiv. of benzaldehyde in toluene solvent: the reactants were mixed at -78 °C and allowed to warm to room temperature overnight. Both alkyl- and aryl-tetraisopropoxy-titanium compounds were used which are generated *in situ* from the corresponding alkyl- or aryl-lithium or *Gignard* compounds and Cl-Ti(OiPr)<sub>3</sub>. It turns out that the presence of the salts, which were formed in the transmetallation step, LiCl and MgXCl, respectively, drastically reduces the enantioselectivity of the titanate produced. In

toluene, these salts were insoluble, and therefore separable by centrifugation. The centrifugation can be performed at room temperature in a tube sealed with a rubber septum and flushed with argon to prevent the decomposition of R-Ti(OiPr)<sub>3</sub>. Then, after achieving the production of the **titanate 2**, Seebach et al. carried out the reaction in a two neck Erlenmeyer flask, a solution of this 0.1 equiv. titanium 2 and 0.12 equiv. Ti(OiPr)<sub>4</sub> in toluene was stirred for a few minutes at room temperature, and 1.2 equiv. of the R-Ti(OiPr)<sub>3</sub> is added. The temperature was maintained at -78 °C for 0.5 to 1.5h, 1.0 equiv. of the aldehyde was added and the reaction was allowed to warm to room temperature overnight without removing the cooling bath. The reaction was subsequently quenched with pure 5M NaOH. Stirring was continued for 10 minutes, Na<sub>2</sub>SO<sub>4</sub> was added and after an additional stirring of 10 minutes, the reaction mixture was filtered through a Celite<sup>®</sup> pad and the solvent removed *in vacuo*. The enantiomeric product was separated from the taddol either by bulb to bulb distillation or flash chromatography.

### **3.4.2 Y.D. Wu et al.—Experimental Studies on the H-bonded Promoted Enantioselective HDA Reaction of Danishefsky's diene with Benzaldehyde**

In Wu's research group, the enantioselective hetero-Diels-Alder (HDA) reaction of Danishefsky's diene with benzaldehyde was achieved catalytically by a series of TADDOL derivative through H-bonding activation, yielding 2-phenyl-2,3-dihydro-4H-pyran-4-one after TFA acid workup in moderate yield and good enantioselectivities.<sup>11</sup> In conjunction with experimental investigations, the mechanism of the catalytic HAD reaction was also studied theoretically using the ONIOM (B3LYP/6-31G\*:PM3) method with trans-1,3-dimethoxy-1,3-butadiene as the model for Danishefsky's diene. The ONIOM method will also be tested out in this thesis too in order to determine the suitability of integrated

MM/MO method of calculation in our elucidation of the relative suitability between the different conformers of the activated pre-TS complex.

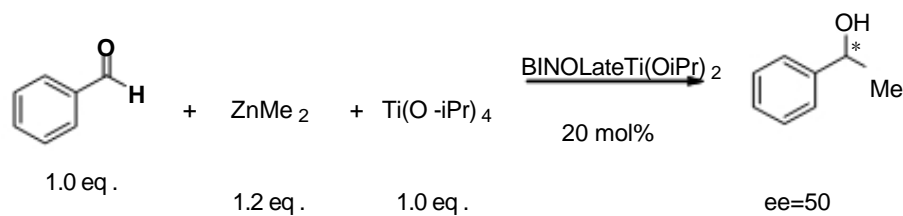
### **3.4.3 P.J. Walsh et al.- Titanium Catalyzed Enantioselective additions of Alkyl groups to Aldehydes**

P.J. Walsh used the catalytic asymmetric addition of alkyl groups to aldehyde as an important reaction in the enantioselective synthesis of secondary alcohol to prove whether there are any mechanistic similarities between the zinc and titanium-based catalysts. While the mechanism of the zinc/amino-alcohol catalysts has received significant attention, the titanium based catalysts have been less well-studied. Based on mechanistic studies on bisulfonamide and BINOL- derived titanium catalysts, the authors described the use of the reaction in the development of new approaches to asymmetric catalysis including applications of diastereomeric catalysts and optimization of asymmetrical catalysts with achiral and meso-ligands.

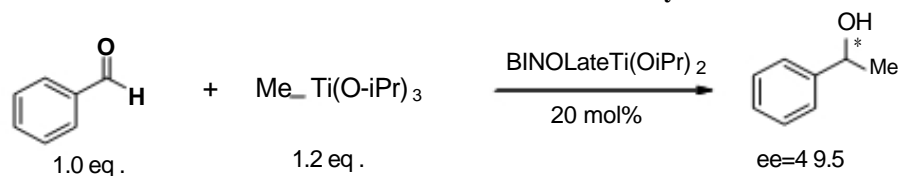
Walsh's article is highly important in this thesis because of the clarification he gave as to the role of dialkyl zinc. He agreed with Seebach's proposal that the role of the dialkyl zinc reagents in titanium taddolate-catalysed addition to aldehyde is not so much to alkylate directly to the aldehyde than to transfer the alkyl group to titanium Taddolate before titanate Taddolate alkylates benzaldehyde in subsequent stages.<sup>12</sup>

The premise of his proposal was based on similar trends in enantioselectivities when dialkyl zinc reagents were used with titanium tetraisopropoxide compared to the use of titanium alkyl species  $R-Ti(OiPr)_3$  generated in situ. Direct conditions were necessary with  $ZnR_2$  and  $R-Ti(OiPr)_3$ , however, and the enantioselectivities were sufficiently different that concrete mechanistic interpretations could not be drawn.

Walsh et al., however, have addressed this issue by performing 2 sets of experiments.



**Scheme 3.4.3-1: Reaction Pathway A**



**Scheme 3.4.3-2: Reaction Pathway B**

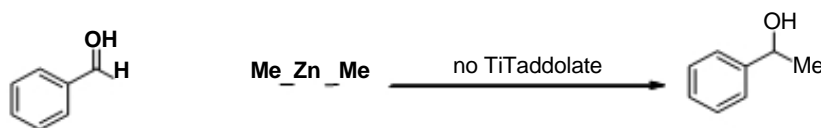
In **reaction pathway A (Scheme 3.4.3-1)**, methyl addition to aldehydes was performed using dimethylzinc,  $\text{Ti(OiPr)}_4$  and 20 mol %  $(\text{BINOLate})\text{Ti(OiPr)}_2$  to give a product of 50% e.e. with benzaldehyde substrate. In scheme 3.4.3-2, which shows the **reaction pathway B (Scheme 3.4.3-2)**, distilled  $\text{Me-Ti(OiPr)}_3$  (120 mol %) was substituted for  $\text{ZnMe}_2$  as the main alkyl group source. It is known that  $\text{Me-Ti(OiPr)}_3$  reacts rapidly with aldehydes to give racemic alcohol on workup.<sup>13</sup> Therefore, they performed the reaction with syringe pump addition of  $\text{Me-Ti(OiPr)}_3$  slowly over 30 min at  $0^\circ\text{C}$  to limit the concentration of  $\text{Me-Ti(OiPr)}_3$  and its uncatalyzed reaction with aldehyde. Under the slow addition conditions, the alkylation of benzaldehyde with  $\text{Me-Ti(OiPr)}_3$  gave product with 49.5% e.e. (vs. 50% e.e. for the reaction with  $\text{ZnMe}_2$ ). Three additional aldehydes were examined. The enantioselective excesses of the alcohol products were all perfectly identical using  $\text{ZnMe}_2/\text{Ti(OiPr)}_4$  vs.  $\text{Me-Ti(OiPr)}_3$ , clearly demonstrating for the first time that the dialkyl zinc reagent is not directly involved in the rate determining C—C bond forming step with the  $(\text{BINOLate})\text{Ti(OR)}_2$  catalyst. The reactions give the same e.e. ratios with and

without dimethyl zinc and therefore have a common titanium alkyl intermediate, which is namely what we have described in Section 3.2.1. The role of the dialkyl zinc reagent is to transfer the alkyl group to titanium derivatives. Furthermore, Walsh et al. went further by experimenting with mixing equi-molar amounts of  $\text{Ti}(\text{OiPr})_4$  and  $\text{ZnMe}_2$  in  $\text{C}_6\text{D}_6$  which resulted in the formation of only  $\text{Me-Ti}(\text{OiPr})_3$  and  $\text{Me-Zn}(\text{OiPr})_2$  by NMR observation, thereby supporting the intermediacy of  $\text{Me-Ti}(\text{OiPr})_3$ .

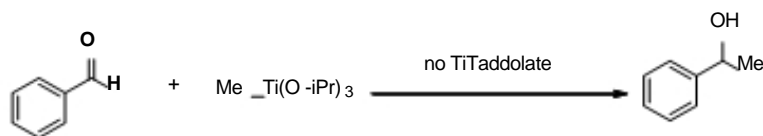
### 3.5 Methodology and Theoretical Calculations

#### 3.5.1 Two types of Uncatalyzed Benchmark Nucleophilic Addition Reactions

Armed with the knowledge that the  $\text{Me-Ti}(\text{OiPr})_3$  may be the actual alkylating agent for the nucleophilic addition of alkyl radical to benzaldehyde, and that even for the alkylation of benzaldehydes by diethyl zinc experimentally goes through the  $\text{R-Ti}(\text{OiPr})_3$  intermediate step, we have 2 types of uncatalyzed benchmark reaction as shown below:



**Scheme 3.5-1 Benchmark uncatalyzed reaction for Monometallic Variant**



**Scheme 3.5-2: Benchmark uncatalyzed reaction for Bimetallic Variant**

In this project, density functional theory (DFT) was used in the Gaussian 03 program to optimize the structures of the molecules, complexes and transition states.<sup>14</sup> The Becke three parameter hybrid functionals (B3) with the correlation functional by Lee, Yang, and Parr (LYP) was used with the 6-31G\* basis set for these calculations.<sup>15-16</sup> Initial

calculations were performed using the semi-empirical methods Austin Method 1 (AM1) and Parametric Method 3 (PM3) followed by the *ab initio* Hartree-Fock method (HF) with the 3-21G basis set. More accurate energies for the optimized structures were calculated using B3LYP theory with the 6-31G\* basis set. The zero point energy correction and the scaling factor were incorporated onto the electronic energy obtained by the DFT method to obtain the relative energies of the species. Solvation is neglected in this study because a relatively non-polar solvent (toluene) was used in this chemical system and it is assumed that the solvent-solute interaction would not be that significant in the DFT calculations in the system.

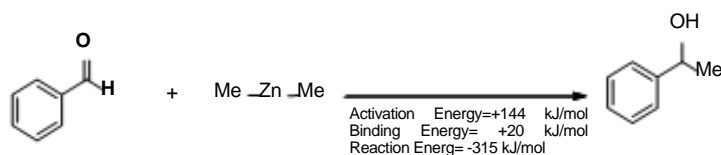
The pre-transition complex which comprises of the benzaldehyde substrate interacting with  $\text{Me}_2\text{Zn}/\text{Me-Ti}(\text{OiPr})_3$  was determined in Gaussian 03 using DFT B3LYP method and using the 6-31G\* basis set. The barrier height of the alkylation nucleophilic addition reaction was determined from the difference between the energy levels of the reactants and the transition state which reveals the C—C bond formation typical of the alkylation of benzaldehyde.

The uncatalyzed reaction between  $\text{Zn}(\text{Me})_2$  to benzaldehyde serves as a model to determine the role of the titanium taddolate catalyst for the monometallic variant of the catalyzed reaction, namely the reaction between  $\text{R-TiTaddol}(\text{OiPr})_2$  and benzaldehyde, whereas the uncatalyzed reaction between  $\text{R-Ti}(\text{OiPr})_3$  to benzaldehyde benchmarks the catalyzed reaction involving the bimetallic variant complex described in the next section, namely the reaction between  $\text{R-Ti}(\text{OiPr})_3\text{-TiTaddol}(\text{OiPr})_2$  and benzaldehyde.

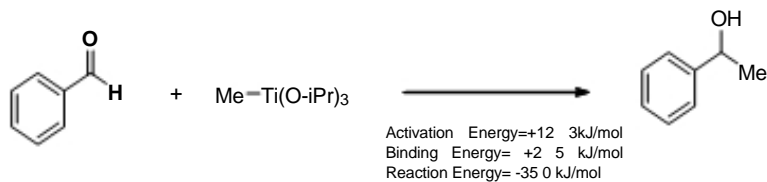


### 3.5.2 Activation Energy Barrier of Uncatalyzed Reaction

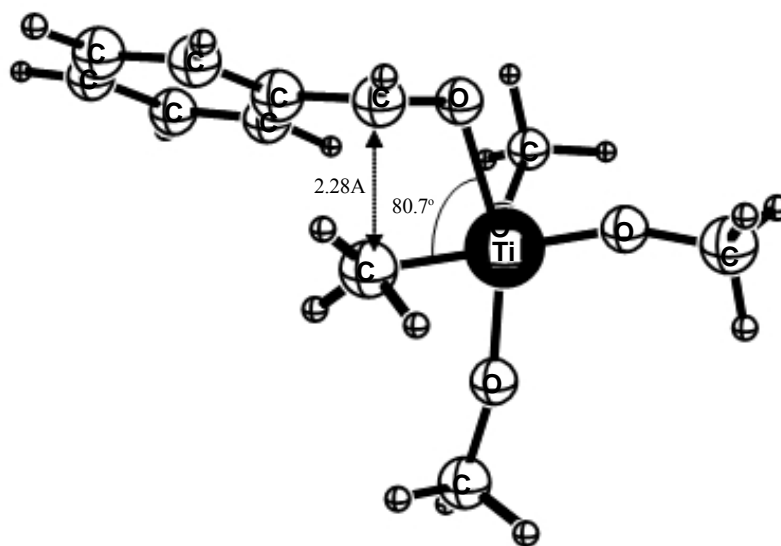
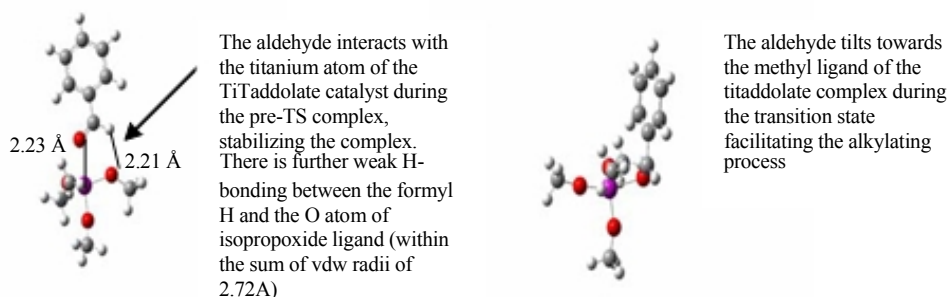
Using the benchmark uncatalyzed reaction as our basis; we begin by calculating the activation energy for the uncatalyzed alkylation reaction. There are 2 “uncatalyzed” reactions we will be looking at, for the mono-metallic and the bimetallic reactions. For each uncatalyzed reaction, we located one transition state which satisfies the one unique imaginary frequency criterion and which corresponds to a saddle point along the PES of the reaction path. The nature of this transition state was further verified by IRC calculations to confirm the reaction coordinate occurs along the C—C bond formation between the benzaldehyde and the alkyl group of the catalyst. The calculated activation barrier for the uncatalyzed reaction elucidated in Scheme 3.5-1 is **144 kJ/mol**; and the binding energy for the pre-TS complex is **20 kJ/mol**. The calculated activation barrier for the uncatalyzed reaction elucidated in Scheme 3.5-2 is **123 kJ/mol** and the binding energy for the pre-TS complex is **25 kJ/mol**. It was observed that methyl titanium triisopropoxide (Me-Ti(OiPr)<sub>3</sub>) acts as a Lewis Acid and electron acceptor and the carbonyl oxygen forms a dative bond with the titanium atom of Me-Ti(OiPr)<sub>3</sub>. In addition, this pre-transition state complex was further stabilized by the presence of weak C-H...O interaction between the carbonyl hydrogen and the oxygen from the isopropoxide ligand of Me-Ti(OiPr)<sub>3</sub>.



*Scheme 3.6-1:- Calculation of barrier height of uncatalyzed reaction (for monometallic variant) using B3LYP/6-31G\* level*



**Scheme 3.6-2:- Calculation of barrier height of uncatalyzed reaction (for bimetallic variant) using B3LYP/6-31G\* level**



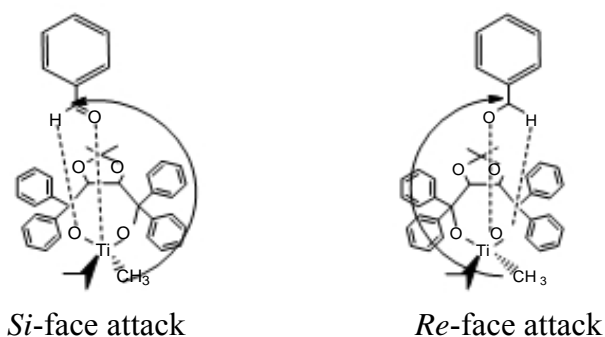
**Fig. 3.6-2:- Geometry of the “Uncatalyzed” Alkylation Reaction (for bimetallic variant)- L-R: Pre-TS complex, TS complex, Bottom: TS complex geometry and bond distances**

### 3.5.3 Monometallic Variant

In this section, we shall look at the mono-metallic variant to interpret the mechanism of the alkylation of benzaldehydes. In this hypothesis, we assume -along the lines of thought presented by E.J. Corey et al. - that the titanium taddolate catalyst acts as a

Lewis acid and the benzaldehyde acts as a substrate and bonds to the titanium taddolate and subsequently stabilized by a weak C-H...O bond. The CH-  $\pi$  forces and H-bonds helps to stabilize the pre-transition complex which would allow the alkylation to take place via the transfer of the alkyl anion (nucleophile) attached to the TiTaddolate to the benzaldehyde leading to an alkoxide intermediate complex which would then be easily H<sup>+</sup>-protonated to yield the secondary alcohol, which is the final product.

In this proposed reaction mechanism, there are 2 enantiofaces of the benzaldehyde substrate which the alkyl group can attack, namely the *Re*-face or the *Si*-face. A little bit of explanation is required here since the stereochemistry assigned to reaction faces differs from one research group to another. According to Seebach et al., using the Cahn-Ingold-Prelog (CIP) priority rules, the *Si*-face of benzaldehyde refers to the side of the formyl carbon which has the anti-clockwise direction in relation to the priority of the attached atoms according to the CIP rule, while the *Re*-face has the clockwise direction.



**Fig. 3.6.2-1 Si and Re-face attack of the alkyl radical on benzaldehyde**

### 3.5.4 Investigation on the pre-TS complexes formed

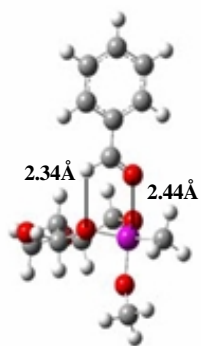
#### 3.5.4.1 Binding Energy (BE) of Benzaldehyde and Alkyl-Titaddolate pre-TS complex

In our monometallic variant of the alkylation process, we begin our study with the alkylated derivative of the TiTaddolate, namely CH<sub>3</sub>-TiTaddolate, or Me-TiTaddolate. In quantum chemical calculations, it is usually difficult for one to model from scratch the real-life system. What we can do is to first build a putative model system, and then scale it up to a simplified real system (which this section touches on) and then move on to the real system. In this section, we examine the individual B3LYP DFT energies of the benzaldehyde and alkyl-Titaddolate and then position the benzaldehyde on the alkylTiTaddolate catalyst in order to calculate the DFT energy of the complex formed. The binding energy (BE) is given by the difference in energies between the individual monomer molecules and the pre-TS complex. For the real system, we attempt to provide the reader with some qualitative insights on the trend between the 2 enantiomers using **ONIOM method** (a variant of the IMOMM method) within the G03 program.

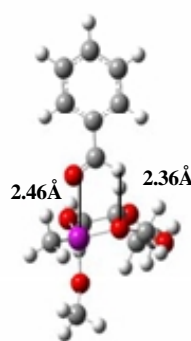
All results stated here were ZPE (calculated at B3LYP/6-31G\* level) corrected and scaled by a common scaling factor of 0.9804.<sup>17</sup> It is very important in the chemical reactions modeled in this project to include the ZPE correction the TiTaddolate molecules are extremely flexible and, together with the large molecular size, results in a substantial vibrational energy of the molecule even at T= 0 K.

We used the hybrid DFT functional B3LYP and 6-31G\* basis set because our preliminary calculations as listed in the table has shown that B3LYP/6-31G\* follows closest in qualitative trend as compared to our benchmark MP2/6-31G\* calculations when

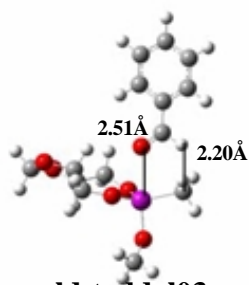
we are doing the pre-TS complex comparison of the different diastereomeric conformers on the Titaddolate-benzaldehyde complex.



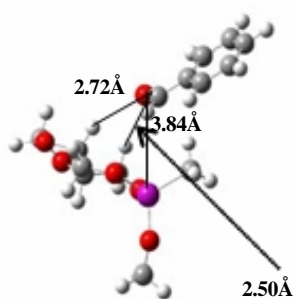
**ald-taddol01**



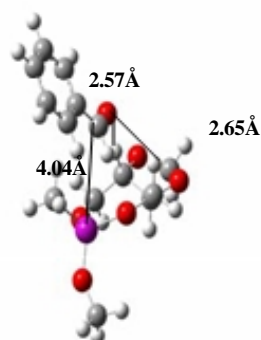
**ald-taddol02**



**ald-taddol03**



**ald-taddol04**



**ald-taddol05**

*Fig. 3.5.4:- Five diastereomeric conformers of benzaldehyde-Titaddolate (simplified) pre-TS complex*

<b>Relative Energies of the Conformers of the pre-T.S. complexes in the Model System</b>					
<b>(ZPE corrected and s.f.=0.9804)</b>					
<i>Pre-TS complexes</i>	Ald-taddol01	Ald-taddol02	Ald-taddol03	Ald-taddol04	Ald-taddol05
Description	cmp-left	cmp-right	cmp-side	cmp-tilt-left	cmp-tilt-right
HF/6-31G*	0.0	2.6	-11.1	-20.0	-20.9
B3LYP/6-31G*	0.0	2.2	- 2.2	-2.9	-1.6
SVWN/6-31G*	0.0	3.7	1.1	17.3	17.8
MPWPW91/6-31G*	0.0	1.9	1.4	0.3	1.7
BPW91.6-31G*	0.0	1.6	1.1	-3.2	-1.7
MP2/6-31G*	0.0	1.9	- 2.2	-6.6	-4.9

**Table 3.6.3-1 Relative Energies of Conformers of Model System**

As seen in the Table 3.6.3-1, our benchmark calculations were based on MP2 method, a post-HF method which could provide a reliable and robust comparison for a DFT method that can best describe the chemical system investigated. We used the 6-31G\* basis set for all our calculations. Next, we ran a whole series of different hybrid DFT functionals, from the conventional B3LYP model, to SVWN, MPWPW91, and B3PW91 and so on. To compare the various DFT methods, we choose a common basis set which is easy to compute but still relatively reliable, namely 6-31G\* polarized basis set as the common basis set in all calculations. It took quite some time to calculate the pre-TS complexes due to the lack of reliable experimentally observed geometry, either from literature or from data which could be derived from Cambridge Crystallographic Structural Database (CCSD). We did manage to find the X-ray crystallographic structures of similar titanates such as spiro-

titanate\* but there is really no crystal structure analysis for Titaddolate which we are looking at. Fortunately, there are CIF files which presents us with a look at the crystal structure of Zr-Taddolates and Hf-Taddolates<sup>†</sup>, which -since they are in the same column as Ti in the Periodic Table- could provide us with a qualitative trend as to the possible starting geometric structures for our species.

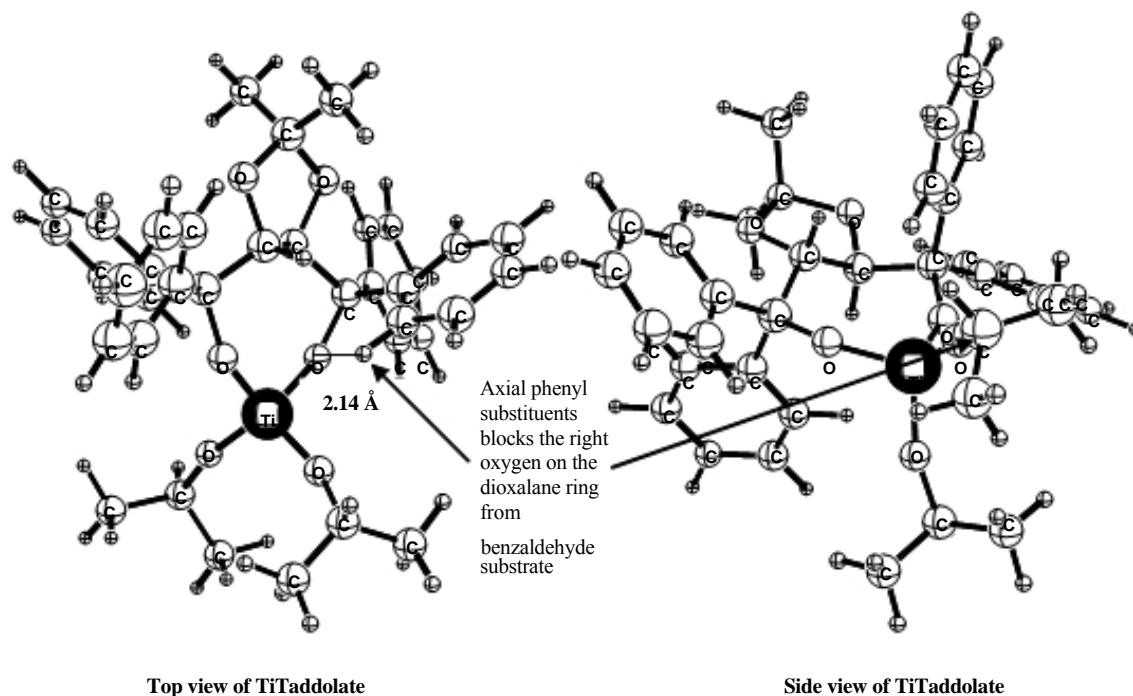
As with other calculation algorithms, we started with a loose geometry at HF/STO-3G, followed by using the geometry obtained to optimize TiTaddolates at a larger basis set, HF/3-21G and finally at the DFT B3LYP/6-31G\* level, reading the force constants previously calculated from HF/3-21G calculations into our DFT calculations. Our experience was that electron correlation is important in this chemical system investigated since the HF calculations are very poor in predicting the relative energies of the conformers. Table 3.6.3-1 showed HF calculations over-estimating the relative energy differences by up to 10kJ/mol with compared with benchmark MP2 calculations. On the other hand, B3LYP/6-31G\* was a more reliable computational method in this chemical system, with results and qualitative trend most resembling the post-HF MP2/6-31G\*. From the comparison of the pre-TS complexes formed in various conformations, we found out that the cmp-left conformer which corresponds to the *S*-product (the more favorable enantiomer experimentally) is lower in energy than the cmp-right conformer, which in turn corresponds to the *R*-product (the less favorable enantiomer) by around 2 kJ/mol. Further addition of the substituents like tetraphenyl substituents yield even greater conformational energy differences. The reason for this difference can be attributed to the fact that the aryl phenyl groups are arranged in a propeller-like configuration in the Taddol moiety and the axial

---

\* Cambridge Crystallography Structural Database, Cambridge, UK; Code: JUPWAS, KOGJAR

† CIF files, not available yet at CCSD were kindly provided by Prof. P.W. Roesky from the Technical University of Berlin

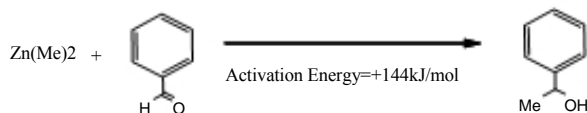
phenyl groups effectively “shield” the docking of the benzaldehyde to the right Taddol oxygen atom, but not the left. Furthermore, our calculations have confirmed the C2 symmetry of Titanium Taddolate molecule; hence it is impossible for the benzaldehyde to circumvent the steric hindrances brought by the 4 phenyl substituents on the oxalane ring by attacking below the plane.



**Fig 3.6.3-1:-The C2 symmetry of the optimized structure of TiTaddolate shows the axial phenyl group blocks the path of docking to the right Taddol oxygen, making *cmp-right* conformer less favorable**

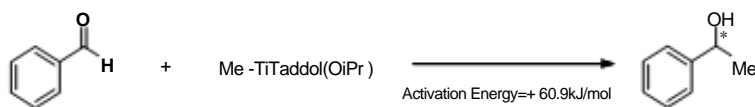
Using B3LYP/6-31G\*, we calculated the optimized energies for the monomer benzaldehyde and the  $\text{Ti}(\text{OiPr})_4$ , the pre-TS complex and we also found the transition state for the alkylation between  $\text{Ti}(\text{OiPr})_4$  and benzaldehyde. The activation energy for the uncatalyzed reaction between dialkyl zinc and benzaldehyde is **+144 kJ/mol**, which is around 20 kJ/mol higher than the activation energy for the uncatalyzed reaction between  $\text{Me-Ti}(\text{OiPr})_3$  and benzaldehyde.





**Scheme 3.6.1:- Uncatalyzed reaction between dialkyl zinc and benzaldehyde**

For the catalyzed reaction, the monometallic variant reaction is shown below:-



**Scheme 3.6.3-2 Monometallic Catalyzed Alkylation Reaction of Benzaldehydes**

The energy barrier height (or the activation energy) for the transition state involving the formation of the more favorable *S*-enantiomer (cmp-left) is calculated as +60.9 kJ/mol for the *S*-enantiomer and +70.6 kJ/mol for the *R*-enantiomer.

Therefore the reaction pathway leading to the *S*-enantiomer is more favorable than the one leading to the *R*-enantiomer. The difference in energy is around 10 kJ/mol, therefore leading to the observed enantiomeric excess ratio of 99.5%.

Furthermore, both *S* and *R* transition states' energy barriers are distinctly lower than that of the uncatalyzed reaction. This proves the fact the Tiaddolate catalyzes the reaction of  $\text{Zn}(\text{Me})_2$  to benzaldehyde. Furthermore, the high enantioselectivity can be explained by the difference in energy barrier heights between the *S* and *R* enantiomers, the difference of 10 kJ/mol barrier makes the *S*-enantiomer the favourable enantiomer.

From the results of the energies calculated at B3LYP/6-31G\* with scaled ZPE correction, the Me-Ti(TADDOL)-(OiPr) is an evidently more reactive reagent and it is also a chiral reagent, as compared to  $\text{Me-Ti}(\text{OiPr})_2$  since it has a lower activation energy for the nucleophilic addition of alkyl group to the benzaldehyde molecule. However, one would be hard pressed to say that the uncatalyzed alkylation in Scheme 3.6.3-1 is a suitable benchmark reaction to determine the catalytic effect of TiTaddolate on the alkylation

reaction since it appears that the Me-TiTADDOL-(OiPr)<sub>4</sub> acts as both a catalyst and a reactant. In fact, strictly speaking, the monometallic variant for the alkylation reaction should just be considered a more active reactant with benzaldehyde.

### 3.6 Bimetallic Variant

The challenging aspect of the alkylation nucleophilic addition reaction of benzaldehyde catalyzed by TiTaddolate lies in the fact that the reaction mechanism which incorporates dialkyl zinc, titanium taddolates and benzaldehydes is totally unknown. To add to the complexity, it is found experimentally that the alkylation reaction does not take place to any appreciable extent unless an excess (1.2 mol equiv.) of titanium tetrapropoxide is added, indicating the importance of incorporating Ti(OiPr)<sub>4</sub> within the reaction mechanism. Walsh et al. has proven experimentally that dialkyl zinc acts as a transferring agent and a source of alkyl groups which transfers the alkyl substituent to titanium taddolates. Titanium taddolate then acts as a nucleophile and a Lewis acid base to “dock” benzaldehyde and undergo a nucleophilic addition reaction where the alkyl group is added to the carbonyl carbon of benzaldehyde to form an alkoxide, which under acid condition, is quickly transformed into secondary alcohol.

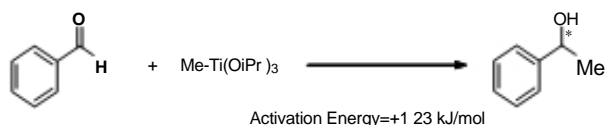
It is, in our opinion, necessary to look into the question of whether under thermodynamically favorable condition, the dual-titanium centered complex may be favored over the single-titanium complex, hence re-emphasizing the role of Ti(OiPr)<sub>4</sub> not only as a removing agent as stated in literature but also as a reactant (in Me-Ti(OiPr)<sub>3</sub> form) which complexes with the original TiTaddolate catalyst to yield the dual-titanium centered complex involved in the C—C bond formation. In fact, Seebach has also suggested in his proposed bimetallic mechanism, that there is a possibility that titanium taddolate might

complex with another titanium taddolate or titanium tetrapropoxide and this aggregated complex might be involved in the transition state complex formed.

In general, we can state that the characteristic features of this reaction are very similar to those of the Ti-Taddolate catalyzed dialkyl zinc addition to aldehydes. It is therefore entirely possible that no zinc center is involved in the rate-determining C—C bond forming step.<sup>18</sup>

### 3.6.1 Uncatalyzed benchmark reaction for bimetallic variant

We have discussed the benchmark reaction in Section 3.5.4, and we shall reproduce the results found here for easy reference. The uncatalyzed benchmark reaction for the bimetallic variant involved the uncatalyzed reaction between the alkylated titanium derivative (Me-Ti(OiPr)<sub>3</sub>) and benzaldehyde as shown below:

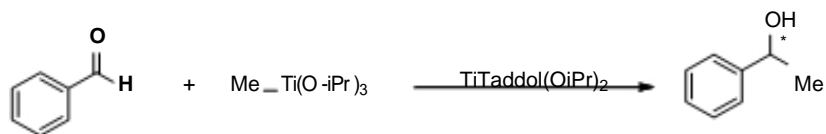


*Scheme 3.6.1:- Uncatalyzed benchmark reaction for bimetallic variant*

The calculated activation barrier of 123.0kJ/mol is lower than the uncatalyzed reaction between the dialkyl zinc and the benzaldehyde (144kJ/mol) This is consistent with experimental results found by Walsh that the alkylation reaction involving the MeTi(OiPr)<sub>3</sub> is faster than with Me<sub>2</sub>Zn.<sup>9</sup>

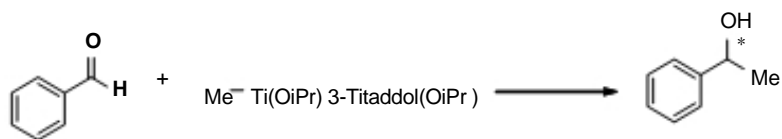
### 3.6.2 Transition States Complexes in Bimetallic Variant

Using DFT B3LYP method and 6-31G\* basis set, we successfully characterized the pre-TS, transition state and post-TS complexes of both the S-enantiomer and R-enantiomer bimetallic approaches.



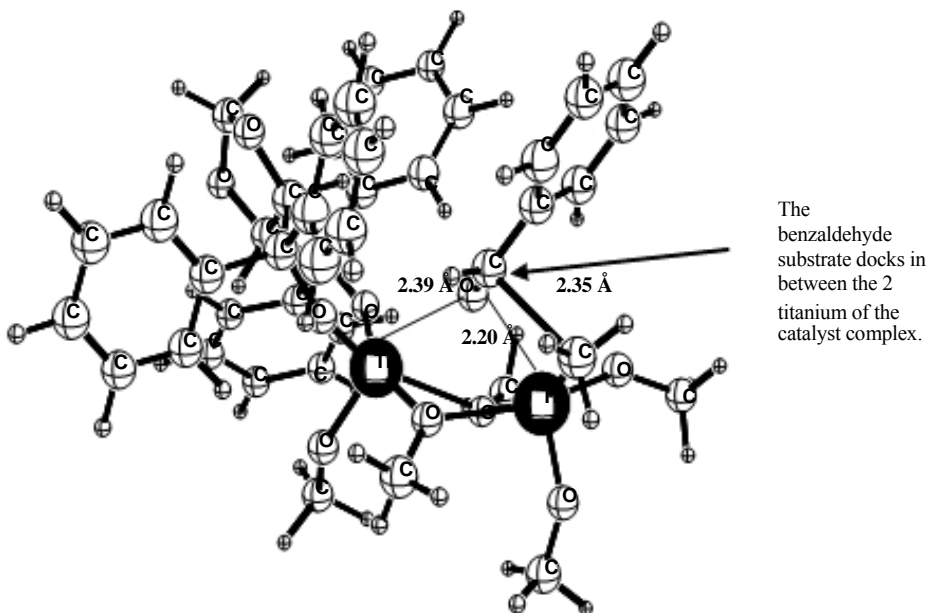
**Scheme 3.6.2-1: Catalyzed reaction involving TiTaddolate(OiPr)<sub>2</sub> as catalyst and Me-Ti(OiPr)<sub>3</sub> as reactant**

This is equivalent to the reaction pathway described below in Scheme 3.6.2-2, where we incorporate the Ti-Taddolate catalyst with the methyl titanium triisopropoxide to form a dual-titanium aggregated complex:-

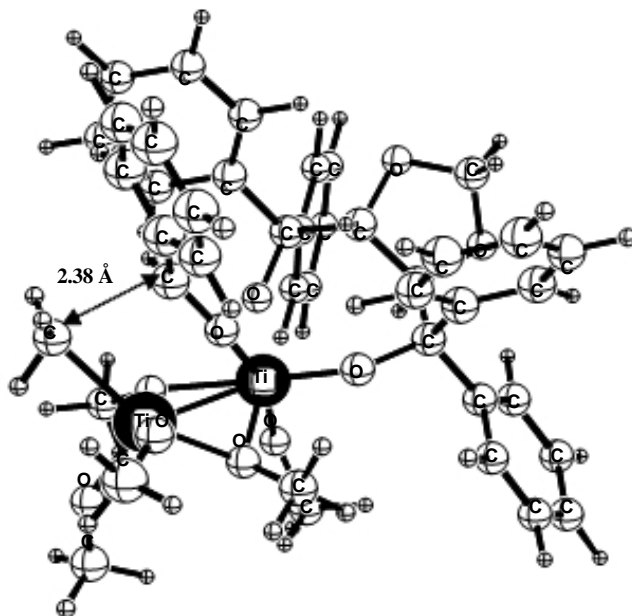


**Scheme 3.6.2-2: Catalyzed bimetallic reaction with the docking complex as a reagent**

The calculated transition states indeed show the complexation of Me-Ti(OiPr)<sub>3</sub>—TiTaddol(OiPr)<sub>2</sub> bimetallic complex, which then alkylates the benzaldehyde attached in between the 2 titanium cores within the Ti-O-Ti-O ring as seen in Figs. 3.6.2-1 and 3.6.2-2.



*Fig. 3.6.2-1: Optimized geometry of TS complex showing benzaldehyde docking in the center of the oxo-titanium ring (S-enantiomer).*



*Fig. 3.6.2-2: Optimized geometry of TS complex showing benzaldehyde docking in the center of the oxo-titanium ring (R-enantiomer).*

The optimized energies are all calculated at DFT B3LYP/6-31G\* with ZPE correction. The activation barrier for the catalyzed S-enantiomer reaction is **44.3 kJ/mol** whereas the activation barrier for the catalyzed R-enantiomer reaction is **67.3 kJ/mol**. This explains the S-enantiomer being favored because of the lower activation barrier by around 23kJ/mol. Several explanations can be gleaned from the optimized geometries of the transition state complexes in order to explain the calculated activation barrier heights. As observed in Fig. 3.6.2-1 and Fig. 3.6.2-2, steric hindrances from the bulky tetraphenyl substituents on the dioxolane ring favours the S-enantiomer configuration where the axial phenyl substituents are out of the way from the benzaldehyde substrate. In R-enantiomer configuration, the steric hindrances caused by the right axial phenyl ring increases the potential energy of the complex. In order to accommodate the benzaldehyde substrate, the

phenyl rings also have to rotate into a less favorable position, therefore incurring torsional strain as well.

The results found shows that indeed a bimetallic complex exists in the transition state of the alkylation reaction between an alkylated Ti derivative and a benzaldehyde and that Seebach's suggestion of his alkylated Ti derivative experiments involving possibly 2 titanium centers is correct.

### **3.7 Further Developments and Qualitative Predictions**

#### **3.7.1 ONIOM Integrated Molecular Orbital/Molecular Mechanics Method**

Even though we have found the reference transition states at the B3LYP/6-31G\* level, there is still more to be done: our B3LYP energies are still not rigorous enough to ascertain quantitatively the actual energy barriers between the 2 enantiomers. Furthermore, we still needed to carry out more rigorous post-HF methods like MP2 theory to confirm whether the bimetallic transition state indeed has relatively lower activation energy for alkylation as compared to the mono-metallic transition state.

However, given the size of our chemical system, which easily involves up to 2000 primitive Gaussians and up to 1000 basis functions for the 6-31G\* basis set, a more efficient way of handling this chemical system may lie in finding a reasonably accurate and computationally inexpensive method to predict the qualitative trends in Titaddolate alkylation of benzaldehydes.

There have been related studies which uses the popular ONIOM method (a type of IMOMM method in G03 program) to study the reaction of Titaddolate on carbonyl compounds<sup>19</sup>. Wu et al. used a customized IMOMM method within G03 to predict the energies of transition state complexes involving BINOLates (an analogue of TADDOLates),

namely (B3LYP/6-G311+G\*\*): PM3). However, using similar ONIOM methods in our system failed, probably because they were using customized PM3 and we used the default PM3 method in Gaussian03. Nevertheless, we tried to use other ONIOM methods to check out the suitability of using Integrated Molecular Orbitals and Molecular Mechanics to compute preliminary optimized structures for further calculations.

### **3.7.2 Introduction on ONIOM methods**

Hybrid techniques that combine 2 or more computational methods in one calculation were first introduced into computational chemistry by K. Morokuma et al. in 1995. These hybrid energy methods such as QM/MM and ONIOM, that combine different levels of theory into one calculation, have been very successful in describing large systems. Geometry optimization methods can take advantage of the partitioning of these calculations into a region treated at a quantum mechanical (QM) level of theory and with the remaining region treated by an inexpensive method such as molecular mechanics (MM) or a less expensive QM level.

Specifically, QM/MM combines a quantum mechanical (QM) method with a molecular mechanics (MM) method, and the more general ONIOM scheme, which can combine any number of molecular orbital methods as well as molecular mechanic methods. The region of the system where the chemical process takes place, for example bond breaking and formation, is treated with an appropriately accurate method, while the remainder of the system is treated at a lower level. QM/MM schemes in particular have been successful in studying enzyme reactions, treating the active site by a high level method, most often DFT and the protein environment by molecular mechanics.

In a 2-layer ONIOM calculation, the total energy of the system is obtained from 3 independent calculations:

$$E_{\text{ONIOM(QM:MM)}} = E^{\text{QM,model}} + E^{\text{MM,real}} - E^{\text{MM,model}} = E^{\text{high,model}} + E^{\text{low,real}} - E^{\text{low,model}}$$

The real system would contain all the atoms within the molecular system and is calculated only at the MM level. The model system contains the part of the system that is treated at the QM level, along with the link atoms that are used to account for the dangling bonds resulting from cutting covalent bonds between the QM and MM regions. To evaluate the ONIOM energy, both QM and MM calculations need to be carried out for the system. Because the positions of the link atoms are determined in terms of the atoms in the real system, the PES and therefore geometry optimization is well defined. The ONIOM gradient is obtained from:

$$\frac{\partial E^{\text{ONIOM}}}{\partial q} = \frac{\partial E_{\text{model}}^{\text{high}}}{\partial q} \cdot \mathbf{J} + \frac{\partial E_{\text{real}}^{\text{low}}}{\partial q} - \frac{\partial E_{\text{model}}^{\text{low}}}{\partial q} \cdot \mathbf{J}$$

where J is the Jacobian matrix, which is needed to convert the coordinate system for the model system to the coordinate system for the real system. The Hessian and other properties can be expressed in a similar fashion.

Because the MM and QM regions are coupled, the optimization must cycle between the regions until both systems' cycles converged. Because the MM region is large but inexpensive to calculate while the QM region is small but expensive, the separate optimization of the MM and QM regions can therefore be more efficient than applying a regular optimization method to the entire system.



### **3.7.3 Problems with the ONIOM method**

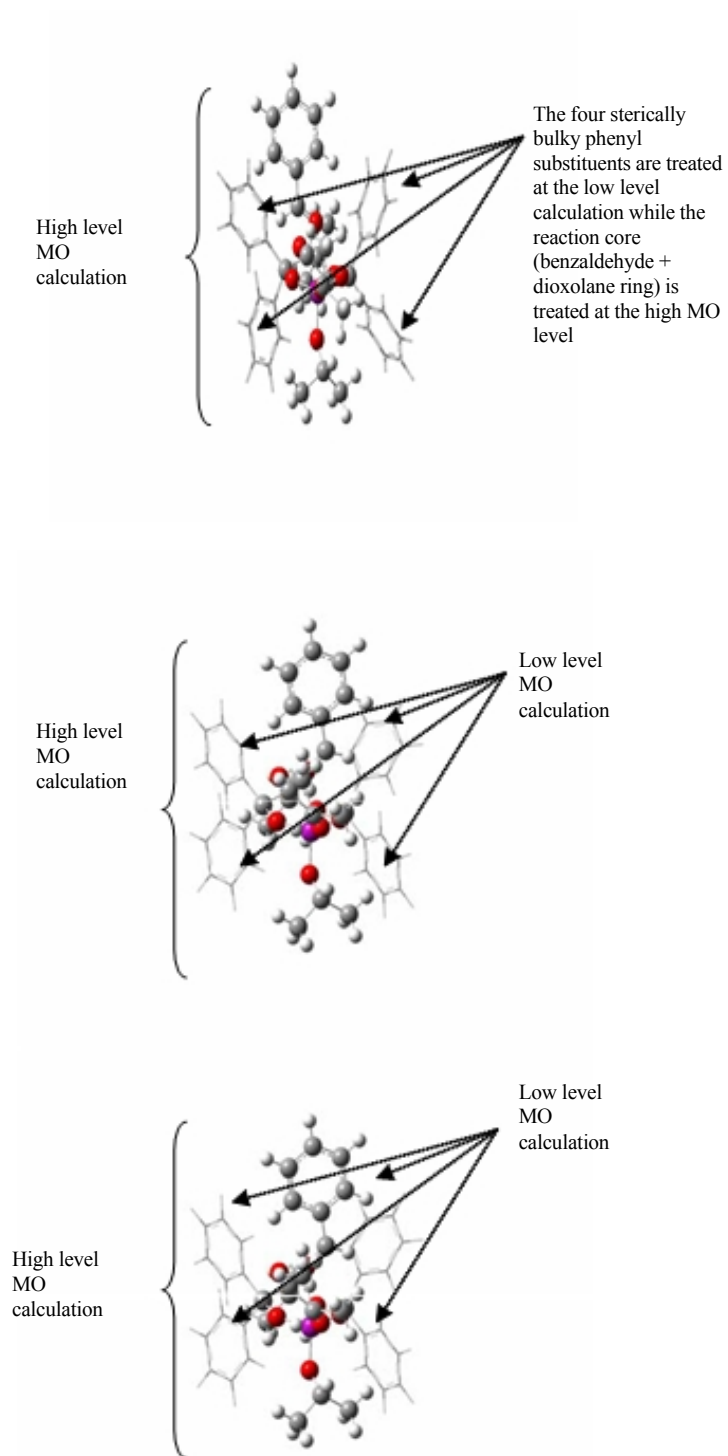
However, completely separating the optimizers for the QM and MM regions (i.e. with no exchange of information between the 2 optimizers) can cause several immediate problems. First, a displacement in the QM region might bring the combined system to a different (but not necessarily lower) region of the PES. Secondly, when the geometrical constraints are applied to the MM region, computation efficiency issues arise that can be dealt with by some integration of the QM and MM optimizers. Such issues can be addressed through a more sophisticated coupled microiteration scheme which is incorporated within the ONIOM process in Gaussian 03 as well as employing electronic embedding techniques which polarizes the QM wavefunction due to the electrostatic interaction with the MM region and therefore produce a more realistic geometry optimization and energy calculation.

## **3.8 Methodology in ONIOM calculations**

### **3.8.1 2-layer ONIOM calculations in titanium taddolate pre-TS complexes**

The goal of an efficient geometry optimization scheme is to find the optimized geometry with the least expenditure of computational effort. Usually the QM calculation on the model system is much more expensive than the MM calculation on the entire real system. A heuristic approach is to minimize the number of expensive QM energy and gradient calculations, even if this results in an increased number of MM calculations on the real system. Due to the large difference in computation cost for the 2 calculations, the overall computation expense will be lowered by the MM calculations. In practice, this goal is accomplished through a microiteration scheme for optimization of the MM region.

The layers defined for the low, and high layers in 2-layer ONIOM calculations are specified in **Figure 3.8.1.a-c**:



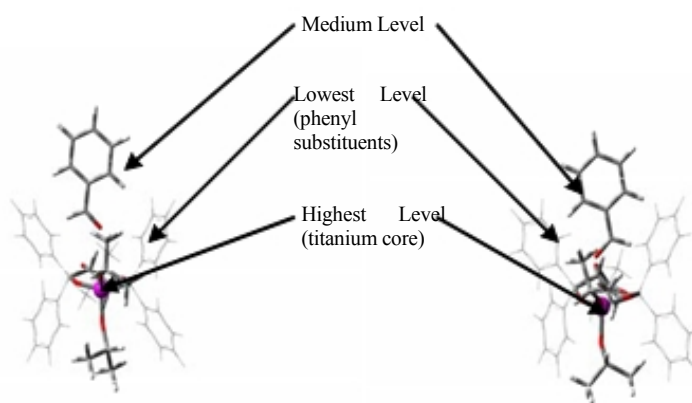
*Fig.3.8.1-a, b, c: optimized geometry of left-cmp, right-cmp and side-cmp*

As illustrated in Fig. 3.8.1 a-c, which presents the optimized ONIOM geometries of the left, right and side pre-TS complexes under B3LYP/6-31G\* for the high layer (represented by the ball and spoke model), HF/3-21G for the low layer (represented by the wireframe model), the ONIOM method used in the titanium taddolate pre-transition state molecular system into 2 distinct layers and use different level of theory and basis sets in order to cut down on overall computation costs. To simulate the effect of the 4 phenyl rings on the molecular system, lower level QM was employed in view of their bulky size, in order to reduce the computation cost. In this case, our ONIOM method is considered IMOMO (integrated molecular orbital-molecular orbital method) which is basically a type of hybrid method which incorporates 2 QM methods, one of which is less computationally expensive as compared to the other. The reaction core is determined by the interacting site of the benzaldehyde substrate to the titanium core and it is calculated using DFT method and the B3LYP/6-31G\* level was employed.

### **3.8.2 3-layer ONIOM calculations in titanium taddolate pre-TS complexes**

However, there have been reports which showed that PM3 calculations on the outer phenyl environment would also reproduce almost the same kind of reliable results on the optimized geometries and relative energies between the conformers. The layers defined for the low, medium and high layers of our second type of calculations are specified in **Figure**

#### **3.8.2:**



**Fig. 3.8.2:-Optimized ONIOM geometries of left and right pre-TS complexes**

As illustrated in Fig. 3.8.2, which presents the optimized ONIOM geometries of the left and right pre-TS complexes under B3LYP/LanL2DZ for the high layer (represented by the titanium core), B3LYP/6-31G\* for the medium layer (represented by the tubes) and the PM3 semi-empirical method for the low layer (represented by the wireframe structure), the ONIOM method used in the titanium taddolate pre-transition state molecular system into 3 distinct layers and use different level of theory and basis sets in order to cut down on overall computation costs. To simulate the effect of the 4 phenyl rings on the molecular system, lowest level MM/semi-empirical calculations were employed in view of their bulky size, in order to reduce the computation cost. In this case, a semi-empirical PM3 method was used. The reaction core is determined by the docking site of the benzaldehyde substrate to the titanium core and it is calculated using DFT method and an appropriate 6-31G\* basis set was employed. The titanium reaction core was described using high-level DFT B3LYP/LanL2DZ method and basis set, which is suitable to describe electronic structure of titanium.

This 3-layers ONIOM method was used to optimize the geometries and the energies of all 3 possible pre-transition state complexes and the same pre-transition complexes were also calculated using DFT methods so that we can benchmark the calculations with non-

ONIOM methods and deduce the computation cost savings attained. This will let us assess whether ONIOM would be a suitable method in the future developments in the titanium taddolate system.

### 3.9 Results and Discussion

The successful implementation of our ONIOM methods on our chemical system investigated indicates the accessibility and the possible deployment of ONIOM in titanium taddolate system.

<b>Whole Real System</b>	<b>Left-cmp</b>	<b>Right-cmp</b>	<b>Side-cmp</b>
B3LYP/6-31G*	-2845.885947	-2845.883916	-2845.88637
(benchmark in hartrees)			
Deviation	0	0.002031	-0.0004188
<b>RE (kJ/mol)</b>	<b>0</b>	<b>5.3</b>	<b>-1.1</b>
B3LYP/6-311+G**	-2846.460895	-2846.45772	-2846.46188
//B3LYP/6-31G*			
Deviation	0	0.0031749	-0.0009825
<b>RE (kJ/mol)</b>	<b>0</b>	<b>8.3</b>	<b>-2.6</b>
<b>Pre-transition state complex between the left and right conformer differs by up to 8kJ/mol</b>			
<b>Whole Real System</b>			
ONIOM	-2278.376213	-2278.372137	-2278.37637
(B3LYP/LANL2DZ:B3LYP/6-31G*:PM3)			
Deviation	0	0.00407587	-0.00015745
<b>RE (kJ/mol)</b>	<b>0</b>	<b>10.7</b>	<b>-0.4</b>
ONIOM	-3064.601125	-3064.599197	-3064.59874
(B3LYP/6-31G*:HF/STO-3G)			

Deviation	0	0.001927887	-0.002380677
<b>RE (kJ/mol)</b>	<b>0</b>	<b>5.1</b>	<b>-6.3</b>

Qualitative trend is consistent with the benchmark results and indicate the feasibility of engaging the ONIOM method to further investigate our titanium taddolate system, more importantly the computation savings of ONIOM method over the entire DFT method on the pre-transition state complex is huge, on average there is a cost savings of 80% in the 3-layered calculations as compared to the single layer calculations.

### **3.10 Conclusion on the Use of ONIOM in structural calculations**

For hybrid techniques such as ONIOM method, geometry optimization can be carried out in a very cost-effective manner by taking advantage of the division of the system into a small but expensive QM region and a large but inexpensive MM region. A series of micro-iterations algorithm incorporated within the new Gaussian 03 program has allowed scientists to investigate previous infeasible large molecular system. It is however not totally fool-proof because the exact geometry of the structures obtained are not entirely consistent with the DFT calculations which form the main gist of the thesis herein. However, the cost savings and the relatively consistent qualitative trends allow us to make good prediction on the reaction mechanism of the most thermodynamically favorable product.

### **3.11 Using Reverse Docking to Find Taddol-Catalyzed Transition States**

Recently, there has been literature which addresses the computational cost issue of Taddolate-mediated hetero-Diels-Alder (HDA) reaction using reverse-docking and molecular mechanics energetics only. Harriman et al. used reverse-docking of a TADDOL

organocatalyst to rigid transition state models of the catalyst-free HDA reaction with reasonable success.<sup>20</sup> Although results indicated a mode of catalysis consistent with experimental data, the relative docking energies between TS-model enantiomers were too great to allow for in-silico correlation to experimentally observed enantiomeric excesses. Nonetheless, the fact that the calculations -which were done at a low level molecular mechanics calculation only and using a relatively computationally inexpensive reverse-docking algorithm, EM-Dock- provides encouraging results for the quick determination of the qualitative trends between the different pathways to the production of the enantiomers gives us another avenue with which to approach the complexity of the Taddol-catalyzed reactions. As stated in the paper, the main factor promoting the HDA reaction appears to be the H-bonding interactions with the aldehyde dienophiles, not unlike the H-bonding reactions of the aldehyde with titanium Taddolates prior to the nucleophilic alkylation addition. Recent publications outline the development of a novel computational procedure, known as reverse-docking, which has proven to be a useful tool of studying the enantioselectivity of several organocatalyzed reactions. Basically, what is done is that a large flexible organocatalyst is docked around the rigid transition state models of the catalyst free reactions (TS-models) generated by ab initio transition state optimization (opt= TS) calculations. The resulting reverse docking poses represent simplified models for the transition states of the organocatalyzed HDA reaction. The conformation space of the catalyst in proximity to the TS models are subsequently sampled stochastically using the docking method EM-dock and the energetically favored paths are analyzed to highlight structure having H-bonding attraction compatible with the organic features in other species,

in other words (aldehyde-oxygen---TADDOL-oxygen distance of less than 4 Å and at an angle of between 100 to 180 degrees).

Using the results from the reverse docking, Harriman et al. seek to find attributes which might contribute to the actual enantioselective difference between the 2 enantiomers using our ONIOM calculations. They settled with the fact that it is a qualitative comparison. Structural analysis of the lowest energy reverse docking poses reveals a common mode of catalyst that is consistent with the principles of molecular recognition, organocatalysis and all available experimental information. There is presence of intramolecular H-bonding within the Taddol catalysis is believed to enhance the acidity of the free hydroxyl proton and allow for a stronger intermolecular H-bond with the carbonyl oxygen of the incoming dienophile. In addition to cooperative H-bonding patterns,  $\pi$ -stacking van der Waals interactions between the aldehydes and the pseudo-equatorial naphthyl ring of the organocatalyst at the transition state may be operative in blocking one of the dienophile face as another factor in the contribution to the enantioselectivity observed

However, the most interesting aspect of this study is the much closer correlation between the calculated relative energies and the experimental relative energies. To the best of our knowledge, this is the first reported use of using quantum chemistry to using a computationally inexpensive reverse docking; and it signified an important step towards the computer assisted design of new organocatalyst.



References:

- <sup>1</sup> Seebach D.; Plattner D.A.; Beck A.K. *Helv. Chim. Acta.* **1992**, 75, 2171 <sup>2</sup>
- Narasaka K. et al. *J. Am. Chem. Soc.* **1974**, 96(24), 7503-7509
- <sup>3</sup> Maruoka, H.; Hayakawa, S.; Yamada, T. *Bull. Chem. Soc. Jpn.* **1988**, 61, 4379 <sup>4</sup>  
Noyori R.; Kitamura M. *Angew. Chem.* **1991**, 103, 34-55
- <sup>5</sup> Seebach D. et al. *Tetrahedron* **1994**, 50, 4363-4384
- <sup>6</sup> Seebach D.; Plattner D.A. et al. *Helv. Chim. Acta.* **1994**, 85, 1436
- <sup>7</sup> Seebach, D.; Plattner, D.A. et al. *Helv. Chim. Acta*, **1996**, 95, 1875
- <sup>8</sup> Walsh P.J., *Titanium-Catalyzed Enantioselective Additions of Alkyl Groups to Aldehydes: Mechanistic Studies and New Concepts in Asymmetric Catalysis*, Accounts of Chemical Research, **2003**, Mar. 11
- <sup>9</sup> Patent European Agency Patent No. 1011736, Seebach D., ZTH, Switzerland, **1998**
- <sup>10</sup> Walsh P.J. et al., *Enantioselective Additions and Mechanistic Studies in Asymmetric Catalysis*, Accounts of Chemical Research, 14 May. **2004**
- <sup>11</sup> Zhang, X.; Du, H.F.; Wang, Z.; Wu, Y.D.; Ding, K., *Experimental and Theoretical Studies on the Hydrogen-Bond-Promoted Enantioselective Hetero-Diels-Alder Reaction of Danishefsky's Diene with Benzaldehyde*, *J. Org. Chem.*, **2006**, 71, 2862-2869
- <sup>12</sup> Weber, B.; Seebach, D., *Ti-TADDOLate-Catalysed, Highly Enantioselective Addition of Alkyl- and Aryl-titanium Derivatives to Aldehydes*, *Tetrahedron* **1994**, 5-, 7473-7484
- <sup>13</sup> Reetz M.T. *Organotitanium Reagents in Organic Synthesis*, Springer-Verlag: Berlin, **1986**
- <sup>14</sup> Gaussian 03, Revision C.02, M. J. Frisch, G. W. Trucks, H. B. Schlegel, G. E. Scuseria, M. A. Robb, J. R. Cheeseman, J. A. Montgomery, Jr., T. Vreven, K. N. Kudin, J. C. Burant, J. M. Millam, S. S. Iyengar, J. Tomasi, V. Barone, B. Mennucci, M. Cossi, G. Scalmani, N. Rega, G. A. Petersson, H. Nakatsuji, M. Hada, M. Ehara, K. Toyota, R. Fukuda, J. Hasegawa, M. Ishida, T. Nakajima, Y. Honda, O. Kitao, H. Nakai, M. Klene, X. Li, J. E. Knox, H. P. Hratchian, J. B. Cross, C. Adamo, J. Jaramillo, R. Gomperts, R. E. Stratmann, O. Yazyev, A. J. Austin, R. Cammi, C. Pomelli, J. W. Ochterski, P. Y. Ayala, K. Morokuma, G. A. Voth, P. Salvador, J. J. Dannenberg, V. G. Zakrzewski, S. Dapprich, A. D. Daniels, M. C. Strain, O. Farkas, D. K. Malick, A. D. Rabuck, K. Raghavachari, J. B. Foresman, J. V. Ortiz, Q. Cui, A. G. Baboul, S. Clifford, J. Cioslowski, B. B. Stefanov, G. Liu, A. Liashenko, P. Piskorz, I. Komaromi, R. L. Martin,

---

D. J. Fox, T. Keith, M. A. Al-Laham, C. Y. Peng, A. Nanayakkara, M. Challacombe, P. M. W. Gill, B. Johnson, W. Chen, M. W. Wong, C. Gonzalez, and J. A. Pople, Gaussian, Inc., Wallingford CT, **2004**.

<sup>15</sup> a) C. Lee, W. Yang, and R. G. Parr. *Phys. Rev. B.* **1988**, 37, 785. b) B. Miehlich, A. Savin, H. Stoll, and H. Preuss. *Chem. Phys. Lett.* **1989**, 157, 200.

<sup>16</sup> A. D. Becke. *J. Chem. Phys.* **1993**, 98, 5648.

<sup>17</sup> Corey E.J.; Bilar, J.C. *J. Am. Chem. Soc.* **1959**, 81, 2620

<sup>18</sup> Seebach, D.; Plattner, D.A.; Beck, A.K; Wang, Y.M.; Hunziker D; Petter W., *Helv. Chim. Acta.* **1992**, 75, 2171

<sup>19</sup> Wu Y.D.; Zhang, X.; Wang Z.; Ding K. *J.Org. Chem.* **2006**, 71, 2862-2869

<sup>20</sup> Harriman, D.J., Lambropoulos, A., Deslongcamps, G. *Tetrahedron Letters* 48 (**2007**), 689-692

# Chapter 4

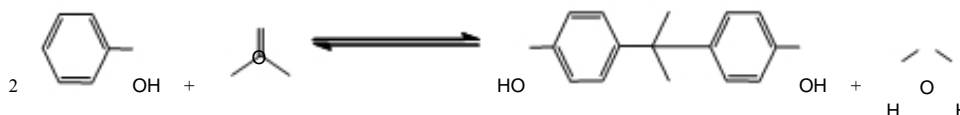
## Acidic Condensation Reaction of Bisphenol-A using Methyl Mercaptans as co-catalysts

---

---

### 4.1 Introduction

Bisphenol A, an industrially important chemical compound, is prepared by the reaction of acetone and phenol to give primarily the condensation product, *p,p'*isopropylidene-diphenol, or BPA.



*Scheme 5.1: Condensation reaction of BPA from acetone and phenol*

It is generally prepared in the presence of an acidic condensation catalyst along with a co-catalyst or catalyst promoter in order to enhance the catalytic effect of the acid on the reaction rate and the chemoselectivity of the condensation reaction.<sup>1</sup> *p,p'*isopropylidene-diphenols are used as reactants in the preparation of indanols<sup>2</sup> and also served as intermediates for stabilizer and dyestuff production.<sup>3</sup>

BPA was first synthesized by Dianin in 1891.<sup>4</sup> It was investigated in the 1930s during the search for synthetic estrogens. At that time, another synthesized compound,

diethylstilbestrol, turned out to be a more powerful estrogen surrogate and, therefore, BPA was not used as a synthetic estrogen. BPA is now mainly used as an important monomer in the manufacture of polycarbonate plastic and epoxy resins. In fact, the main driver for BPA is currently based on the global demand of polycarbonate and epoxy resins. In 2002, an estimated production value of US\$ 2.5 billion was achieved.<sup>5</sup> Polycarbonates are an unusual and extremely useful class of polymers and sold under a variety of trade names. Polycarbonate resin is used in automotive components, glazing sheet and optical media such as CD and DVD. Epoxy resins are used in protective coatings, electrical laminates and encapsulations, bonding adhesives and glass fiber-reinforced materials.

Strong mineral acids such as HCl or H<sub>2</sub>SO<sub>4</sub> can, therefore, be used as catalysts for the condensation production of BPA. HCl is much preferred due to its lower boiling point and the relative ease of removal from the reaction mixture. In industrial process applications, infrastructural and production costs are usually prohibitively exorbitant and whatever unnecessary by-products, if any, should be either easily eliminated from the effluent stream or avoided altogether. In recent years, instead of strong mineral acids, strongly acidic cation exchange resins have been used, with or without activity enhancing modifiers as co-catalysts. Resin catalysts eliminate catalyst recycle issues and greatly mitigate equipment corrosion and wastewater treatment problems. To compensate for any drop in reaction activity, reaction temperature with resin catalysts are usually increased to 70-80 °C compared to 50 °C with concentrated aqueous or gaseous dry HCl catalyst.

Compounds that contain mercaptan-moieties like alkyl thiols which hydrolyze to mercaptan groups are used in industries in catalytic amounts of 1% or less of the

feedstock to improve both the formation rate and the chemical yield of BPA. In this thesis, we attempt to explain how mercaptans act as suitable co-catalysts by increasing the reaction rate of the condensation reaction between phenol and acetone as well as to understand the detailed mechanism in the formation of BPA.

Presently, the most common used catalyst, both for its small molecular weight as well as its ease of removal in resin exchange columns, is methyl mercaptan or methanethiol (MeSH), which is a colourless gas with a pungent smell similar to that of rotten cabbages. Other examples of mercaptan promoters are 3-mercaptopropionic acid and 2,2-bismethylpropane. We propose that the effect of the methyl mercaptan co-catalyst could be attributed to the stabilization of the transition state in the formation of the carbonium cation intermediate during the rate-determining steps. In addition, the comparatively lower  $\Delta G^\circ$  of the intermediates and products formed also contributes to the thermodynamically favored pathway. Industrially, newer ion exchange catalysts are modified to introduce mercapto groups that accomplish the same result while keeping the promoter bound to the resin. In other words, the methyl mercaptan catalysts are immobilized and the catalysis of the acetone and phenol are considered heterogeneous catalysis.

There are several advantages in having an immobilized thiol-promoter ion exchange catalyzed BPA process:

1. Much lower investment and maintenance costs due to the use of less costly materials of construction
2. Minimal waste water production leading to drastic reduction in the size of the treating system

3. Simpler purification system in that catalyst recovery and recycling are not required.

It is essential to note that in modern industrial processes, it is commonplace to use resin catalyzed processes with thiol enhancing promoters rather than the convention HCl catalysed process and they retain an advantage in less costly construction materials. There are dozens of literature articles which explain the production economics for BPA using resin catalysts (mercapto-thiol approach) versus using the conventional mineral acids.

#### **4.2 Methyl Mercaptan as Co-catalyst in BPA Condensation Reaction**

It was discovered by the end of the 1940s that the use of mercapto substituted aliphatic carboxylic acids as catalyst promoters increases the condensation reaction rate between phenols and ketones to such an extent that the reaction time could be cut to 1/10<sup>th</sup> the time previously required with just an acid catalyst.<sup>6</sup>

Subsequently, industrial chemists found out that the contact time of the acid-catalyzed reaction between phenol and ketones could be further improved by the use of methyl mercaptans (MeSH).<sup>7</sup> Not only was the contact time reduced, the use of gaseous methyl mercaptan in the reaction mixture also allows one to run the reaction with only minimal amounts of this co-catalyst or catalyst promoters without the formation of any excessive amounts of by-product formation or BPA product disintegration. Furthermore, methyl mercaptan could also be used in a continuous-flow stirred tank reactor (CSTR), which streamlines the production process of BPA by providing a constant supply of products eluted from the reaction mixture compared to a conventional batch reactor. It is also easily separated from the reactor reaction mixture effluent containing BPA since it is

highly volatile. This avoids the presence of sulphur contaminants in the final product. Since then, the use of gaseous free methyl mercaptan has been the co-catalyst of choice in the acid-catalyzed phenol-acetone reactions.

### **4.3 Improvements on Mercaptan Co-catalysts**

Given the rapid development in the industrial catalyst industry, new inventions have emerged regularly to improve on the methyl mercaptans as co-catalysts in the production of BPA.

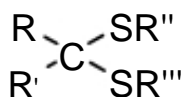
Methyl mercaptans might have been a catalyst promoter of choice in the previous century, but with the focus on logistics efficiency and green chemistry, the prevalent use of methyl mercaptans has been put to question. Firstly, methyl mercaptan is difficult to handle because it is gaseous at room temperature and pressure. This makes the shipping of methyl mercaptan inefficient because it must first be pressurized to a liquid state to economically transport sufficient amounts required for the manufacture of BPA at a plant located some distance from the site producing methyl mercaptan. In addition, since methyl mercaptan is hazardous, -and pungent as well-, shipping this material to certain locations might be restricted by environmental laws, hence resulting in its limited availability in these areas. As a result, some BPA plants must now either produce methyl mercaptan on site, or switch an alternative catalyst promoter which does not have the volatility or other inherent disadvantages of methyl mercaptan.

There have been a number of patents sent to the United States Patent and Trademark Office detailing new mercaptan-based catalysts which are also just as efficient in the yielding BPA.<sup>8</sup> In some of these cases, the co-catalyst has the same selectivity towards bisphenol-A as methyl mercaptan, without the formation of any by-product

sulphur species at levels greater than with the use of methyl mercaptan but which is not as volatile as methyl mercaptan. More importantly, it is at liquid state at room temperature and pressure, henceforth rendering it easily and economically transportable. In addition, they are stable during transportation. In the chemical industrial, which differs from bench top experiments in the manner that shipping and handling of feedstock are important issues, these improved mercaptan-based co-catalysts could possibly represent a substantial savings in industrial production costs of BPA.

#### 4.3.1 Dithiolketals as Mercaptan Co-catalysts

Palmer and Wong <sup>8</sup> discovered a catalyst promoter of the following structure, a class of dithiolketals, which enhances the chemical yield of BPA within the reaction mixture in the presence of an acid catalyst:-

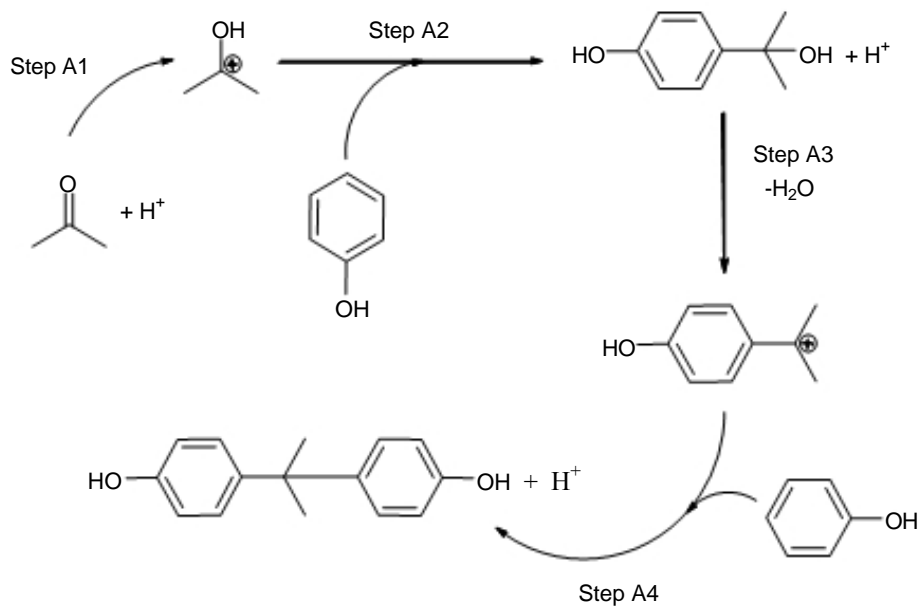


*Fig. 4.3.1-1: Patented dithioketane co-catalyst*

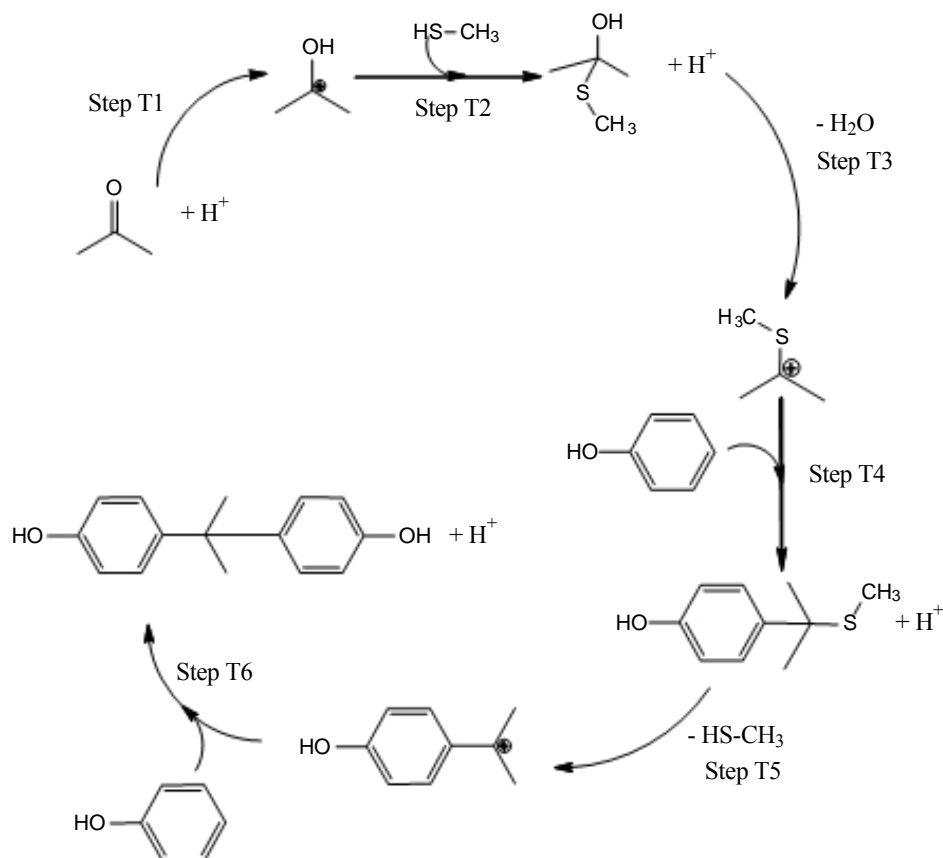
In this dithioketane co-catalyst, the composition of which is made up of 2, 2-bis(thiomethyl)propane as a backbone. The R, R', R'', R''' represent alkyl radicals attached to the thiol and carbon atoms accordingly. This dithioketal catalyst, a specific class of dithioacetals (if R=H) is added in the liquid phase to the reaction mixture or to any reactant with just as high activity and selectivity as methyl mercaptan, with the added advantage that its relatively low volatility and stability in liquid state during transport makes it a good drop-in replacement to its predecessor. Dithioketal dissociates into acetone and the methyl mercaptan catalysts. In the section 4.3.2, we will model this reaction to determine its viability in the overall reaction.



Armed with the knowledge of organic chemical reaction mechanism as well as an abundant source of literature on the typical mechanisms of carbocation chemistry, possible reaction schemes of the acid-catalyzed reaction and the methyl mercaptan cocatalyzed reaction are shown in **Fig. 4.3.1-1** and **Fig. 4.3.1-2** :-



**Fig 4.3.1-1: Proposed schematic reaction pathways for acid -catalyzed reactions of BPA**



**Fig 4.3.1-2: Proposed schematic reaction pathways for mercaptan catalyzed reactions of BPA**

This chapter elucidates the reaction pathways of the proposed reaction mechanisms using quantum mechanical DFT theory. The computational results would shed light on the reasons behind the observed increase in reaction rate of condensation of BPA when methyl mercaptan is added as a co-catalyst or catalyst promoter.

### 4.3.2 Experimental and Theoretical Calculations on Methyl Mercaptans Co-catalysts

We shall examine the improvement of the co-catalyst proposed by Palmer and Wong in the overall determination of the transition states in the condensation of BPA. The dithioketals catalyst promoter composition can be added to the reaction mixture or to any one of the reactants in the liquid phase or gaseous phase. Since the dithioketal

catalyst promoter composition is in the liquid state during the shipping and handling, it is preferred to add it to the reaction mixture or to any reactant in the liquid phase. Hence, in our calculations, we will employ the Polarizable Continuum Model or PCM (solvent = water) to simulate the solvation effects of this chemical reaction. The PCM model allows us to provide a more realistic and consistent comparison with the experimental data. More importantly, unlike the theoretical study on titanium taddolate catalyzed alkylation reaction of benzaldehydes in Chapter 3, where the solvent toluene is a relatively non-polar organic solvent, water is a highly polar solvent and many of the species calculated (e.g. carbocation species in Steps A2 and T4) are also strongly polar, therefore the solvent effect is expected to be important in the reactions investigated. As a consequence, it is essential to incorporate solvent effects into the calculations in this chemical system in order to obtain more realistic results to compare with experimental data.

#### **4.4 Calculations: Heats of Formation of BPA condensation reaction**

We commence our investigation by doing a preliminary study on the heats of formation of the reactants, intermediates and products involved in our initial proposed mechanism of the condensation reaction. Using solvated AM1 (SAM1) semi-empirical method in Spartan 04 program, with solvent being water, we obtained the solvated heats of formation of the molecules involved in the 2 pathways as shown in **Fig. 4.4-1** and **Fig.**

**4.4-2:-**

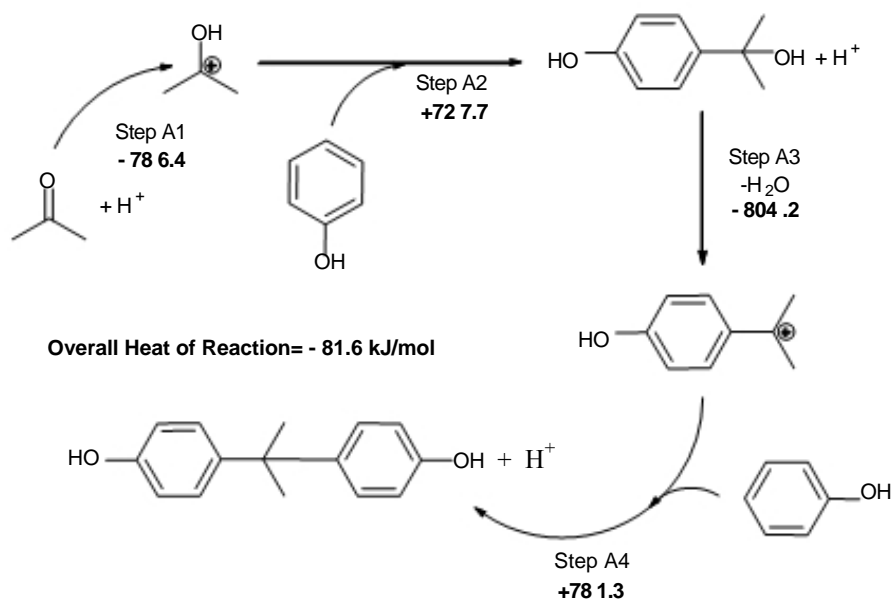


Fig. 4.4.1:- SAM1 calculations of Heats of Formation (in kJ/mol) of Steps A1-A4

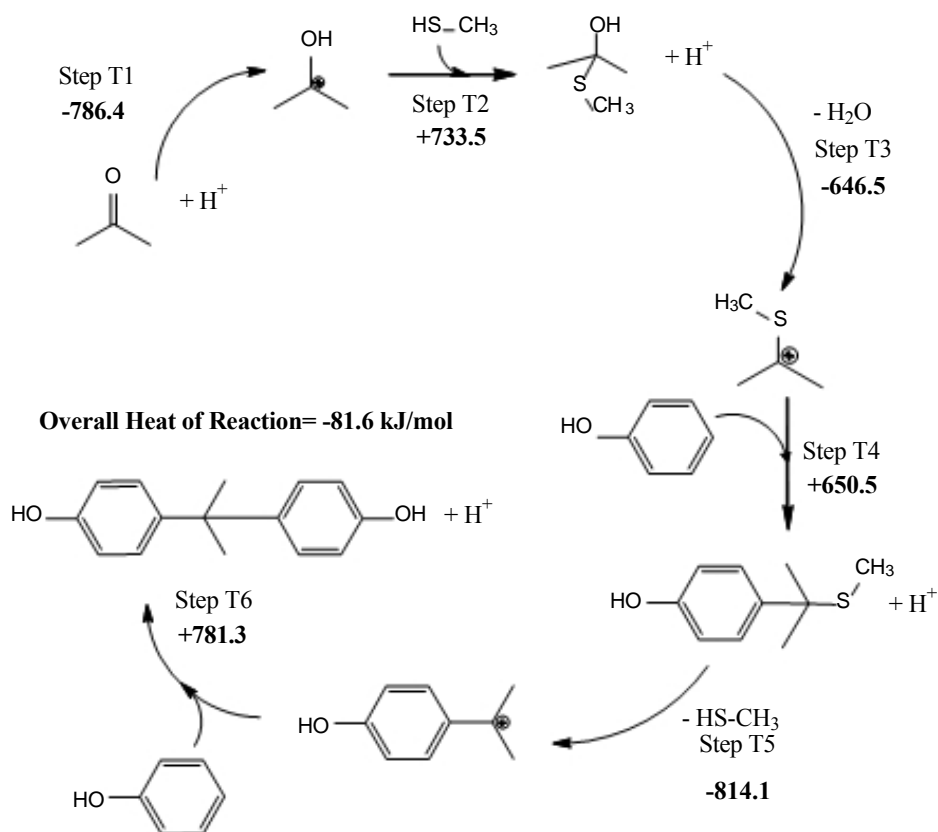
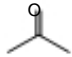
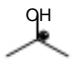
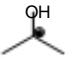
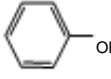
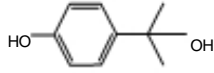
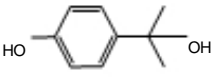
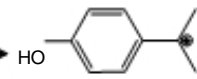

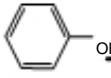
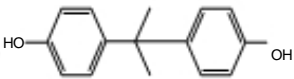
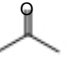
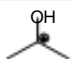
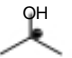
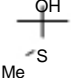


Fig. 4.4.2:- SAM1 calculations of Heats of Formation (in kJ/mol) of Steps T1-T6

Subsequent to the SAM1 preliminary calculations, where we found that the overall methyl mercaptan-catalyzed pathway is thermodynamically exothermic ( $\Delta H_{\text{reaction}} = -81.6 \text{ kJ/mol}$ ), we upgraded our calculations to DFT theory and employed B3LYP/6-31G\* level to calculate the energies of the reactants and intermediates involved in both reaction pathways. The DFT energies are listed in Table 4.4.3 and 4.4.4 respectively on the following page:-

Acid Cat.	Reactants	Products	$\Delta H_{\text{rxn}}$ (kJ/mol)		
<b>Step A1</b>	 +	$\text{H}^+ \longrightarrow$ 			
Energies in hartrees	-193.15569	0	-193.47933	<b>-849.7</b>	
<b>Step A2</b>	 +	 $\longrightarrow$  + $\text{H}^+$			
Energies in hartrees	-193.47933	-307.46487	-500.62080	0	<b>+849.1</b>
<b>Step A3</b>	 +	$\text{H}^+ \longrightarrow$  + $\text{H}_2\text{O}$			
Energies in hartrees)	-500.62080	0	-424.55346	-76.42372	<b>-935.7</b>
<b>Step A4</b>	 +	 $\longrightarrow$  + $\text{H}^+$			
Energies in hartrees	-424.55346	-307.46487	-731.66760	0	<b>+920.8</b>

**Table 4.4.3: B3LYP/6-31G\* energies with scaled ZPE correction in acid-catalysed pathway**

Mercaptan Cat.	Reactants	Products	$\Delta H_{\text{rxn}}$ (kJ/mol)	
<b>Step T1</b>	 +	$\text{H}^+ \longrightarrow$ 		
Energies in hartrees	-193.15569	0	-193.47933	<b>-849.7</b>
<b>Step T2</b>	 +	$\text{MeSH} \longrightarrow$  + $\text{H}^+$		

Energies in hartrees	-193.47933	-438.69830	-631.85779	0	<b>+839.8</b>
<b>Step T3</b>		$\text{H}^+$		$+\text{H}_2\text{O}$	
Energies in hartrees	-631.85779	0	-555.76936	-76.42372	<b>-880.3</b>
<b>Step T4</b>				$+\text{H}^+$	
Energies in hartrees	-555.76936	-307.46487	-862.90429	0	<b>+866.3</b>
<b>Step T5</b>		$\text{H}^+$		$+\text{MeSH}$	
Energies in hartrees	-862.90429	0	-424.55346	-438.6983	<b>-912.4</b>
<b>Step T6</b>				$+\text{H}^+$	
Energies in hartrees	-424.55346	-307.46487	-731.66760	0	<b>+920.8</b>

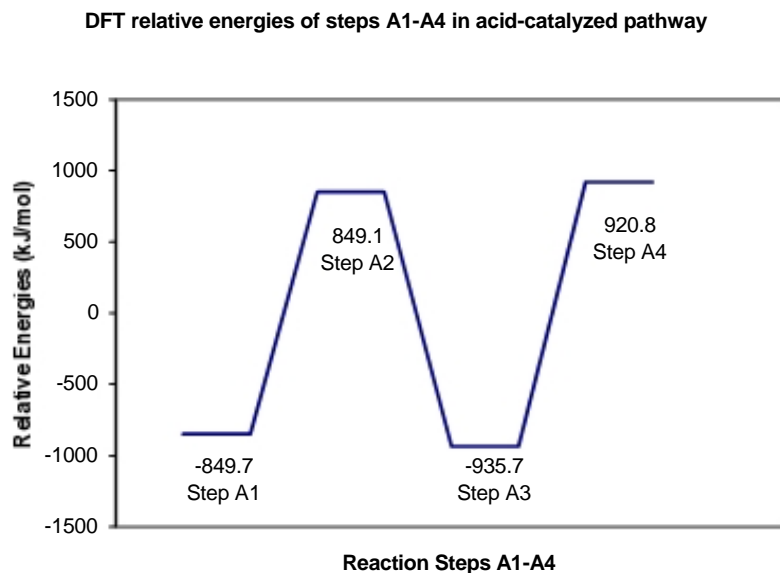
**Table 4.4.4: B3LYP/6-31G\* electronic energies with scaled ZPE correction in mercaptan-catalysed pathway**

Since electronic energies for the  $\text{H}^+$  proton cannot be obtained from DFT calculations, we incorporated empirical values derived from real-life experiments. We searched assiduously through the scientific databases and available literature to obtain the heat of formation for  $\text{H}^+$  proton from experiments, namely those of Truhlar et al. whose group carried out both experimental as well as high-level theoretical calculations on the  $\text{H}^+$  ion energetics. The widely accepted value for the heat of formation of  $\text{H}^+$  and the solvated Gibbs free energy of solvation of  $\text{H}^+$  are +1530.0 and -432.6 kJ/mol, respectively.<sup>9</sup>

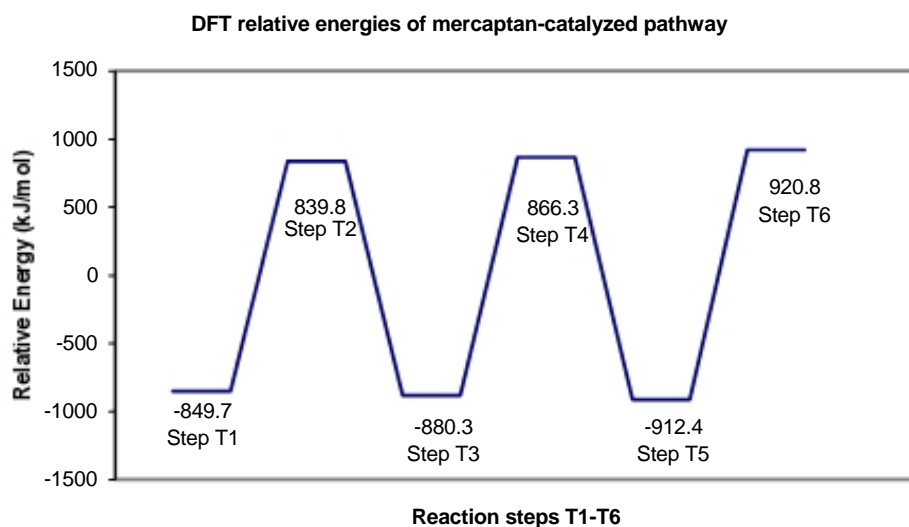
#### 4.4.1 Discussion and interpretation on the $\Delta E$ values of the reaction steps

The solvated AM1 (SAM1) calculated values provided us with a preliminary overview of the energy reaction profile of the condensation reactions via these 2 pathways. Not surprisingly, for reactions which required  $H^+$  protonation, the reaction is highly exothermic ( $\Delta E_{\text{reaction}} = \sum H_f, \text{products} - \sum H_f, \text{reactants}$ ); where reactions involve deprotonation, the reaction is highly endothermic.

The overall heat of formation reaction energies are still exothermic for both acid-catalyzed and mercaptan-catalyzed reactions, being -81.6 kJ/mol for both pathways and the DFT energy profile of the steps in both pathways are illustrated in **Fig. 4.4.1-1** and **4.4.1-2**:-



**Fig. 4.4.1-1**:- DFT energies of the Steps A1-A4 in acid-catalyzed pathway



*Fig. 4.4.1-2:- DFT energies of the Steps T1-T6 in mercaptan-catalyzed pathway*

#### **4.4.2 Problems with Protonation-Deprotonation Hypothesis**

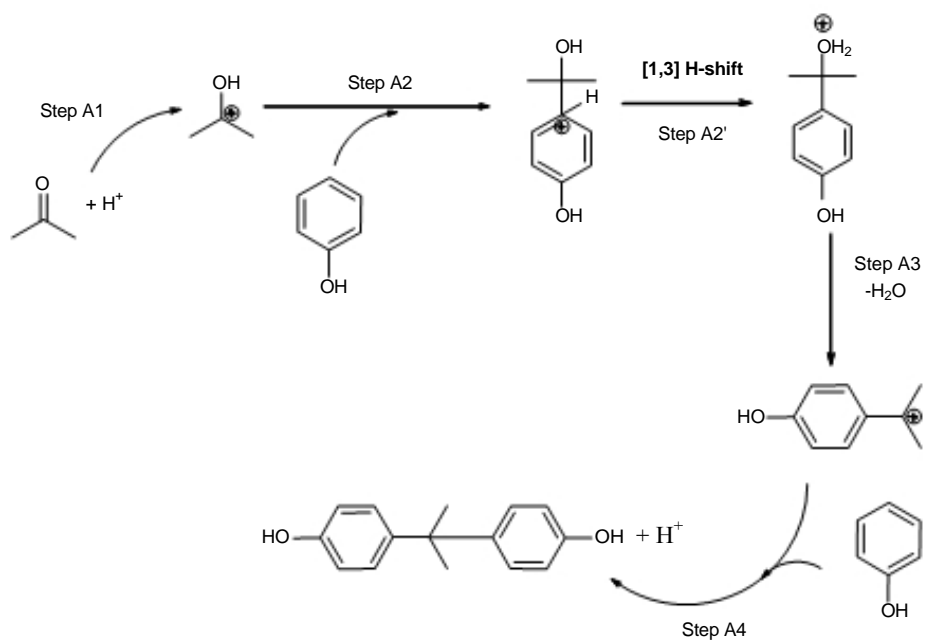
A brief glance at the energy profiles of the 2 reaction pathways as shown in Fig. 4.4.2-1 and 4.4.2-2 shows that the “protonation-deprotonation” hypothesis is not viable because the energy profile has to go through high peaks and sinking valleys to reach the final BPA product. It would be rather improbable that the reaction has to go through such thermodynamically unfavorable steps. In fact, the protonation/deprotonation step involving the addition or removal of  $H^+$  directly is not thermodynamically favorable. This led us to seek for other reaction mechanisms which could give a more reasonable thermodynamical deprotonation of  $H^+$  proton in steps A2 and T4, i.e., via a less thermodynamically extreme pathway. We subsequently explored the possibility of an alternate protonation/deprotonation step through [1,3] hydrogen-shift reaction from one C atom to another O or S (in mercaptan-catalyzed case) atom. An ideal situation would be that protonation/deprotonation of a molecule takes place via this hydrogen transfer from the deprotonating molecule (the H-donor) to the protonating molecule (the H-acceptor).



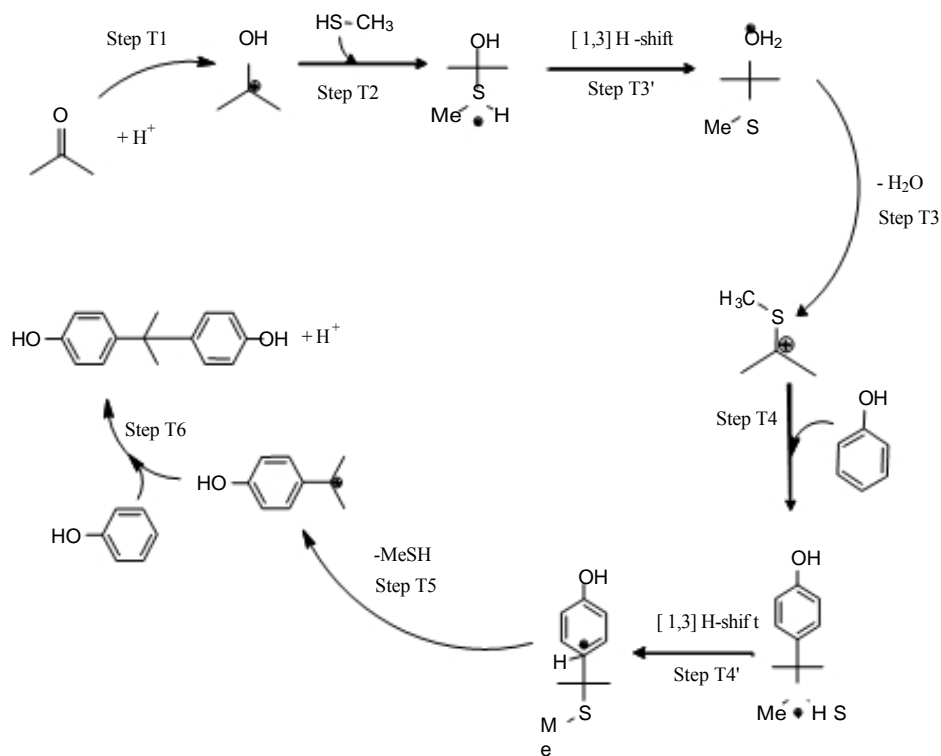
After the [1,3] H-shift rearrangement, “deprotonation” can take place in a milder step of condensation reaction to condense out H<sub>2</sub>O or MeSH. The transition states involving [1,3] H-shift in both reaction pathways were successfully located and the resultant energy profile indeed follows the initial predicted downward slope, presently a more thermodynamically favorable reaction profile and consistent with the observed reaction kinetic data.<sup>10</sup> These [1,3] H-shift transition states and the revised energy profile will be presented in the following sections.

#### **4.4.3 Reaction Mechanism Involving C—C Bond Forming and [1,3] H-shift Rearrangement Reaction Transition States**

Other than the conventional C—C bond formation required in the build-up to the final bisphenol-A product, we propose that there exists another type of transition states at steps A2 and T4 which precludes the “deprotonation” of H<sup>+</sup> and that is where the 1,3-H shift reactions takes place to transfer the H atom from a more electropositive atom to a more electronegative atom (like O or S), the H<sup>+</sup> is then condensed out as H<sub>2</sub>O or MeSH, which will therefore act as a milder form of deprotonation. The revised reaction mechanism is provided in **Fig. 4.4.3-1** and **4.4.3-2**:-



**Fig 4.4.3-1: Acid-catalysed revised reaction mechanism incorporating [1,3] H-shift in protonation/deprotonation steps**



**Fig 4.4.3-2: Mercaptan-catalysed revised reaction mechanism incorporating [1,3] H-shift in protonation/deprotonation steps**

Using DFT theoretical method of calculations, we utilized B3LYP and 6-31G\* as our level of theory and basis set, respectively, to calculate the relative energies of the individual steps in the acid and mercaptan-catalyzed pathways. The relative energies are benchmarked against the initial steps of each pathways, i.e. Step A1 and Step T1 for the acid and mercaptan pathways, respectively. The equations are kept consistent with same mass equivalence in the following steps to allow comparison of the relative energies with respect to the first steps of each pathway.

## **4.5 Methodology and Theoretical Calculations**

### **4.5.1 Optimal Method of Calculation—DFT B3LYP/6-31G\***

Structures along the reaction pathway were optimized at HF/3-21G level and then force constants were read from our previous calculations and finally optimize our structures at B3LYP/6-31G\* level. Based on our benchmarking calculations, B3LYP/6-31G\* is found to be a suitable level of theory to calculate the energies of the molecules examined.

The experimental gas-phase proton affinity of acetone is readily available from the United States National Institutes of Standards and Technology's Computational Chemistry Comparative Benchmark Database (NIST's CCCBDB) as 812.0 kJ/mol.<sup>11</sup> Our calculated gas-phase proton affinity of 816.9 kJ/mol is in good agreement with the experimental value. Reasonable agreement is also obtained for the proton affinities of methanol and methane thiol as shown in Table 4.5.1:-

Molecule	CCCBDB experiment proton affinity (kJ/mol) <sup>12</sup>	Calculated proton affinity (B3LYP/6-31G*) (kJ/mol)
Acetone	812.0	816.9
Methanol	754.3	752.9
MeSH	773.4	775.4

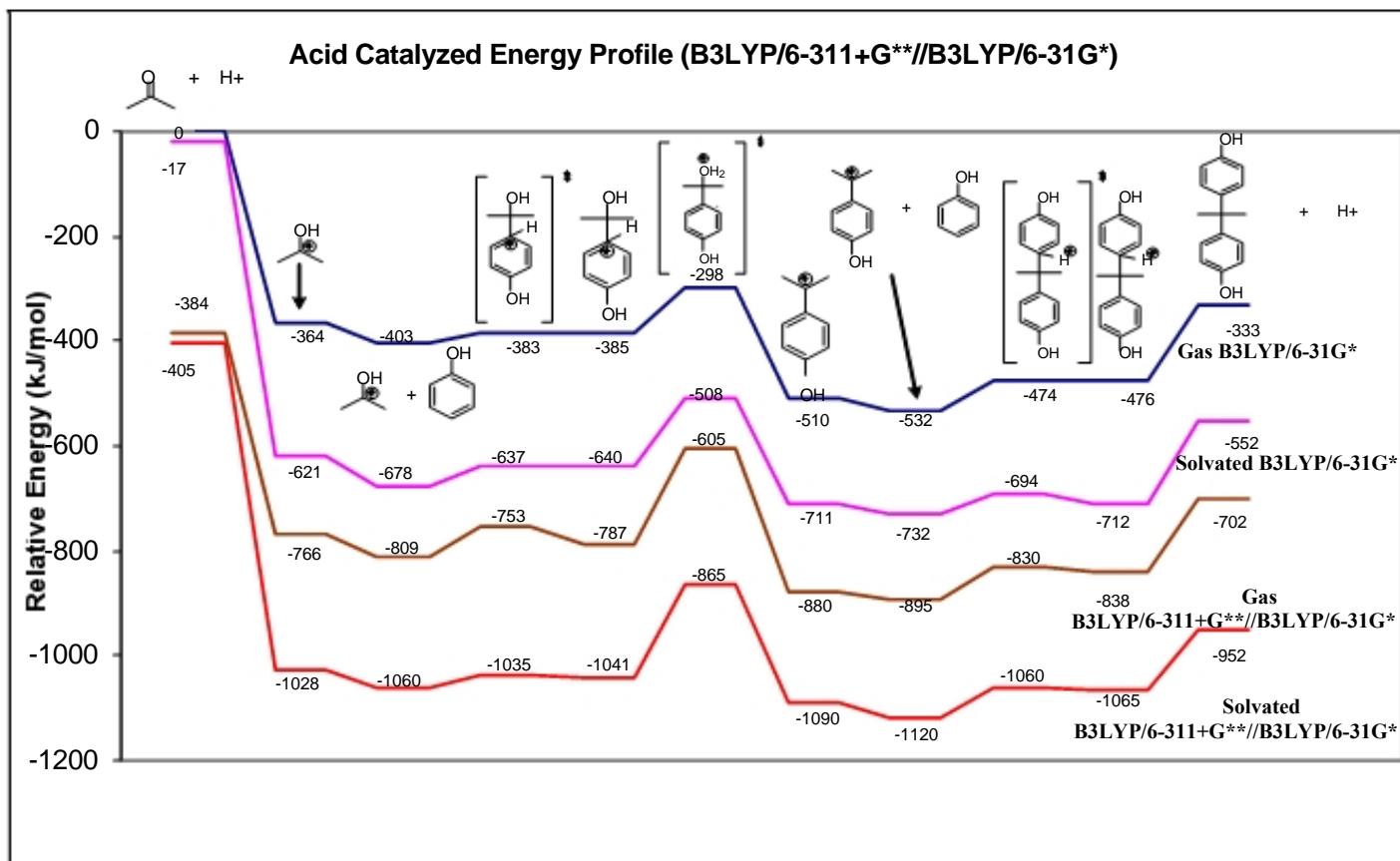
*Table 4.5.1:- Calculated B3LYP/6-31G\* values and experimental gas phase proton affinities*

#### 4.5.2 Energies and Frequency Calculations

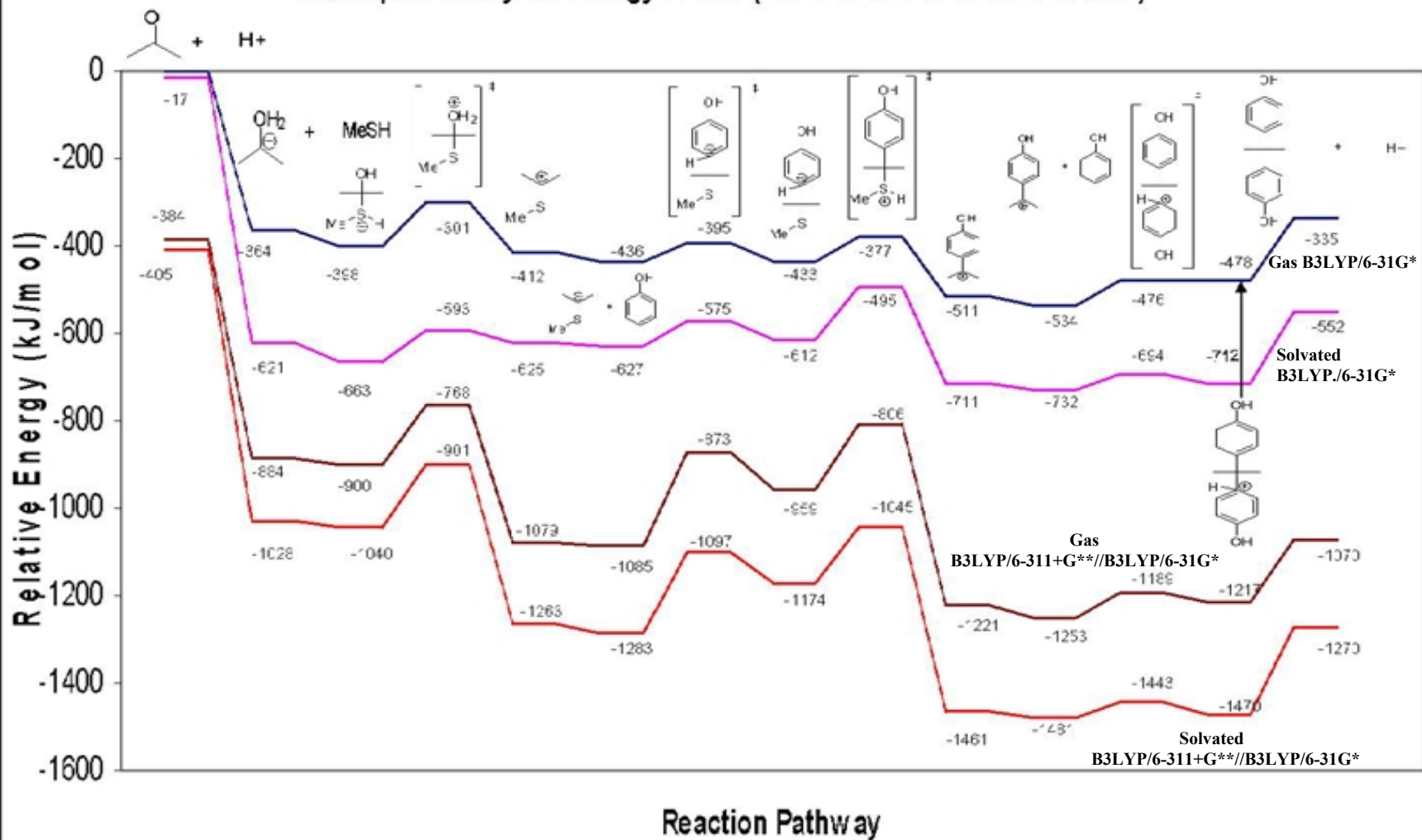
Using DFT B3LYP/6-31G\* as our computational level, we subsequently optimized the geometries of the pre-TS, TS, post-TS, intermediates and products of steps A1-A4 as well as steps T1-T6. In all cases, frequency calculations were also performed to confirm the nature of stationary points as minima (with all real frequencies) or transition states (with one imaginary frequency). The calculated relative energies include ZPE correction and are scaled by a common scaling factor of 0.9804.

#### 4.6 PES Energy Profile of Acid and Mercaptan Catalyzed Pathways

The schematic potential energy profiles of the acid and mercaptan pathways are shown in **Fig. 4.7.1** and **4.7.2**. The potential energy curves are referenced with respect to the first equation, i.e., Step A1 and Step T1 and they are all mass-balanced to ensure consistency in our relative energy calculations:-



### Mercaptan Catalyzed Energy Profile (B3LYP/6-311+G\*\*//B3LYP/6-31G\*)



## 4.7 Transition States and Conformers of Acid Pathway

In this section, we shall examine the mechanism and the associated transition states in detail for the conventional acid catalyzed pathway. The explanation for the transition states and intermediates of the mercaptan-enhanced catalysis will be investigated in the next section 5.9. We shall also investigate the different conformers which can be found along the transition reaction steps, since there are several degrees of freedom along the rotatable hydrocarbon and thiol bonds.

### 4.7.1 C—C bond forming transition states in Acid Pathway

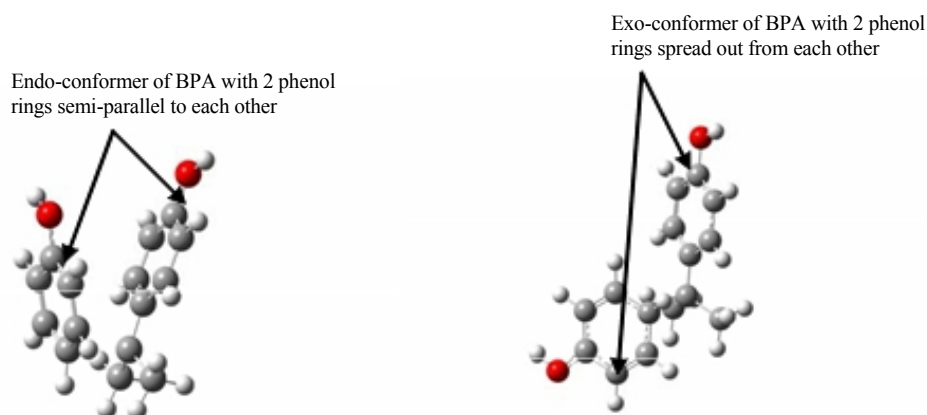
The most important step in the condensation reaction between acetone and phenol molecules to form BPA would be the quintessential C—C bond formation. BPA is made of the build-up of carbon skeleton composed by linking 2 phenol moieties at the 1, and 3 carbons of the acetone molecule, eliminating water molecule as a side product. Therefore, it is not surprising that the C—C bond formation would be found in the transition states along the pathway. Without C—C bond forming transition states, BPA would not be produced from the smaller constituent molecules. In our acid pathway, the transition states which corresponds to the C—C bond formation of the acetone and phenol moieties occur at step A2 and A4. At Step A2, the C atom of the phenol moiety attached itself to the C atom at the third position of the acetone moiety as shown:



**Fig 4.7.1-1:- Cis- and trans-conformers (with respect to the hydroxyl group of the phenol moiety and the hydroxyl group of the alkyl moiety) of the C-C transition state complex of Step A2**

Specifically, in step A2, we found 2 possible conformers of the transition state complexes, namely the *cis*- and the *trans*-conformer. The conformers differ in the orientation of the hydroxyl functional groups with respect to one another. The energy barrier heights for the transition state involving *cis*- and *trans*-conformers are 19.5 kJ/mol and 20.0 kJ/mol respectively. Given a difference of 0.5 kJ/mol, it is difficult to predict the *cis/trans* preference of the reaction step on the basis of such a small energy difference.

In step A4, the second phenol molecule attaches itself on the phenolic propylidene cation, the transition state complex, which is similar to step T6 which shows another C—C bond forming process between the C atom at the *para* position of the phenol moiety with the middle C atom of the propylidene moiety in 2 ways, the *endo*-conformer and the *exo*-conformer approach:-



**Fig. 4.7.1-2:- Endo and Exo transition states of Step A4**

This time, the energy barrier height between the reactants of Step A4 to the transition state of the complexes is differs by a greater magnitude. We found that not only is the *exo*-transition state (where the 2 phenol rings are spaced out in wing-like



configuration) lower in energy than the *endo*-transition state (where the 2 phenol rings exhibit weak  $\pi$ -stacking interaction); the activation energy for the *exo*-transition state is also lower than the activation via the *endo*-transition state as shown:-

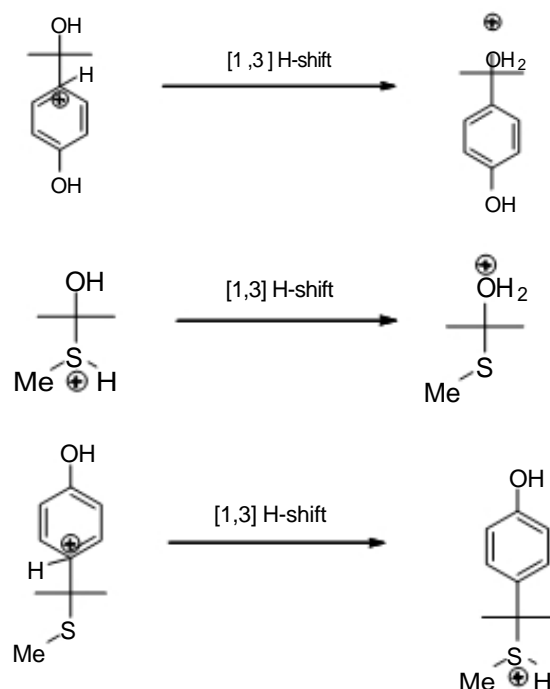
**Energy barrier height for *exo*-TS= 58.0 kJ/mol (gas phase)/ 38.3 kJ/mol (solvated)**

**Energy barrier height for *endo*-TS= 63.9 kJ/mol (gas phase)/ 45.0 kJ/mol (solvated)**

The difference in activation energies of the 2 approaches are of the order of around 5.9 kJ/mol, which means that according to the Arrhenius equation, the *exobisphenol-A* product will be the dominant product, whereas only a little of *endobisphenol-A* will be formed (e.r= 95:5).

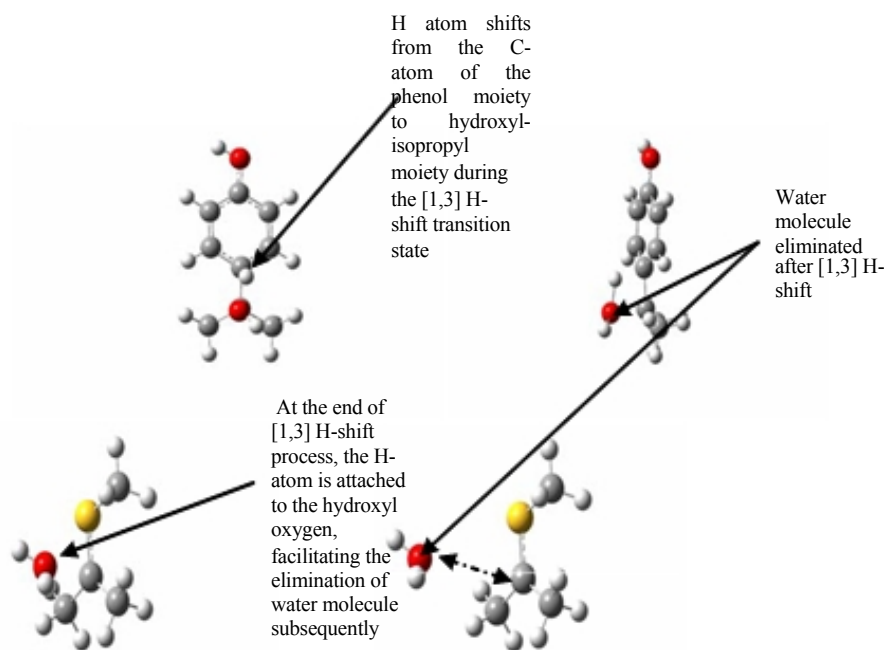
#### 4.7.2 [1,3] H-shift Transition States

As stated at the outset, if we were to incorporate the “protonation-deprotonation” hypothesis in our reaction mechanism elucidation, our reaction profile will shoot up and down along the reaction pathway and it would be inconceivable for a reaction to undergo such drastic PES surface. The loss of a H-proton straight out would require too high an energy of dissociation. Given the fact that [1,3] H-shift is a possible pathway which might temper the peaks and valleys seen in our original PES curve and that it is frequently encountered in literature<sup>13</sup>, we sought to find the transition states which corresponds to the 1,3-Hydrogen shift; in other words, transition states which correspond to a H atom moving along the reaction co-ordinate from the donor atom to the acceptor atom as shown in the **Fig. 4.7.2-1** below:-



*Fig. 4.7.2-1: Examples of [1,3] H-shift in the revised reaction mechanism*

A possible explanation would be that the 1,3 H-shift involve a possible “H-bridge” where the H-atom will be in between the donor C atom and the acceptor C atom, instead of forming a carbonium ion as an intermediate using the principles of Hammond’s postulate as well as our chemical intuition that the H-bridge would facilitate the transfer of the H-atom from the thiol moiety to the hydroxyl functional group. This reaction would possibly be similar to the hydrogen halide (HX) electrophilic addition reaction to alkenes, which has been proven quantum mechanically to involve a H-bridge as an intermediate, counter to having a carbonium entity as once thought. Subsequently, we successfully found the transition states which corresponds to the correct reaction coordinate of 1,3 H shift. The transition states of Step A2 are shown below:-

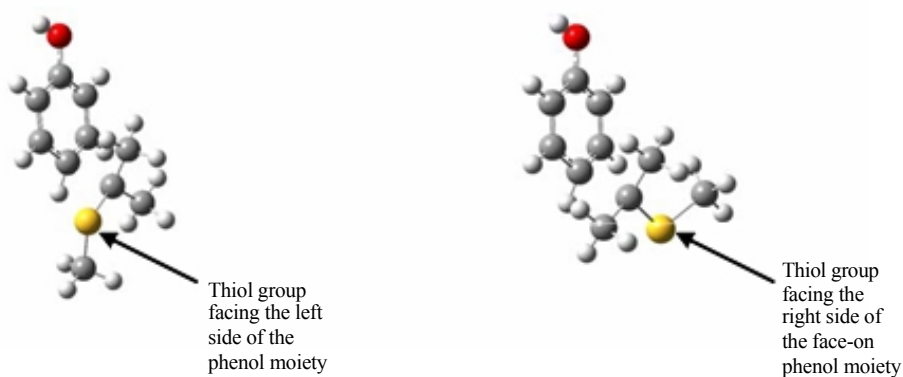


*Fig. 4.7.2-2:-[1, 3] H-shift transition state of Step A2, showing the elimination of H<sub>2</sub>O in the elimination step later.*

## 4.8 Transition States of Mercaptan Pathway

### 4.8.1 C—C bond forming transition states

In the mercaptan catalyzed pathway, we also found the C—C bond forming essential to the construction of the bisphenol-A molecule. The first C—C bond forming transition state exists at Step T4 and the transition states can go through 2 pathways, the left-TS and the right-TS as shown below:-



*Fig 4.8.1: Transition state complexes in left-cmp and right-cmp in Step T4 in the gas phase*

The energy barrier heights of the 2 complexes are very similar and we thought in reality, the reaction will not present any preferable pathways since the relative energies between the 2 conformers are highly similar:-

**Energy barrier height of left-TS= 6.8 kJ/mol (gas phase)/ no left-TS located (solvated)**

**Energy barrier height of right-TS= 7.0 kJ/mol (gas phase)/ 5.8 kJ/mol (solvated)**

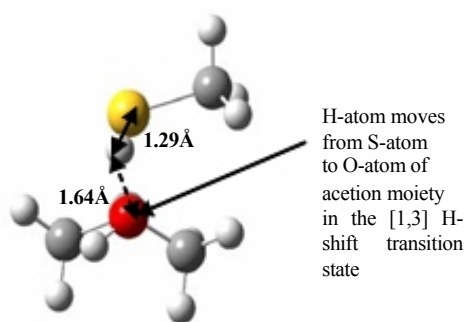
However, in the solvated phase, using PCM model (solvent=water), the transition state of left-TS complex shows 2 imaginary frequencies; in other words, this is a second-order transition state in the solvated phase and therefore not a real transition state. The right-TS in step T4 still shows only one unique imaginary frequency. Hence, there is a difference between the gas-phase and the solvated-phase calculations of the transition states.

What is more interesting though, especially for the sharp reader, is the fact that the average barrier height between the Step T4 and its analogous reaction in the acid pathway, Step A2 is quite different. The average energy barrier height of the acid pathway Step A2 is 19.8 kJ/mol in the gas phase and 40.5 kJ/mol in the solvated phase, whereas the average energy barrier height of mercaptan pathway Step T4 is 6.9 kJ/mol and 5.8 kJ/mol in the solvated phase. This relative energy difference between the 2 activation energies (of around **35 kJ/mol**) for the formation of the quintessential phenolic propylidene cation- which would then react with the 2<sup>nd</sup> phenol molecule to form the product BPA- explains the enhancement effect on the catalytic reaction brought by the addition of the co-catalyst methyl mercaptan. Ceterus paribus, the acid catalyzed reaction has a catalytic effect on the condensation reaction between phenol and acetone but the

methyl mercaptan further decreases the activation energy of the formation of phenolic propylidene cation.

#### 4.8.2 [1,3] H-shift Transition States

The [1,3] H-shift transition states were also found using B3LYP/6-31G\* in the methyl mercaptan pathway. In step T2, the H atom moves from the S-donor atom of the methyl mercaptan moiety to the O-atom of acetone.



*Fig. 4.8.2-1: H-atom from MeSH moves from the S-atom to the O-atom of acetone*

This [1,3] H-shift resembles that of a sigmatropic rearrangement, which is a process in which a  $\sigma$ -bonded substituent group migrates from one atom to another neighbouring atom. One  $\sigma$  bond is broken in the starting moiety, a new  $\sigma$  bond is formed in the product. This sigmatropic suprafacial [1,3] H-shift effectively tempers the protonation-deprotonation energy profile on the PES curve and creates a thermodynamically favorable reaction profile.

Another [1,3] H-shift is seen in step T6 where the H-atom now moves from the S-atom of MeSH moiety to the phenol ring before being eliminated as part of a water molecule:-

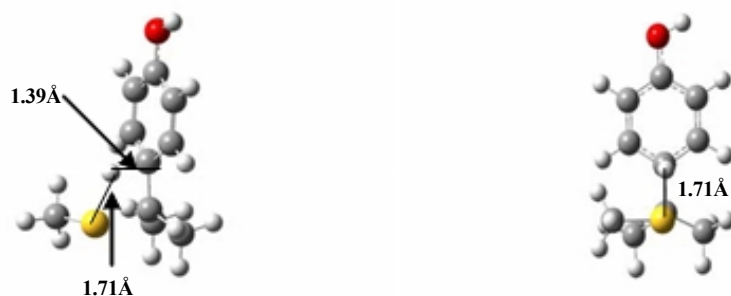


Fig. 4.8.2-2: Another example of the [1,3] H-shift leading to thiolpropylidene cation

## 4.9 Discussion and Interpretation

### 4.9.1 Stability of carbocation intermediates

It is a well-known fact that more highly substituted carbocations are more stable than less highly substituted ones. In other words, the stability order of carbocations is in the order of *tertiary* > *secondary* > *primary* > *methyl*. It may be suggested that the reason why as the reaction progresses down the reaction pathway of both acid-catalyzed and mercaptan catalyzed condensation of BPA, the carbocation intermediate formed moves from secondary carbocations (e.g. aa04 and tt06) to tertiary carbocations (e.g. aa06 and tt10) before the final production of the quintessential carbocation aa08/tt12, which are equivalent could be due to the relative stability of the latter tertiary carbocations compared to the former secondary carbocations. The reason for the structure of the final product can be illustrated by Hammond's postulate which states that the structure of a transition state resembles the structure of the nearest stable species. Transition states for endothermic states structurally resemble products and transition states for exothermic steps structurally resemble reactants. Although there is no precise thermodynamic relationship between the stability of a high-energy carbocation intermediate (which is

determined by  $\Delta G^\circ$ ) and the reaction rate (which is determined by  $\Delta G^\ddagger$ ), it is generally observed that when comparing 2 similar reactions, the more stable intermediate forms faster than the less stable one.

An explanation of the relationship between the reaction rate and intermediate stability was first advanced in 1955. Known as the Hammond postulate, this explanation is not a thermodynamic law; rather, it is a reasonable account of observed facts. It intuitively links reaction rate and intermediate stability by looking at the energy level and structure of the transition state.

#### **4.9.2 Energy barriers of transition states formed**

As we have seen in the energy profiles of the acid and mercaptan pathways, the overall condensation reaction of BPA from acetone and phenol reactants is exothermic, much of which is contributed by the protonation of acetone in steps A1 and T1. Both pathways require an acidic environment; therefore mercaptan is not so much a catalyst as a co-catalyst in the greater scheme of things. Industrially, mineral acids like HCl and H<sub>2</sub>SO<sub>4</sub>, immobilized and attached to acidic ion-exchange resin columns are still the main catalyst with which the condensation reaction takes place. Chemical engineers and process technologists are constantly on the look out for new catalysts that can enhance the rate of reaction of the acid catalysis of BPA by further reducing the energy barrier height of the C—C bond formation as exemplified in steps A2 and T4 respectively. As we have calculated from DFT methods, the activation energy barrier for the first C—C bond formation between the acetone moiety and the first phenol molecule was reduced by 13 kJ/mol via introducing methyl mercaptan MeSH into the reaction mixture. The reduction

in activation energy is not as impressive as in the Taddol project but it does explain the increase in reaction rate of the overall condensation reaction.

Reviewing the energy profiles of the acid and methyl-mercaptan pathways also reveal the fact that the potential energy surface is smoother in the methyl mercaptan pathway as compared to the acid pathway. We propose that methyl mercaptan enhances the catalytic effect of the proton on the condensation reaction by further lowering the entire energy surface as well as tempering the peaks and valleys seen in the conventional acid pathway.

Further calculations were done to improve our calculations on the PES surface. We went on to optimize the reactants in all steps using B3LYP/6-311+G\*\*, this time also including the solvation effects since in experiments, the condensation reactions take place in the ion-exchange resin columns with water as an effluent medium. The model used for the solvation effects in our calculations is PCM, solvent=water.

Introducing the solvated phase of the reactants under a larger basis sets produced a similar but more distinctive reaction energy profile as shown in the above energy profiles.

#### **4.9.3 Further developments by calculating single point reaction energy barrier heights at B3LYP/6-311+G\*\***

In order to further ascertain the relative energy differences of the energy barriers of the important transition states at step A2, T4 and T6. We did single point energy calculations of the transition states and the constituent monomers at 2 further DFT calculations, namely the B3LYP/6-311+G\*\* and B3LYP/6-311++G(3df, 2p). Our results revealed the same trend as determined in the B3LYP/6-31G\* method and basis set. The B3LYP/6-31G\* results are benchmarked against the B3LYP/6-311+G\*\* results. The single point results are indicated in **Fig. 4.7.1** and **4.7.2**.



## 4.10 Future Developments through Kinetic Studies of BPA condensation

Kinetic studies are classical methods for elucidating reaction mechanisms. Determining the rate-determining step would greatly aid the understanding of the organic reaction under investigation. Kinetic studies may not guarantee useful results as the quintessential C-C bond formation step in production of BPA may be located after the rate-determining step. One assumption that kinetic studies may prove or disprove is that the “protonation” and “deprotonation” steps take place under the [1,3] H-shift mechanism. Proving that the sigmatropic suprafacial [1,3] H-shift exists in the actual reaction mechanism is a crucial test for reaction pathways proposed here.

### References:

---

<sup>1</sup> Costin D.N., E.A.P.T., Patent No. 3627839, 1999

<sup>2</sup> Voges H.W., Ullmann's Encyclopedia of Industrial Chemistry, 6<sup>th</sup> ed.; Wiley-VCH: Weinheim, 2003, Vol. 25, 636

<sup>3</sup> Krimm, H.; Schnell, H., Br. Patent 905,994, 1962

<sup>4</sup> Zincke T., Mittheilungen aus dem chemischen Laboratorium der Universitat Marburg, Justus Liebigs Annalender Chemie, 343 (1905), 75-131

<sup>5</sup> Rohm Hass, <http://www.amberlyst.com/bpa.htm>

<sup>6</sup> De Jong J.I.; Dethmers F.H.D., *The formation of 2,2-bis(4-hydroxyphenyl)-propane (bisphenol A) from phenol and acetone*, Rec. Trav. Chim. (1965), 84, 4, 460-464

<sup>7</sup> Williamson J., U.S. Patent No. 2-730-552, 1956

<sup>8</sup> Palmer D.; Wong P.K., U.S. Patent No.6-465-697, 2002

<sup>9</sup> M.W. Palascak, G.C.Shields, *Accurate Experimental Values for the Free Energies of Hydration of H<sup>+</sup>, OH<sup>-</sup>, and H<sub>3</sub>O<sup>+</sup>*, J. Phys. Chem. A, **108** (16), 3692-3694, 2004

- 
- <sup>10</sup> Rahimi A., Farhangzadeh S. Iranian Polymer Journal, Vol. 10 Number 1 (2001) 29-32
- <sup>11</sup> Trott, W.M.; Blais, N.C.; Walters, E.A., *Molecular beam photo- ionization study of acetone and acetone-d<sub>6</sub>*, **J. Chem. Phys.**, 1978, 69, 3150
- <sup>12</sup> Hunter, E.P., Lias, S.G., *Evaluated Gas Phase Basicities and Proton Affinities of Molecules: An Update*, **J. Phys. Chem. Ref. Data**, 1998, 27, 3, 413-656
- <sup>13</sup> Hudson E.; David J., Journal of Organic Chemistry 2003, 68,7, 2735-2740
- <sup>14</sup> J. C. Rienstra-Kiracofe, G. S. Tschumper, H. F. Schaefer III, S. Nandi, G. B. Ellison, *Atomic and Molecular Electron Affinities: Photoelectron Experiments and Theoretical Computations*, Chemical Reviews, 102, 231-282 (2002)

# Chapter 5

## Conclusion

---

---

### 5.1 A common thread between the projects

According to the textbook by D.E. De Vos et al., *Chiral Catalyst Immobilization and Recycling*, the enantioselective catalysis in industrial production of important chemicals has become the cornerstone of the chemical industry.<sup>1</sup> This Masters thesis therefore deals with not only the theoretical aspects of the abovementioned chemical reactions, but also the industrial application of using the most suitable catalyst for large scale production of the desired products.

Large scale preparation of single enantiomers has now become an objective that is within the reach of industry. This means, whereas in the past, chemically important molecules like bisphenol-A might require high overhead costs- in terms of continuous supply of fresh catalysts- to produce, now the entire process would be streamlined within CSTR (continuously stirred tank reactors) with immobilized catalyzed like mercaptan -linked acidic ion exchange resin columns.

As enantioselective catalysis begins to be integrated in process schemes throughout the chemical industry, issues such as separation and reuse of expensive catalysts now come to the foreground. It is no longer sufficient for industrial and chemical engineers to just produce the most efficient heterogeneous catalysts for industrially important chemical reactions; they must also be working with material and surface chemists to

produce a heterogeneous inter-phase within which catalyst would be most efficiently recovered and recycled for subsequent reactions.

C—C bond formation plays a central role in organic synthesis. These reactions can be catalyzed by acids, bases and transition metal complexes via various routes such as nucleophilic addition, including alkylation in the case of the first Taddol project described in Chapter 3. Catalytic C-C bond formation is therefore one of the most actively pursued in the field of asymmetric catalysis because of its prime importance in the synthesis of fine chemicals, mainly for pharmaceutical and agrochemical products.

In asymmetric catalysis, a general rule of thumb is to work on the following three areas<sup>2</sup> :

- 1) The chiral modification of metallic and oxidic heterogeneous catalysts;
- 2) The immobilization of homogeneous catalysts; and,
- 3) The application of chiral polymers.

Deducing a suitable catalyst for a production reaction might be the holy grail for industrial chemists, but scaling it up to large scale production requires a whole slew of thoughtful consideration and if successful, a patent review process. Such was the case with both titanium taddolate and methyl mercaptan catalysts in this thesis.

## References:

---

<sup>1</sup> D.E.De Vos, I.F.J. Vankelecom, P.A. Jacobs, *Chiral Catalyst Immobilization and Recycling*, Wiley-VCH, 2000

<sup>2</sup> Hans-Ulrich Blaser, Benoit Pugin, Martin Studer, *Enantioselective Heterogeneous Catalysis: Academic and Industrial Challenges*, “Chiral Catalyst Immobilization and Recycling”, 1, 1, Wiley-VCH, 2000